

***Characterization of Neuronal SNARE Protein Amisyn and Its Role  
in Neurotransmission***

**Dissertation**

for the award of the degree  
“Doctor of Philosophy (Ph.D.)”  
Division of Mathematics and Natural Sciences

within the doctoral program “Molecular Biology of Cells”  
of the Georg-August University School of Science (GAUSS)

submitted by  
Jialin JIN

from Beijing China

Göttingen, September 2021

Thesis committee members:

Supervisor, reviewer: **Dr. Ira Milosevic**

Synaptic Vesicle Dynamics

European Neuroscience Institute

University Medical Center Göttingen

Göttingen, Germany

and

Wellcome Centre for Human

University of Oxford

Oxford, England

PhD committee member, reviewer: **Prof. Dr. Peter Schu**

Department of Cellular Biochemistry

University Medical Center Göttingen

Göttingen, Germany

PhD committee member: **Dr. Brett Carter**

Synaptic Physiology and Plasticity

European Neuroscience Institute

University Medical Center Göttingen

Göttingen, Germany

Thesis examination broad member:

**Prof. Dr. Rubén Fernández-Busnadiego**

University Medical Center Göttingen

Institute for Neuropathology

Göttingen, Germany

**Prof. Dr. Jochen Staiger**

Center for Anatomy, Dept. of Neuroanatomy

University Medical Center Göttingen

Göttingen, Germany

**Prof. Dr. Halyna Shcherbata**

Research Group Gene Expression and Signaling

Institute of Cell Biochemistry

Hannover Medical School

Hannover, Germany

Date of the oral examination: 29.10.2021

I hereby declare that I prepared this PhD thesis, entitled “*Characterization of Neuronal SNARE Protein Amisyn and Its Role in Neurotransmission*” on my own and with no other sources and aids than those cited.

Jialin JIN

17 September 2021

Göttingen

# Contents

<b>List of Figures</b> .....	<b>V</b>
<b>List of Tables</b> .....	<b>VII</b>
<b>List of Abbreviations</b> .....	<b>VIII</b>
<b>Abstract</b> .....	<b>1</b>
<b>1 Introduction</b> .....	<b>3</b>
1.1 Neuronal Communication via Synaptic Neurotransmission .....	3
1.2 The recycle Process of the Synaptic Vesicles at the Presynaptic Side .....	5
1.3 Exocytosis .....	6
1.4 Amisyn and Its Links to Exocytosis .....	12
1.5 The Patch Clamp Technique as an Effective Tool in Neuroscience .....	15
1.6 Aim of the study .....	18
<b>2 Materials and Supplementary Method</b> .....	<b>22</b>
2.1 Chemicals and Reagents .....	22
2.2 Solutions .....	24
2.3 Antibodies .....	26
2.4 Consumables and Kits .....	27
2.5 Plasmids .....	28
2.6 Primers .....	28
2.7 Equipment .....	30
2.8 Bacteria and Virus .....	31
2.9 Softwares .....	31
2.10 Supplementary Method .....	32
2.10.1 Protein Expression and Purification Procedure .....	32

2.10.2	Biochemical procedures .....	33
<b>3</b>	<b>Results .....</b>	<b>34</b>
3.1	PI(4,5)P <sub>2</sub> -dependent Regulation of Exocytosis by Amisyn, the Vertebrate-specific Competitor of Synaptobrevin 2 .....	34
3.2	Amisyn regulates release probability at the neuronal synapse .....	92
3.3	GST pull-down of amisyn (Supplementary results) .....	135
<b>4</b>	<b>Discussion .....</b>	<b>138</b>
4.1	Investigation of Amisyn's N-terminal Domain .....	140
4.2	Investigation of the Mechanism of Amisyn-Syntaxin Association .....	140
4.3	Investigation of Exocytosis Inhibition by Amisyn .....	141
4.4	Investigation of Novel Amisyn Interactors.....	143
4.5	Electrophysiological and Behavioral Characteristics of Amisyn Mutant Mice .....	144
4.6	Investigation of the Levels and Distribution of Various Neuronal Proteins in Amisyn Mutant Mice Brains .....	148
<b>5</b>	<b>Summary and Outlook .....</b>	<b>150</b>
5.1	Summary of Thesis Work .....	150
5.2	Future Perspectives .....	152
	<b>Reference .....</b>	<b>154</b>
	<b>Acknowledgement .....</b>	<b>167</b>
	<b>Curriculum Vitae .....</b>	<b>169</b>

## List of Figures

Figure 1 Neurons and their connection .....	4
Figure 2 Synaptic vesicle recycling procedure on the presynaptic side .....	6
Figure 3 Details of exocytic process .....	9
Figure 4 Sequence and structure of the amisyn .....	14
Figure 5 Procedures of patch clamp .....	16
Figure 6 Whole-cell voltage-clamp setup for brain slice recording .....	17
Figure 7 Scan of SDS gel from the first pull-down experiment .....	135
Figure 8 Scan of SDS gel from the second pull-down experiment .....	136
Figure 9 Volcano plot of the mass spec result of amisyn pull-down experiment .....	137
<b>Chapter 3.1</b>	
Figure 1 Amisyn forms SNARE complex with syntaxin-1 and SNAP-25 and inhibits liposome fusion <i>in vitro</i> . .....	68
Figure 2 Amisyn binds to membranes by its N-terminal PH-domain .....	71
Figure 3 Recombinant amisyn binds to plasma membranes <i>in vitro</i> .....	73
Figure 4 PI(4,5)P <sub>2</sub> levels control membrane binding of amisyn in PC12 cells .....	75
Figure 5 Liposome binding of amisyn is dependent on PI(4,5)P <sub>2</sub> .....	77
Figure 6 Stimulation recruits amisyn-EGFP to the plasma membrane of PC12 cells .....	78
Figure 7 Amisyn, but not amisyn SNARE-domain, reduced number of released vesicles but did not alter rates of vesicle fusion in bovine chromaffin cells .....	81
Figure 8 Model of the role of amisyn in secretory vesicle exocytosis .....	83
Suppl. Figure S1 Amisyn is a conserved, vertebrate-specific protein that forms SNARE complex with syntaxin-1 and SNAP-25 .....	84
Suppl. Figure S2 Purification of recombinant amisyn (WT and AADD mutant) proteins. ....	86

Suppl. Figure S3 Specificity of custom-made anti-amisyn polyclonal rabbit antibody .....	88
Suppl. Figure S4 Amisyn interaction with liposomes requires the presence of phosphatidylinositol bisphosphates or phosphatidylinositol trisphosphate .....	89
Suppl. Figure S5 Amisyn, but not amisyn SNARE-domain, reduced the number of released vesicles but did not alter rates of vesicle fusion in bovine chromaffin cells. .....	90
<b>Chapter 3.2</b>	
Figure 1 Enrichment of amisyn in the hippocampus and the generation of amisyn mutant mice with conditional potential, C57BL6/N-STXBP6 <sup>tm1a</sup> .....	120
Figure 2 Protein expression and mRNA transcription levels in amisyn mutant mice .....	122
Figure 3 Behavioral characterization of amisyn mutant mice .....	124
Figure 4 mEPSC recordings in CA1 neurons from amisyn mutant mice brain slices .....	126
Figure 5 Amisyn mutation altered vesicle release probability in neurons from CA1 and CA3 areas .....	128
Figure 6 High frequency stimulus train recording revealed that amisyn's absence influences the releasable pool size .....	129
Figure 7 Amisyn mutant mice had impaired SC-LTP .....	131
Suppl. Figure S1 EPSCs response to 10-stimuli train with different frequencies ....	132
Suppl. Figure S2 Habituation showed no anxiety difference between amisyn mutant mice and WT mice .....	133
Suppl. Figure S3 No difference in CaV $\alpha$ 2 $\delta$ 4 expression level between amisyn mutant and wild type animal's hippocampus.....	134

## List of Tables

Table 1 Chemicals, their supplier and catalog number used in this thesis.....	22
Table 2 Buffers and solutions used in this study .....	24
Table 3 Antibodies used in experiments presented in this thesis .....	26
Table 4 Kits and consumable products used in experiments presented in this thesis	27
Table 5 Plasmids used in experiments presented in this thesis .....	28
Table 6 Primers used for genotyping samples .....	28
Table 7 Primers used for qPCR .....	28
Table 8 Equipment used in this study .....	30
Table 9 Bacteria and viruses used in the study .....	31
Table 10 Software programs used in study .....	31

## List of Abbreviations

°C	Celsius degree
ASD	autism spectrum disorder
CATCHR	complex associated with tethering containing helical rods
DG	dentate gyrus
DMEM	Dulbecco's modified eagle's medium
DNA	deoxyribonucleic acid
EDTA	ethylenediaminetetraacetic acid
EGTA	ethylene glycol tetraacetic acid
EPM	elevated plus maze
EPSC	excitatory postsynaptic current
EPSP	excitatory postsynaptic potential
FBS	fetal bovine serum
GABA	γ-amino butyric acid
GFP	green fluorescent protein
GST	glutathion-S-Transferasen
HEPES	4-(2-hydroxyethyl)-1-piperazineethanesulfonic acid
IPTG	Isopropyl β-D-1-thiogalactopyranoside
KD	knockdown
kDa	kilo daltons
KO	knockout
LDCV	large dense core vesicles
LTP	long term potentiation
mass spec	mass spectrometry
mEPSC	miniature excitatory postsynaptic current
MF	mossy fibre
Munc13/18	mammalian uncoordinated-13/18
NOR	novel object recognition
NSF	soluble N-ethylmaleimide-sensitive factor

NT	neurotransmitter
PBS-T	phosphate buffered saline triton X 100
PI(4,5)P <sub>2</sub>	phosphatidylinositol 4,5-bisphosphate
PKC	protein kinase C
PLC	phospholipase C
PM	plasma membrane
PMSF	phenylmethylsulfonyl fluoride
PPR	pair pulse ratio
PTP	post tetanic potentiation
P <sub>r</sub>	release probability
Rab	Ras-related protein
RIM	Rab3-interacting molecule
RRP	readily releasable pool
SC	Schaffer collateral
SDS-PAGE	sodium dodecyl sulfate polyacrylamide gel electrophoresis
SH3	Src-homology 3
SM	Sec1/Munc-18-like
SNAP	synaptosomal-associated protein
SNARE	soluble N-ethylmaleimide-sensitive factor attachment protein receptors
SRP	slowly releasable pool
STP	short term plasticity
STXBP	syntaxin binding protein
SV	synaptic vesicle
TBS-T	Tris-buffered saline and Tween 20
VAMP	vesicle-associated membrane protein
WT	wild type

## **Abstract**

Neurotransmission is a complex bioprocess that involves a series of complex interactions between proteins and lipids. Exocytosis, which directly mediates neurotransmitter release, is one of the most important steps in the neurotransmission process and has been intensively studied for the last three decades. Various exocytosis regulators have been reported and described in detail, including Munc18, synaptotagmin, complexin, and tomosyn. Among these regulators, amisyn (known as syntaxin bind protein 6) has been rarely studied due to technical challenges related to its expression and lack of specific antibodies. Although studies on amisyn date back to 2002, only 6 publications have focused on this protein. Thus, the basic structural, functional, and physiological characteristics of amisyn remain unclear.

As a member of the SNARE family, amisyn is a 24 kDa protein comprising a C-terminal VAMP2-like SNARE domain and an unknown N-terminal domain. Amisyn can bind with syntaxin-1 and SNAP-25 to form a SNARE complex. The amisyn-SNARE complex is fusion-inactive because amisyn does not contain a transmembrane domain. Thus, amisyn is speculated to be an inhibitor of exocytosis. This thesis work addresses the function of amisyn in neuronal and neurosecretory cells, including the function of amisyn's N-terminal domain. Furthermore, for the first time, the consequences of amisyn's ablation in a mammalian model were studied systematically.

In the first study, we conducted a sequencing analysis to determine the potential structure of the N-terminal domain of amisyn. In the following experiment, we confirmed this speculation and determined that the N-terminal domain of amisyn is a pleckstrin homology domain. This pleckstrin homology domain could bind with phosphatidylinositol 4,5-bisphosphate lipids. Further experimental results suggested that the pleckstrin homology domain of amisyn was involved in both SNARE complex formation and the exocytosis inhibitory process of amisyn. In chromaffin cells, external full-length amisyn could change the size of the readily releasable pool and slowly releasable pool, whereas the SNARE domain of amisyn failed to achieve this. Based on these data, we constructed a new model to explain the role of amisyn in

neurotransmission. In this new model, amisyn associates with the phosphatidylinositol 4,5-bisphosphate in the plasma membrane and competes with VAMP2 to form the fusion-inactive SNARE complex. In this way, amisyn can achieve an inhibitory effect. In the second study, we characterized the physiological properties of amisyn using a newly generated amisyn mutant mouse line. We also studied the behavioral and proteomic properties of amisyn-deficient animals. We first determined which synaptic and signaling proteins are altered in the hippocampi of amisyn mutants; the RNA and protein levels were unaltered for all tested candidates, except for VAMP2, rab3a, and  $\alpha$ -synuclein. Next, we conducted electrophysiological and behavioral assays to characterize neurotransmission in amisyn mutant animals. We found increased vesicle release probability and enlargement of the readily releasable pool in amisyn-deficient synapses. Further experiments on plasticity revealed that long-term potentiation was abolished in amisyn mutant animals, which was consistent with the results from the behavioral assays, thereby indicating an impairment of learning and memory formation in amisyn mutant animals.

The new findings reported in this doctoral thesis further our understanding of amisyn and its roles in neurotransmission, allow us to characterize exocytosis more precisely, and enhance our understanding of the pathological mechanisms underlying some amisyn-related diseases.

# **1 Introduction**

## **1.1 Neuronal communication via synaptic neurotransmission**

One of the most important organs in the human body is the brain, which accounts for only 2% of body weight and consumes 20% of daily energy consumption (Herculano-Houzel, 2012). The brain is a multidimensional complex consisting of proteins, genes, cells, and synapses interacting with each other within a dynamic neurochemical environment (Raichle & Mintun, 2006). Two different types of cells are distributed in the brain: neurons and glia. Electrically excitable neurons are the basic structural and functional units of neuronal networks (Kandel, 2012). Unlike neurons, glial cells mainly provide structural support to neurons and maintain homeostasis of the nervous system. The number of glial cells in the brain is 10 times more than that of neurons (Herculano-Houzel, 2014; Marina et al., 2018).

Neuronal communication is the basis of basic brain functions such as motor control, learning, cognitive processes, and memory formation, and understanding its molecular mechanisms is essential for the study of brain functions (Monje, 2018). As a basic unit of neuronal communication, a single neuron consists of a cell body, called the soma, and several processes (Luo, Sui, Wang, & Chae, 2015). The soma contains the nucleus and most important organelles. Usually, one neuron has multiple short processes, called dendrites, which can receive input signals from other neurons. All neurons have only one axon, which is a long projection that, as opposed to dendrites, is able to project output information flow from the soma to the soma/dendrites of other neurons. This juxtaposition of an axon and its receptive site (dendrite or soma) is called a synapse. The axonal terminal part of a synapse is called the presynaptic side, whereas the other part is called the postsynaptic side. The space between the presynaptic and postsynaptic sides is called the synaptic cleft (Brodal, 1980). Neural signals can pass from one cell to another across synapses. This information passing process is called neurotransmission.

There are two main types of neurotransmission at synapses: electrical and chemical. Electrical neurotransmission involves an electrical nerve impulse that propagates along the axon until it reaches the gap junction. This nerve impulse is usually a

voltage change called an action potential. At the gap junction, the action potential from the output cell can induce a new action potential at the input cell (Miller & Pereda, 2017).

Chemical neurotransmission is achieved by the release of chemical signaling molecules called neurotransmitters (NTs) at the presynaptic side when an action potential arrives. NTs are usually stored in small (approximately 40 nm) lipid membrane surrounded spheres called synaptic vesicles (SVs) at the bouton of the presynaptic side. After SVs release NTs into the synaptic cleft, NTs then specifically bind to receptors on the postsynaptic membrane; in turn, this opens voltage-gated ion channels, which results in a directional ion flow across the membrane that forms an electrical signal that can propagate the signal to the next neuron. In some cases, if NTs bind with metabotropic receptors, a second messenger cascade happens at the postsynaptic side (Sinha & Mukhopadhyay, 2020). This messenger cascade also facilitates signal transmission.

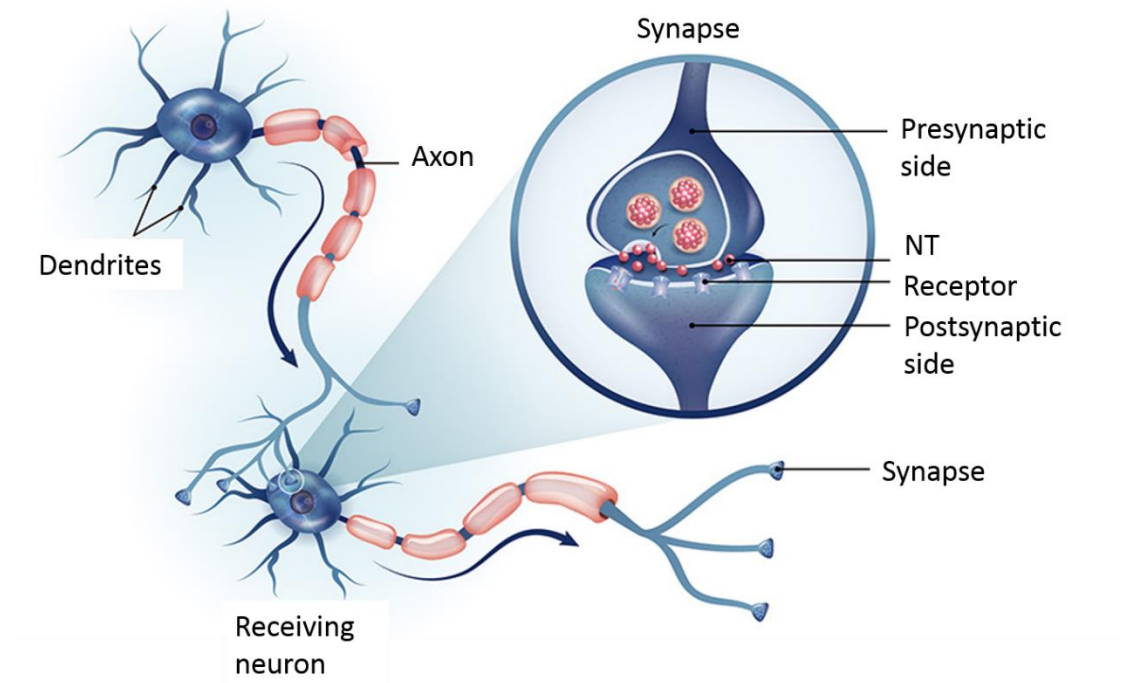


**Figure 1** A schematic diagram of neurons and their connection. A neuron consists of a cell body (soma), dendritic branches, and a long projection that transports information to other neurons (axon). A synapse (magnified part) is formed by an axon of the presynaptic neuron and the dendrite of the postsynaptic neuron. NTs are released from the presynaptic side and

conjugate with the receptors on the postsynaptic side. (Figure: gemetex.com)

## 1.2 The recycle process of the synaptic vesicles at the presynaptic side

At the presynaptic terminals, a series of biochemical reactions and events are involved in the release of NTs. After arrival of the action potential, SVs are first recruited to a specific electron-dense area of the bouton called the active zone. The arrival of an action potential triggers the opening of voltage-gated calcium channels and increases the intracellular calcium concentration. High calcium concentration further triggers a SNARE-dependent SV fusion process called exocytosis (Jahn & Fasshauer, 2012). During exocytosis, SVs are recruited at the active zone and secrete NTs after fusion with the plasma membrane. Usually, the SV reserve at synaptic terminals is insufficient for exocytosis to occur multiple times. Thus, neurons must replenish SVs in an efficient process called endocytosis, during which the excess SV membrane and proteins are recycled to the plasma membrane (Saheki & De Camilli, 2012). The recycled material can be used to form new SVs, and peripheral proteins become attached to them to guarantee that they are ready for the next round of fusion. This entire procedure is called SV recycling (Reese, 1973; Sudhof & Rizo, 2011).

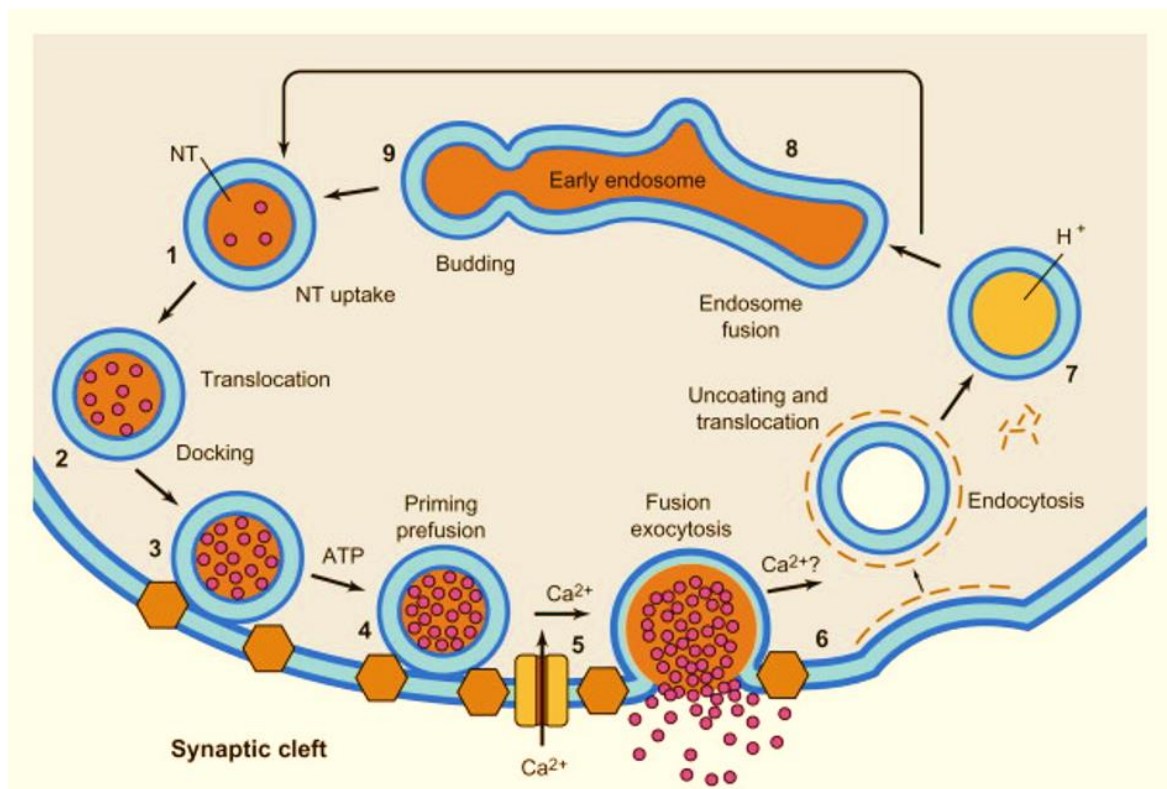


**Figure 2** A diagram of the synaptic vesicle recycling procedure on the presynaptic side. First, NTs are released from SVs through exocytosis (2-5), which involves a sequence of steps, including mobilization of NT-filled SVs to the specialized sites for release called the active zone (2), where the vesicles are docked (3), followed by the activation of release machinery by priming (4) and finally undergoes calcium-triggered vesicle fusion (5). Then, the excessive membrane and proteins are retrieved by endocytosis (6). Finally, new vesicles are formed subsequently and filled with NTs again (7,8) to participate in the next cycle of fusion events. (Figure modified from: Pigino et al., 2012)

### 1.3 Exocytosis

As described in the previous section, exocytosis mediates the secretion process of NTs. Regulated exocytosis is crucial for all biological secretion processes, including neurotransmission. Exocytosis is the result of a series of complex protein-protein and protein-lipid interactions.

The whole exocytosis process is composed of several steps. First, the vesicle recruits and docks at the release site. Second, calcium influx occurs, which initiates vesicle fusion. Finally, NTs are released into the synaptic cleft (Jahn & Fasshauer, 2012; Sudhof & Rizo, 2011). After decades of research, several important proteins involved in exocytosis have been identified and described. Most of the underlying mechanisms and properties of exocytosis have been well studied *in vitro*, *in vivo*, and *in silico* (Neher, 2006).

Before exocytosis starts, SVs initially remain at the presynaptic terminal and cluster to form functionally distinguished pools, called vesicle pools. Several proteins including synapsins, intersectin, Rab3, and SH3, are involved in the formation of vesicle pools (Bykhovskaia, 2011; Lledo et al., 1994; Ma, Niu, & Ma, 2008; Milovanovic & De Camilli, 2017; Shupliakov & Brodin, 2010). According to the demand of transmission, vesicles can move from one pool to another or even to the neighboring synapses.

Among the vesicle pools is a specific pool that comprises the most active vesicles that participate in recycling and fusion. This pool, which is called the readily releasable

pool (RRP), is transiently active once the release process starts (Kaeser & Regehr, 2017; Rosenmund & Stevens, 1996). However, most vesicles in the RRP are not in the fusion state at this time point. Hence, active SVs must be transported to the active zone on the plasma membrane so that they can be ready for release. This transporting event is achieved by a protein complex composed of Rab3 interacting molecule (RIM), mammalian uncoordinated 13 (Munc13), ELKS, Calpastatin (CAST), Liprin, Bassoon, and Piccolo (Schoch & Gundelfinger, 2006); these proteins can couple SVs with calcium channels on the plasma membrane and manipulate short- and long-term synaptic plasticity.

In the following step, SVs recruited at the active zone are docked on the plasma membrane and primed for fusion. The docking of SVs refers to the contact between the vesicle and plasma membranes. Then, docked SVs are primed by a series of reversible interactions and finally activate the release process. Several proteins are involved in docking and priming, and most of these proteins are from conserved protein families such as soluble N-ethylmaleimide-sensitive factor (NSF) attachment protein receptors (SNARE), Sec1/Munc-18-like (SM), and complex associated with tethering containing helical rods (CATCHR) proteins (de Wit, 2010; Jahn & Fasshauer, 2012). Active zone proteins, including Munc13 and RIM, also participate in the docking and priming of SVs and help to prime and fix the vesicle onto the plasma membrane (Magdziarek et al., 2020; Zarebidaki et al., 2020).

After docking and priming, the fusion of the vesicle begins. The formation of the SNARE complex is crucial for fusion. SNARE proteins contain a conserved homologous stretch of 60-70 amino acids called a SNARE motif. Four SNARE motifs spontaneously form a thermostable sodium dodecyl sulfate (SDS) and protease-resistant coiled-coil bundle complex (Terrian & White, 1997; Weimbs, Mostov, Low, & Hofmann, 1998). The kernel of this SNARE complex is a 16 layers of amino acid side chains that are perpendicular to the axis of the complex. Among these 16 layers, there is a unique central layer, also known as the 0-layer, which is hydrophilic and is made up of three glutamine (Q) and one arginine (R) (Fasshauer, Eliason, Brunger, & Jahn, 1998; Sutton, Fasshauer, Jahn, & Brunger, 1998). Each of

these four amino acids is from a different protein and combined via ionic interaction. According to the type of this particular amino acid from the 0-layer, SNARE proteins can be distinguished into four different subfamilies, as follows: Q<sub>a</sub>, Q<sub>b</sub>, Q<sub>c</sub>, and R (Fasshauer et al., 1998; Kloepper, Kienle, & Fasshauer, 2007; Stein, Weber, Wahl, & Jahn, 2009). Although a single SNARE protein can participate in fusion alone *in vitro*, only the SNARE complex together with its regulators can accomplish the whole fusion process *in vivo* (Weber et al., 1998).

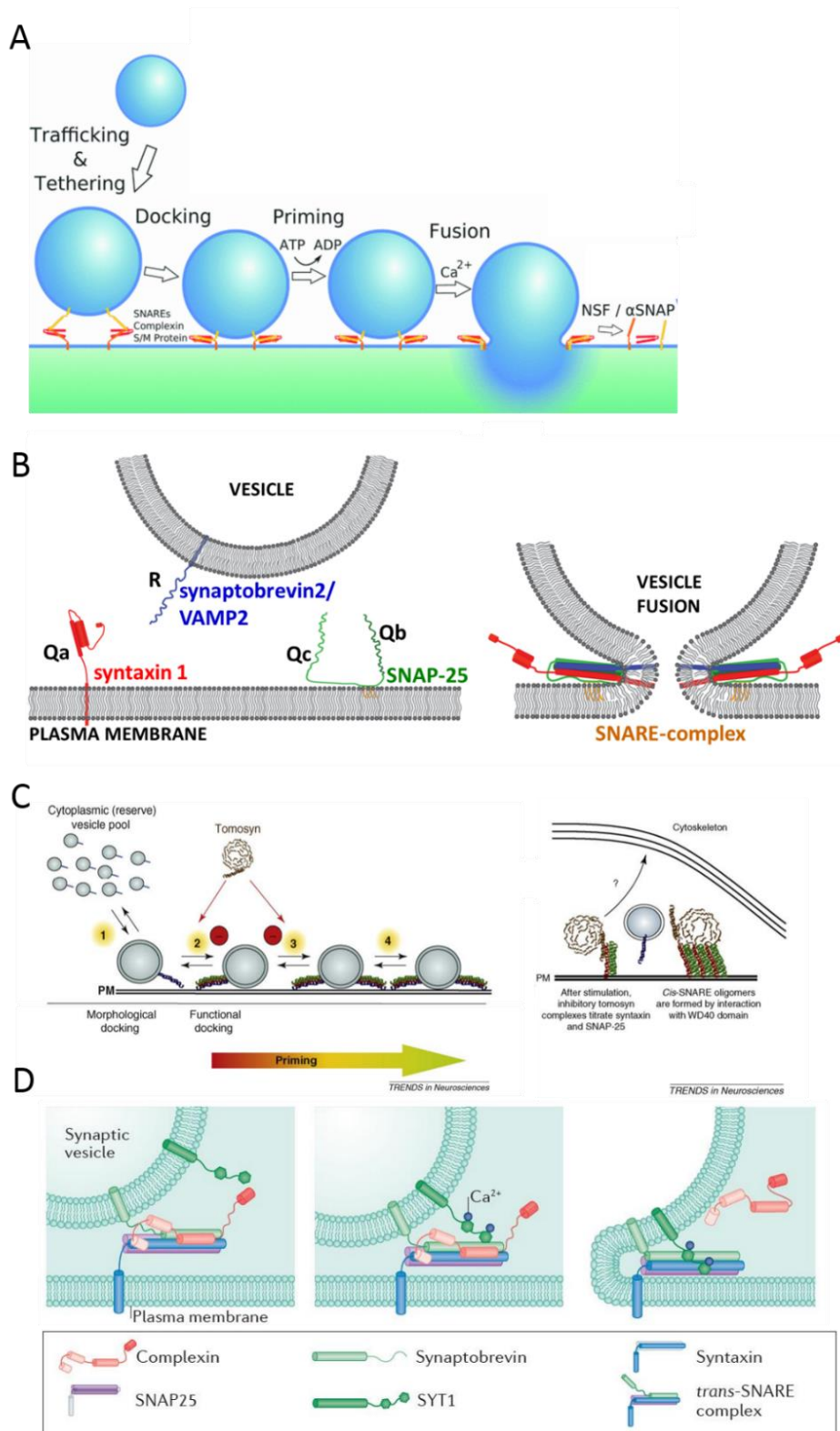


**Figure 3** Details of the exocytic process. (A) A diagram showing the main procedure of exocytosis, including trafficking/recruitment, docking, priming, and fusion. (B) A diagram of the formation of a neuronal SNARE complex. The conjugation of two Q-SNARE proteins (syntaxin-1 and SNAP-25) with R-SNARE assists in the docking and priming of the vesicle

to the plasma membrane. During vesicle fusion, the SNARE complex helps to fix and stabilize the fusion pole. (C) A putative model for the whole inhibitory process of tomosyn after stimulation. After stimulation, syntaxin is phosphorylated, which promotes its interaction with tomosyn. Hence, more tomosyn are recruited to the membrane and form a fusion-inactive SNARE complex with syntaxin and SNAP-25 (left). After fusion, the WD domain of tomosyn enhances the oligomerization of the cis-SNARE complex and reduces vesicle priming (right). (D) A molecular clamp model explains how complexin inhibits spontaneous vesicle release while promoting calcium-evoked vesicle release. In this case, complexin binds to the SNARE complex and prevents spontaneous release. When calcium concentration increases, complexin unbinds the SNARE complex to leave space for synaptotagmin to bind to the SNARE complex and active zone. (Figure created by combining parts of original figures from: Milosevic & Sorensen, 2014; Ashery et al., 2009; Trimbach et al., 2016)

In a neuron, the SNARE complex involved in the SV fusion is called the neuronal SNARE complex (Sollner, Bennett, Whiteheart, Scheller, & Rothman, 1993); this complex consists of three different SNARE proteins, as follows: syntaxin-1, SNAP-25 (synaptosomal-associated protein of 25kDa), and VAMP2 (vesicle-associated membrane protein2)/synaptobrevin (Bennett, Calakos, & Scheller, 1992; Oyler et al., 1989; Trimble, Cowan, & Scheller, 1988). Syntaxin-1 is a Q<sub>a</sub>-SNARE protein, SNAP-25 is a Q<sub>b/c</sub>-SNARE protein, and VAMP2 is an R-SNARE protein. Other than the SNARE motif, syntaxin-1 also contains a C-terminal transmembrane domain that fixes syntaxin to the plasma membrane and an H<sub>abc</sub> domain that can bind with Munc-18, a SNARE complex regulator. Munc-18 belongs to the SM protein family and assists in the formation of the neuronal SNARE complex and acts as a switch for fusion (Wang et al., 2020). SNAP-25 has two SNARE motifs (b and c) (Blasi, Chapman, Link, et al., 1993; Oyler et al., 1989). Unlike syntaxin-1, SNAP-25 does not contain a trans-membrane domain, but has a linker domain that can attach it to the plasma membrane via a palmitoylation interaction. The combination of syntaxin-1 and SNAP-25 forms an acceptor complex that can be associated with VAMP2 in the

following step. Given that both syntaxin-1 and SNAP-25 are distributed on the plasma membrane, they are also identified as target-SNARE or t-SNARE proteins, whereas VAMP2 is classified as a vesicle SNARE or v-SNARE protein because it is located on SVs (Baumert, Maycox, Navone, De Camilli, & Jahn, 1989; Trimble et al., 1988; Veit, Sollner, & Rothman, 1996). Thus, the formation of the neuronal SNARE complex facilitates the docking and fixing of vesicles at the plasma membrane.

Other than Munc-18, the formation of SNARE is regulated by several proteins. Vesicle protein synaptotagmin-1 and 2 act as a trigger for the formation of the SNARE complex (Geppert, Archer, & Sudhof, 1991; Perin, Fried, Mignery, Jahn, & Sudhof, 1990; Zhou et al., 2015). As calcium interactors, synaptotagmin-1 and 2 can bind with  $Ca^{2+}$  and initiate the complex formation process (Bowers & Reist, 2020; Misura, Scheller, & Weis, 2000; Xu, Mashimo, & Sudhof, 2007). Hence, calcium concentration is a key parameter of SNARE-mediated fusion. Similarly to Munc-18, Munc-13 and CAPS can bind with syntaxin-1 and partially open the Munc-18/syntaxin-1 dimer to activate syntaxin-1 (i.e., reverse it from a closed to an open state) (reverse it from a closed to an open state) (Prinslow, Stepien, Pan, Xu, & Rizo, 2019; Wang et al., 2020).

Complexins are another SNARE regulatory protein family. Complexins are small cytosolic proteins without a complex structure that also have a central helix-like SNARE motif (McMahon, Missler, Li, & Sudhof, 1995). This structure allows them to bind with the SNARE complex and regulate vesicle fusion. Interestingly, these proteins have both inhibitory and promoting effects on fusion regulation. They can act as a clamp and inhibit the spontaneous fusion of SVs (Glick & Rothman, 1987); this clamp is released when action potential-induced calcium ions bind to synaptotagmin. Thus, complexin can act as an exocytosis promoter in a high-calcium environment (Thorsten Trimbuch, 2016).

Similar to complexins, tomosyn, which is also known as syntaxin binding protein 5 (STXBP5), contains a VAMP-type R-SNARE motif. Tomosyn can bind with syntaxin and further form the SNARE complex with SNAP-25 (Fujita et al., 1998). The tomosyn-SNP25-syntaxin complex can compete with the VAMP2-SNARE complex

and lead to reduced vesicle release probability and inhibition of vesicle docking and priming (Ashery, Bielopolski, Barak, & Yizhar, 2009). Experimental evidence has shown that downregulation of tomosyn promotes synaptic transmission in the mammalian hippocampus, but inhibits insulin secretion in beta cells (Ben-Simon et al., 2015; Ferdaoussi et al., 2017).

After vesicle fusion and NT release, the SNARE complex fully presents in the plasma membrane due to the fusion. The residue of the SNARE complex after fusion is called the cis-SNARE complex. Then, the complex disassembles with the help of an adaptor protein, called alpha-SNAP, and a hexameric ATPase, called NSF (Clary, Griff, & Rothman, 1990; Littleton et al., 2001). Finally, SNAREs and other proteins are retrieved from the plasma membrane and get ready for the next round of exocytosis.

#### **1.4 Amisyn and its links to exocytosis**

Amisyn, also known as syntaxin binding protein 6 (STXBP6), is a 24 kDa protein that was first reported in 2002 by Scales (Scales, Hesser, Masuda, & Scheller, 2002). Cytogenetically, the amisyn gene is located at chromosome 14 position 14q11.2 (Castermans et al., 2008). It was identified when a search based on the homology with the expression sequence of tomosyn's SNARE domain was performed. Like tomosyn, amisyn has a SNARE C-terminal domain, which forms a spiral coil and allows amisyn to form a SNARE complex with syntaxin-1 and SNAP-25 (Scales et al., 2002). Amisyn's SNARE domain binds to syntaxin-1's and SNAP-25' SNARE domains and can largely enhance the stability of the amisyn-syntaxin complex. Circular dichroism analysis has shown that the amisyn-SNARE complex has higher thermostability than the VAMP2-SNARE complex. As well as a SNARE domain, amisyn also contains an N-terminal domain, the detailed function of which has remained unclear until the study showed in the chapter 3.1 (Kondratiuk et al., 2020). In general, this N-terminal domain is a pleckstrin homology (PH) domain that can transiently associate with phosphatidylinositol 4,5-bisphosphate (PI(4,5)P<sub>2</sub>) lipids on the plasma membrane. A detailed analysis and explanation are shown in the chapter 3.1. The lack of any transmembrane anchor on amisyn makes it a cytosolic protein rather than a membrane

or SV protein. In addition to syntaxin-1 and PI(4,5)P<sub>2</sub>, amisyn also interacts with syntaxin-4. (Scales et al., 2002). Other interactions of amisyn with proteins/lipids warrants additional research.

Similar to tomosyn, amisyn is a brain-enriched protein. Its transcription mainly occurs in the cortex and hippocampus, especially in the dentate gyrus, according to data presented in the Allen Brain Atlas (<https://portal.brain-map.org/>). Amisyn is also found in organs other than the brain, including the heart, kidney, liver, and adrenal gland, as well as in COS, Hela, and beta-insulin cell lines (Collins et al., 2016; Scales et al., 2002).

Given that amisyn can form the SNARE complex in much the same way as tomosyn, it is involved in the regulation of exocytosis. Similarly to tomosyn, the amisyn-SNARE complex may compete with the VAMP2-SNARE complex and inhibit the secretion process. The external SNARE motif of amisyn can inhibit the exocytosis of norepinephrine in cracked PC12 cells (Scales et al., 2002). Further experiments have shown that amisyn overexpression in PC12 cells inhibits both basal and stimulated exocytosis. However, mutation on the SNARE motif can eliminate such inhibitory effects (Constable, Graham, Morgan, & Burgoyne, 2005).

Immunofluorescence experiments have suggested that amisyn overexpression has no effect on NT loading. Amperometry recordings in amisyn-expressing chromaffin cells have confirmed the inhibitory effect of amisyn on secretion (Constable et al., 2005). The results have shown that a significant number of cells expressing amisyn failed to respond to calcium stimulation. Furthermore, the number of spikes detected per cell was found to be significantly reduced in amisyn-expressing cells. Interestingly, amisyn with a mutation on the SNARE motif has a similar inhibitory effect to wild type (WT) amisyn. As well as a reduction in spike number, amisyn causes an increase in the spike foot charge and duration, which indicates that amisyn may play a role in vesicle fusion (Constable et al., 2005).

Amisyn is involved not only in neurosecretion but also in insulin secretion. Recent research on beta cells has revealed that amisyn can be recruited to the exocytosis site in beta cells by cAMP-sensor Epac2 (Gucek et al., 2019). In a beta cell, amisyn helps

to close the pore and restrict insulin release, which could explain the high expression level of amisyn in some patients with type 2 diabetes mellitus (Barg & Gucek, 2016; Collins et al., 2016).

Amisyn is also linked with other diseases, such as cancer and autism (Castermans et al., 2008). Ultrastructural analysis of blood platelets of patients with autism spectrum disorder complicated with haploinsufficiency of the amisyn genes demonstrated the morphological abnormalities of dense-core granules (Castermans et al., 2010). Differential expression of amisyn can be used as an indicator of lung adenocarcinoma (Lenka et al., 2017; Y. Liu et al., 2021).

So far, no effective animal model for amisyn has been established, except the newly released CRISPR knockout (KO) mouse model introduced by Liu et al in 2021 (C. Liu et al., 2021). No behavioral impairment has yet been reported in this mouse model. Moreover, these animals reportedly gained less weight than WT animals. Remarkably, only the SNARE motif of amisyn is knocked out in this mouse model, whereas the N-terminal is fully expressed in KO mice. Furthermore, Liu and colleagues only performed some behavioral assays (T maze, open field, and Morris water maze tests) and a gene analysis with this mouse model, which means that some phenotypes of these KO mice may not have been observed in their experiments.

In conclusion, prior to the experiments presented in this thesis, only the SNARE domain of the amisyn structure had been partially studied. Although studies have reported on amisyn for 20 years, only its potential inhibitory effect in exocytosis is known.



isolated from the entire membrane. With further manipulation, the current flow through the pipette can be monitored using a microelectrode inside the pipette (Sakmann & Neher, 1984).

The patch clamp can be classified into different modes, that are distinguished by different patching configurations. Among these configurations, field recording and whole-cell configuration are the most commonly used.

Technically, field recording is not a patch clamp technique because the recording pipette does not form a “patch” on the cell membrane. In the field recording configuration, the recording pipette is directly placed in the tissue nearby the plasma membrane. Thus, extracellular electrical parameters can be collected via detecting electrodes. Usually, changes in extracellular current/voltage are very small; therefore, field recording requires a high-power amplification of signals.

Figure 5 shows the whole-cell configuration patch clamp procedure. For an accurate measurement, the patching area should be kept in a closed stable electrical environment with no leak current passing by. This requires a perfect seal between the pipette and the cell membrane. The sealing level of the patching can be described by the resistance of the pipette tip, whereby a higher resistance suggests a better seal. If the pipette tip is simply placed onto the cell membrane, it can only achieve a seal resistance of 10–100 M $\Omega$ . By applying a slight suction onto the membrane via the pipette, the patched area of the membrane is sucked into the pipette with a “ $\Omega$ ” formation. With such manipulation, the seal resistance may reach an order of 10–100 G $\Omega$ . An even stronger suction is required to rupture the patched membrane for the whole-cell configuration. Usually, a good seal after rupture refers to a seal resistance of around 1 G $\Omega$ , which ensures quality of measurements. After the membrane has been broken, the solution inside the pipette can flow into the cell as the intercellular solution, and the current through the cell membrane can be detected (Segev, Garcia-Oscos, & Kourrich, 2016).

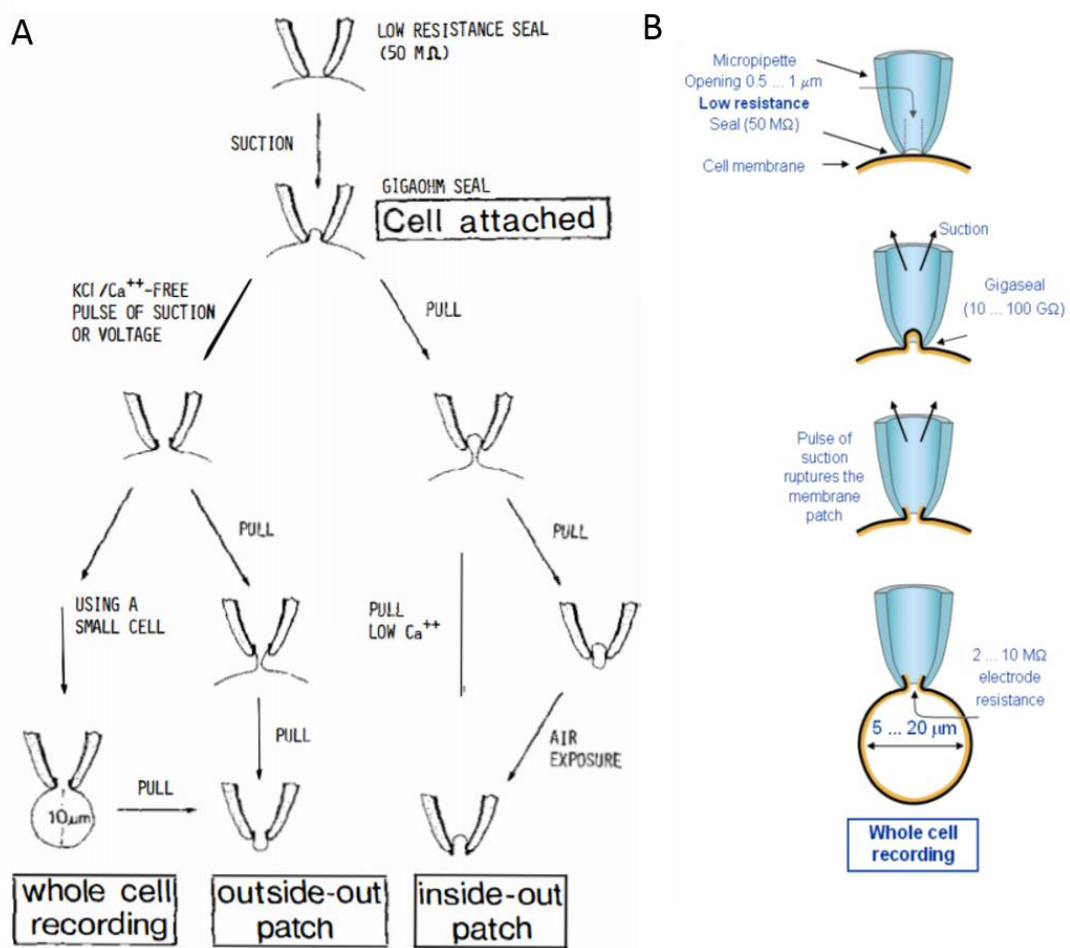


**Figure 5** Patch clamp procedures. (A) A diagram of the procedures of three different patch clamp configurations: whole-cell, outside-out, and inside-out. (B) Detailed procedure required for the whole-cell patch clamp configuration (Figure from Sakmann & Neher, 1984; Malmivou, 2017).

Two main recording modes can be achieved using the patch clamp – the voltage-clamp and current-clamp mode. In the voltage-clamp mode, the membrane potential is kept at a constant preset value while recording the current flow through the membrane. Figure 6 shows a circuit sketch of the voltage-clamp mode. The circuit includes a negative feedback amplifier that compares the detected membrane voltage with the preset voltage to adjust the membrane potential by injecting current. The circuit is grounded via an electrode soaked in the extracellular bath solution.

In the current clamp, the membrane current is kept constant while measuring the change in membrane potential by monitoring the injected electric quantity. A

voltmeter replaces the feedback amplifier in the current clamp circuit.

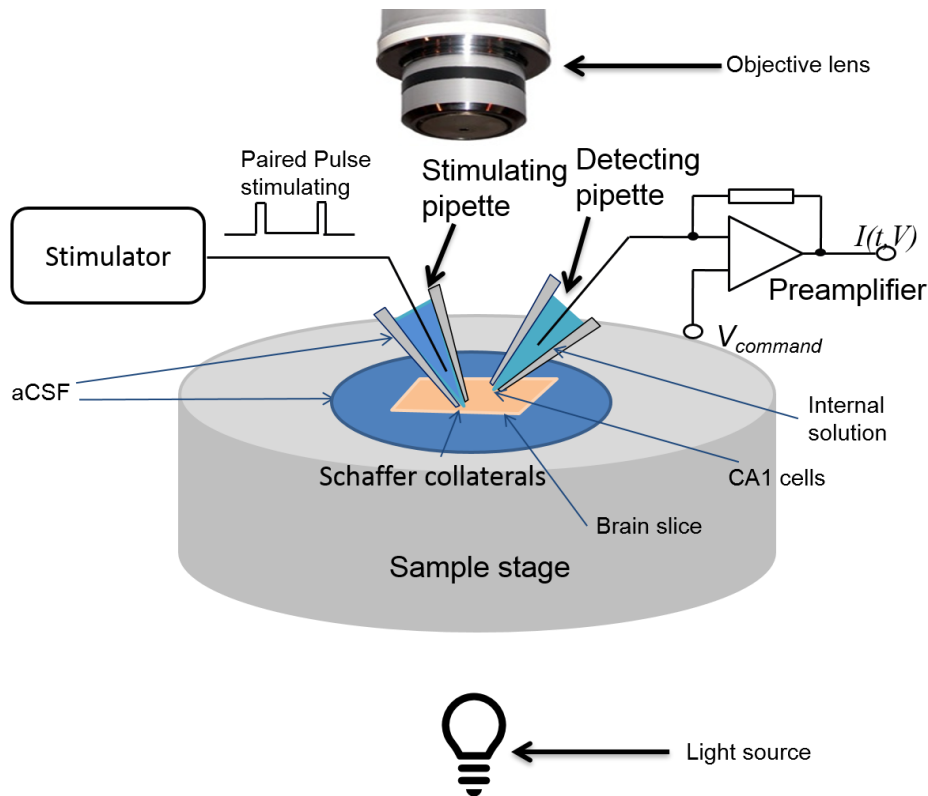


**Figure 6** A diagram of a whole-cell voltage-clamp setup for a brain slice pair-pulse excitatory postsynaptic current recording. The brain slice is placed on the sample stage of the microscope. Two pipettes are attached to the slice, as follows: the left one is the stimulation pipette, which delivers voltage/current stimulation to the neurons, and the right one is the recording pipette, which is attached to the target neuron in a whole-cell configuration. The circuit of the voltage clamp is shown beside the pipette.

As discussed in the previous section, information in the nervous system is often propagated as electrical signals. Hence, the patch clamp allows direct measurement of detailed electrophysiological processes. For instance, a patch clamp can measure current flow at a very small area of the membrane that only includes a signal ion channel. This allows the properties of individual ion channels and other ion-channel-related issues to be investigated (Sigworth & Neher, 1980). In living tissues, the patch clamp technique can be used to investigate the electrical properties of a substantial part of the neuron, and contributes to our understanding of passive and

active biophysical properties of excitable cells. Whole-cell recordings can be applied to neurons in several different types of preparations, including cultured neurons, dissociated neurons, brain slices, and even awake animals (Ince et al., 1986; Segev et al., 2016; Yoshimura, Furue, Ito, & Nakatsuka, 2002).

### **1.6 Aim of the study**

Exocytosis is a crucial process in neurotransmission, and several regulators of exocytosis have been identified and characterized in detail. The key steps in exocytosis are vesicle recruitment, docking, priming, and fusion, which have been studied for several decades. However, the regulators of exocytosis, especially negative regulators and their mechanisms, are unclear. The SNARE complex, as an important participant of exocytosis, is involved in the docking, priming, and fusion of vesicles. As discussed in the previous sections, the neuronal SNARE complex consists of three individual SNARE proteins – syntaxin-1, SNAP-25, and VAMP2. However, there are other proteins that contain the SNARE motif besides these three proteins. Proteins with the SNARE motif can interact with the neuronal SNARE complex and regulate exocytosis via such interactions. Tomosyn, as a well-known negative exocytosis regulator belonging to this subfamily, binds with syntaxin-1 and competes with VAMP2. Different experiments in both *in vitro* cell lines and *in vivo* animal models have characterized the regulatory mechanism and physiological properties of tomosyn.

As a SNARE protein from the same subfamily, amisyn also has a VAMP2-like SNARE motif, and can form a SNARE complex with syntaxin-1 and SNAP-25. However, compared to its “family member”, amisyn has received limited attention in previous studies, and the structure and function of its N-terminal remain unclear. Moreover, until 2021, no animal model for amisyn research had been established. Considering the enrichment of amisyn in the brain, especially in the hippocampus, it may play an essential role in neurotransmission and memory formation. It is therefore essential to create a representative mammalian model to investigate the effects of amisyn on brain function, and at several levels.

In the first part of this research, we focused on studying the detailed mechanism of the formation of the amisyn-syntaxin-SNAP-25 complex and the function of the N-terminal domain of amisyn. According to sequence analysis, 32% of the amisyn protein sequence is similar to the Sec3-like protein sequence, which contains a PH domain. Thus, we attempted to characterize the lipid-binding ability and N-terminal domain of amisyn, and then tested whether amisyn can still form the SNARE complex if it loses its SNARE or N-terminal domain. Finally, we evaluated whether the secretory inhibitory ability of amisyn is affected when amisyn is incomplete or mutated.

In the second part of this research, we focused on the characterization of the physiological function of amisyn in a newly established amisyn mutant mouse line. This mouse line, called STXBP6<sup>tm1a</sup>, can reduce amisyn expression in the hippocampus by 90%. Using this mouse line, we studied several important issues, as follows: (1) I began by characterizing the biochemical properties of the amisyn protein and its mutants, and determined whether amisyn interacts directly with other syntaxin proteins besides syntaxin-1 and whether amisyn may be a competitor of the SNARE protein tomosyn in exocytosis; (2) I performed electrophysiology-based and behavioral assays to characterize neurotransmission in hippocampal neurons that lack amisyn. Amisyn has been reported to be enriched in the hippocampus; thus, I used a whole-cell patch clamp to characterize miniature excitatory postsynaptic currents (mEPSCs) and evoked EPSCs of the neurons in the CA1 and CA3 regions. Furthermore, the release probability and synaptic plasticity were examined; (3) Next, I employed proteomics-based methods (e.g., western blotting) to investigate the levels and distribution of various neuronal proteins in amisyn mutant brains.

These results enhance our understanding of the relationship between amisyn and other synaptic/neuronal proteins. During this research, I used animals of different ages for different experiments. For behavioral experiments, I used animals older than 3 months to avoid anxiety in the mice. For long-term synaptic potentiation (LTP) recordings, I used P11-15 mice to achieve a more stable baseline. For CA3 region electrophysiology experiments, I used P18-P25 mice to achieve a good slice quality

while avoiding the influence of neurodevelopment.

Altogether, my Ph.D. thesis work contributes to the detailed understanding of amisyn, a protein that is fundamental to our knowledge of neuronal cell physiology. This work may also help unravel the complex pathological processes that occur in diabetes and autism.

## 2 Materials and Supplementary Method

### 2.1 Chemicals and reagents

The Chemicals used in this study are listed below in Table 1.

Table 1 - List of chemicals, their supplier, and catalog number used in this thesis

<b>Chemical</b>	<b>Supplier</b>	<b>Catalog</b>
2-Mercaptoethanol	Carl Roth	422.3
4',6-Diamidino-2-phenylindole (DAPI)	Carl Roth	6335.1
Acetic acid (CH <sub>3</sub> COOH)	Carl Roth	X895.2
Acrylamide	Carl Roth	3029.2
Agarose	Biozym	840004
Ammonium chloride (NH <sub>4</sub> Cl)	Carl Roth	K298.1
Ammonium Persulfate (APS)	AMRESCO	486
Ampicillin sodium salt	Carl Roth	K029.1
Bicuculline	Sigma-Aldrich	14340
Bovine serum albumin (BSA)	Carl Roth	CP84.2
Bromophenol blue	Carl Roth	T116.1
Calcium chloride (CaCl <sub>2</sub> )	Carl Roth	CN93.1
Cesium methanesulfonate (CsMeSO <sub>4</sub> )	Sigma-Aldrich	C1426
Cholera Toxin Subunit B (Recombinant), Alexa Fluor™ 594 Conjugate	Thermo Fisher	C22842
Chloramphenicol	Sigma-Aldrich	C0378-5G
Complete ULTRA Tablets, EDTA-free, Protease Inhibitor Cocktail	Sigma-Aldrich	5892953001
CNQX	Tocris	0190
Creatinephosphokinease	Sigma-Aldrich	C3755
DAPI	Carl Roth	6335.1
D-APV	Tocris	0106
Dimethyl sulfoxide (DMSO)	Sigma-Aldrich	41639
Dithiothreitol (DTT)	Carl Roth	6908.1
DMEM powder	Gibco® (Life Technologies)	52100-021
DMEM, high glucose, pyruvate	Thermo Fisher	41966-052
DNase	Sigma-Aldrich	D4227
Ethanol absolute	VWR	20,816,298
Ethidium bromide	VWR	E406
Ethylenediaminetetraacetic acid (EDTA)	Carl Roth	8043.2
Fetal Bovine Serum, qualified, heat inactivated	Thermo Fisher	10500064
Fura-4F	Invitrogen	F14174
Furaptra	Invitrogen	M1290
Gelatin from cold water fish	Sigma-Aldrich	G7765

Glucose	Sigma-Aldrich	G8270
Glutamax	Gibco® (Life Technologies)	35050-061
Glutaraldehyde	ApplieChem	A3166.0100
Glycerol	Carl Roth	7530.1
Glycine	Carl Roth	3908.3
Goat Serum	Life Technologies	10000C
Halt™ Protease & Phosphatase single use Inhibitor Cocktail (100X)	Thermo Fisher	78442
HEPES	Carl Roth	HN77.2
IPTG	Carl Roth	2316.3
Insulin-selenium-transferrin(ITS-100X)	Gibco® (Life Technologies)	51500-056
L-Cysteine	Sigma-Aldrich	C7352
Lipofectamine 2000 Reagent	ThermoFisher Scientific	11668-019
Luminata™ Forte Western HRP Substrate	Millipore	WBLUF0500
Lysozyme	Sigma Aldrich	10837059001
Magnesium chloride (MgCl <sub>2</sub> )	VWR	8.14733.0100
mCLING-Atto 647	Synaptic System	710 006AT1
Methanol	VWR	20903.368
Methyl nadic anhydride (MNA)	Sigma Aldrich	45347
Mg-Adenosine triphosphate (ATP)	Sigma-Aldrich	A9187
Mowiol 4-88	AppliChem	A9011
Na-GTP	Sigma-Aldrich	G8877
NBD	ThermoFischer Scientific	S1167
Opti-MEM	Gibco® (Life Technologies)	31985070
Oregon Green™ 488	ThermoFischer	O-10241
Osmium Tetroxide	Sigma Aldrich	O5500
PageRuler Plus Prestained Protein Ladder	Thermo Scientific	26619
Papain	Worthington Biochemical	LS003127
Paraformaldehyde (PFA)	BioChemica	A3813
Penicillin/ Streptomycin	Life Technologies	15140122
Phosphocreatine kinase	Roche	10 127 566001
PhosStop tablets	Sigma-Aldrich	4906837001
PMSF	Carl Roth	6367.2
Poly-L-Lysine	Sigma-Aldrich	P-8920
Potassium chloride (KCl)	Volu-Sol	83608.26

Potassium dihydrogen phosphate (KH <sub>2</sub> PO <sub>4</sub> )	Carl Roth	3904.1
Potassium phosphate dibasic (K <sub>2</sub> HPO <sub>4</sub> )	Carl Roth	P749.2
Proteinase K	Roche	3115879001
PreScission Protease	GE Healthcare Life	27084301
QX-314	Sigma-Aldrich	21306-56-9
Rhodamine	ThermoFischer Scientific	R302
Skim Milk Powder	Fluka	70166
Sodium bicarbonate (NaHCO <sub>3</sub> )	Sigma-Aldrich	71631
Sodium cacodylate	Carl Roth	5169.1
Sodium chloride (NaCl)	AppliChem	A1430,0010
Sodium creatine phosphate hydrate	TCI chemical	C0397
Sodium deoxycholate	Sigma-Aldrich	30970
Sodium dodecyl sulfate (SDS)	Sigma-Aldrich	L4509-500G
Sodium hydroxide pellets (NaOH)	Carl Roth	6771.1
Tetramethylethylenediamine (TEMED)	Sigma-Aldrich	T7024
Tetraethylammonium chloride (TEA-Cl)	Fluka	86616
Tetrodotoxin (TTX)	Tocris	T-550
TMA-DPH	Invitrogen	T204
Tranferrin Alexa 546	ThermoFischer Scientific	T133443
Tris(hydroxymethyl)aminomethane (Tris)-Base	Sigma-Aldrich	T1503
Tris(hydroxymethyl)aminomethane (Tris)-HCl	Carl Roth	9090.2
Triton X-100	Carl Roth	3051.3
Trypsin-EDTA (0.05%), phenol red	Gibco® (Life Technologies)	11580626
Tween-20	AMRESCO	777
Vitamin C	Sigma-Aldrich	A5960
Yeast extract powder	Chemsolute	LP0021B

## 2.2 Solutions

The various buffers and solutions used in the study are listed in Table 2.

Table 2 - List of buffers and solutions used in this study

Solution	Recipe
4% paraformaldehyde (PFA)	4% PFA in PBS, pH 7.4; heat PBS to 58° C, add sodium hydroxide drop wise until PFA dissolves
5% milk	5% skim milk powder in TBS-T
Artificial cerebrospinal fluid (aCSF)	125mM NaCl, 26mM NaHCO <sub>3</sub> , 2.5mM KCl, 1.25mM NaH <sub>2</sub> PO <sub>4</sub> , 1mM MgCl <sub>2</sub> , 2mM CaCl <sub>2</sub> , and 25mM glucose, pH 7.4, osmolarity ~305 mOsm/L
Elution buffer	100mM NaCl, 50mM Tris, 15mM Reduced GSH,

	pH 7.8
Internal solution (mini)	130mM CsMeSO <sub>4</sub> , 5mM TEA-Cl, 5mM NaCl, 10mM HEPES, 4mM MgCl <sub>2</sub> , 0.1mM EGTA, 10mM Na-creatinephosphate, 4 ATP and 0.4 GTP, pH 7.35, osmolarity ~300 mOsm/L
Internal solution (EPSC)	130mM CsMeSO <sub>4</sub> , 2.67mM CsCl, 10mM Hepes, 1mM EGTA, 3mM QX-314-Cl, 5mM TEA-Cl, 15mM Creatinephosphate disodium, 4mM Mg-ATP, 0.3mM Na-GTP, 5mM Creatinephosphokinease, pH7.4, osmolarity~ 305mM
Bacteria lysis buffer	150mM NaCl, 50mM HEPES, 2mM EDTA, 2mM DTT, pH 7.4
Mowiol-488® mounting medium	3.6 M glycerol, 3 M Mowiol 4-88, 133 mM Tris-Base in dH <sub>2</sub> O. Stir for several hours at 45°C, centrifuge at 5000 g for 15 min, collect supernatant, store at -20°C
PC-12 cell culture medium	DMEM (high-glucose + L-Glutamate) + 10% Fetal Bovine Serum + 6% Penicillin-Streptomycin + 2% Glutamax
PC-12 lysis buffer	1.5% DDM, 1% cocktail inhibitors in PBS
Phosphate buffered saline (PBS)	137 mM NaCl, 2.7 mM KCl, 10 mM Na <sub>2</sub> HPO <sub>4</sub> x 2H <sub>2</sub> O, 2 mM KH <sub>2</sub> PO <sub>4</sub> in dH <sub>2</sub> O, p.H. 7.4, autoclave
PBS-T	1% Tween-20 in PBS
PreScission Protease Cleavage Buffer	150mM NaCl, 50mM Tris, 1mM EDTA, 1mM DTT, pH 7.0
Running Buffer	125 mM Tris Base, 0.96 M Glycine, 0.5% SDS
SDS loading buffer	62.5 mM Tris, pH 6.8, 50% (v/v) Glycerol, 12% (w/v), SDS, 0.06% (w/v) Bromophenol blue, (5% 2-Mercaptoetanol added before use)
SNET buffer	20 mM Tris (pH 8.0), 5 mM EDTA (pH 8.0), 400 mM NaCl, 0.5 % (w/v) SDS in dH <sub>2</sub> O
Sucrose cutting solution	26 NaHCO <sub>3</sub> , 1.25 NaH <sub>2</sub> PO <sub>4</sub> , 4 KCl, 10 glucose, 230 sucrose, 0.5 CaCl <sub>2</sub> , and 10 MgSO <sub>4</sub>
TAE buffer	40 mM Tris, 19 mM CH <sub>3</sub> COOH, 1 mM EDTA, in dH <sub>2</sub> O, pH 8.0
TBS-T	1% Tween-20 in TBS
Transfer Buffer	25 mM Tris-Base, 0.2 M Glycine, 20% (v/v) Methanol in dH <sub>2</sub> O
Tris buffered saline (TBS)	20 mM Tris-Base, 150 mM NaCl in dH <sub>2</sub> O, pH 7.6

## 2.3 Antibodies

All antibodies used for immunocytochemistry and western blot analysis are listed in

Table 3.

Table 3- Antibodies used in experiments presented in this thesis

<b>Antibody</b>	<b>Source &amp; identifier</b>	<b>Species</b>	<b>Concentration</b>
$\alpha$ -synuclein	Synaptic system 128002	Rabbit	1:1000 in 5% milk
$\beta$ -actin	Millipore C4	Rabbit	1:1000 in 5% milk
amisyn	Custom-made Aminchen 172	Rabbit	1:500 in TBS-T
amisyn	Sigma-Aldrich HPA003552	Rabbit	1:500 in 5% milk
CaV $\alpha$ 2 $\delta$ 4	Alomone Labs ACC-104	Rabbit	1:200 in 1% BSA
CDK5	Santa Cruz sc-173	Rabbit	1:200 in 5% milk
CREB	Cell signaling 9197	Rabbit	1:1000 in 5% milk
Donkey Anti-Goat IR800	Li-Cor 926-32214	Goat	1:7000 in 5% milk
EEA1	Synaptic system 237002	Rabbit	1:1000 in 5% milk
Endophilin A1	Santa Cruz sc-247945	Goat	1:2000 in 5% milk
ERK1/2	Cell signaling 9102	Rabbit	1:1000 in 5% milk
GAPDH	Sigma-Aldrich G9545	Rabbit	1:1000 in 5% milk
GluA2	Millipore MAB397	Mouse	1:1000 in 5% milk
GST	Millipore ABN116	Rabbit	1:10000 in 5% milk
Goat Anti-Rabbit IR 680	Li-Cor 926-68021	Rabbit	1:7000 in 5% milk
Goat Anti-Mouse IR 800	Li-Cor 926-32210	Mouse	1:7000 in 5% milk
Homer1	Synaptic system 160003	Rabbit	1:1000 in 5% milk
HPRT	Abcam Ab97698	Rabbit	1:2000 in 5% milk
Munc18	Synaptic system 116002	Rabbit	1:1000 in 5% milk
Na <sup>+</sup> /K <sup>+</sup> ATPase	Synaptic system 130930	Rabbit	1:1000 in 5% milk
P-ERK1/2	Cell signaling 9101	Rabbit	1:1000 in 5% milk
P-CREB	Cell signaling 9198	Rabbit	1:1000 in 5% milk
PSD-95	Synaptic system 124011	Mouse	1:1000 in 5% milk
Rab3a	Synaptic system 107102	Rabbit	1:5000 in 5% milk
Rab3a/b	Synaptic system 107011	Mouse	1:1000 in 5% milk
Rab7a	NovusBio NBP1-05048	Rabbit	1:1000 in 5% milk
Rabphilin3	Synaptic system 118002	Rabbit	1:1000 in 5% milk
RIM1	Synaptic system 140003	Rabbit	1:1000 in 5% milk
RPL7	Abcam ab72550	Rabbit	1:6000 in 3% BSA
SNAP-25	Synaptic system 116002	Rabbit	1:1000 in 5% milk

SNAP47	Synaptic system 110162	Rabbit	1:1000 in 5% milk
Synapsin 1/2	Synaptic system 106002	Rabbit	1:1000 in 5% milk
Synaptotagmin1	Synaptic system 105011	Mouse	1:1000 in 5% milk
Synaptophysin1	Synaptic system 101011	Mouse	1:5000 in 5% milk
Syntaxin1A	Synaptic system 110302	Rabbit	1:1000 in 5% milk
Syntaxin16	Synaptic system 110162	Rabbit	1:1000 in 5% milk
VAMP2	Synaptic system 104211	Mouse	1:1000 in 5% milk

## 2.4 Consumables and kits

The kits and consumables used are listed in Table 4.

Table 4 - Kits and consumable products used in experiments presented in this thesis

<b>Product</b>	<b>Supplier</b>	<b>Catalog number</b>
Amicon Ultra-1PLHK Ultracel-PL100kDa (15ml)	EMD Millipore™	UFC910096
12-well TC plate	CytoOne	CC7682-7512
96-well TC plate	CytoOne	CC7682-7596
Borosilicate glass with filament	Science Product	GB150-TF-8P
Cell scraper	StarLab	CC7600-0202
Coverslips 18 mm (1.5H thickness)	Mariefeld	17580
Cryogenic vial 2 mL	Fisher Brand	1050026
Cuvettes polystyrol/polystyrene	Sarstedt	67-742
Eppendorf tubes (1.5 mL)	StarLab	E1415-1500
Eppendorf tubes (2 mL)	StarLab	S1620-2700
G-coupled magnetic beads	Invitrogen	10007D
GFP-Trap®_A	Chromtek	gta-10
GoTaq Flexi DNA polymerase kit	Promega	M8291
iTaq™ Universal SYBR Green Supermix	Bio-Rad	172-5124
Microscope slides	Carl Carl Roth	2111
Needles 24G	B.Braun	465 7675
Needles 27G	B.Braun	465 7705
Nitrocellulose membrane	BIO-Rad	1620115
PageRuler Plus Prestained Protein Ladder	Thermo Scientific	26619
Pasteur pipet plastic	Carl Carl Roth	EA63.1
PCR plate 384-well skirted ABI-Type (Universal)	StarLab	E1042-3840
Petri dish 10 cm	Sarstedt	82.1473.001
Petri dish 2 cm	Sarstedt	82.1135.500
Pierce BCA Protein Assay Kit	Thermo Scientific	23225
QuickChange II XL Site-Directed 30rx Kit	Agilent Stratagene	200522-5

Razor blade from the supermarket	-	-
Super Frost slide	Th. Geyer	769 5019
Syringe 1 ml	VWR	613-2040
Syringe 50 ml	VWR	613-2053
Tips 10 µL TipOne	StarLab	S111-3210
Tips 1000 µL TipOne	StarLab	S1111-6001
Tips 200 µL TipOne	StarLab	S1120-8800
Tubes 15 mL	Sarstedt	62.554.502
Tubes 50 mL	Corning	430829
Whatman Western Blot Paper	Th. Geyer	4-01-60-0041

## 2.5 Plasmids

The list of plasmids used in the study is in Table 5. Plasmids were used to express the mentioned protein in experiments.

Table 5 - Plasmids used in experiments presented in this thesis

Plasmid name	Vector	Protein	Fluorescence marker
pEGFP-amisyn-N1	pEGFP	Amisyn	EGFP
PEGFP-amisyn-SNARE-motif-N1	PEGFP	Amisyn SNARE domain	EGFP
pGEX-6p1-amisyn	pGEX_6p1	Amisyn(SV)	-
pGEX-6p1-amisyn-PHMutant	pGEX_6p1	Amisyn(SV)-K30A, K32A, K60D, K62D	-
pGEX-6p1-amisyn-GFP-N1	pGEX_6p1	Amisyn	GFP
pGEX-6p1-amisyn-SNARE-motif-N1	pGEX-6p1	Amisyn SNARE domain	-

## 2.6 Primers

Primers used for genotyping and quantitative PCR are listed below in Table 6 and 7.

Table 6 – Primers used for genotyping samples

Primer	Sequence
CSD-F	TGCTCAAGGTGGAATGATTGTCC
CSD-ttR	CAAGTGCACAATTACAGCTCTCAGG
CSD-loxF	GAGATGGCGCAACGCAATTAATG
CSD-R	ATGTGTAAGCACAAAAGGAAATGGG

Table 7-Primers used for qPCR

Protein	Gene	Primer
mAmisyn	STXBP6	F AGCACGGCCTCAGAAAAGTG

		R	AGGATGCTGTTTCCTCCCATA
mPSD95	DGL4	F	TGAGATCAGTCATAGCAGCTACT
		R	CTTCCTCCCCTAGCAGGTCC
mRPL7	RPL7	F	CTGCTGGGCCAAAACTCTCA
		R	CCTTCAACTCTGCGAAATTCCTT
mCAMK4	CAMK4	F	CTCTCACACCCGAACATCATAAA
		R	CTCACTGTAGTATCCCTTCTCCA
mCAMK2B	CAMK2B	F	CGTTTCACCGACGAGTACCAG
		R	GCGTACAATGTTGGAATGCTTC
mCREB	CREB1	F	CAGTGGGCAGTACATTGCCAT
		R	CTGCTGTCCATCAGTGGTCTG
mPKC	PRKCA	F	GTTTACCCGGCCAACGACT
		R	GGGCGATGAATTTGTGGTCTT
mPKA	PRKACA	F	AGATCGTCCTGACCTTTGAGT
		R	GGCAAACCGAAGTCTGTCAC
mCDK5	CDK5	F	CCCTGAGATTGTGAAGTCATTCC
		R	CCAATTTCAACTCCCCATTCCT
mRhoA	RHOA	F	AGCTTGTGGTAAGACATGCTTG
		R	GTGTCCATAAAGCCAACTCTAC
mSTX1a	STX1A	F	CCCACAAGGAGATACATTCCCA
		R	AACGAAATCCAAAACGGCAGT
mTomosyn	STXBP5	F	CCAGAGCCATGCAAGCCTATC
		R	CAGAGTGTGAGAAAGTCAACGAT
mComplexin2	CPLX2	F	AAGAGCGCAAGGCGAAACA
		R	TGGCAGATATTTGAGCACTGTG
mSTX2	STX2	F	TGTGGAGAAGGATCATTTTCATGG
		R	TGCTCAATAGACTTCAGCTTGC
mSTX4	STX4	F	CCCGGACGACGAGTTCTTC
		R	TTTGATCTCCTCTCGCAGGTT
mSNAP-25	SNP25	F	CAACTGGAACGCATTGAGGAA
		R	GGCCACTACTCCATCCTGATTAT
mMunc13-1	UNC13A	F	CATCCTCCTGGACGCTCATTT
		R	TTCTCCCCAGCCAAAGTAATTC
mMunc18	STXBP1	F	GTGGACCAGTTAAGCATGAGG
		R	GCTCTCGGCGCTTGTTGAT
mSV2A	SV2A	F	GGCTTTCGAGACCGAGCAG
		R	GACCTTCGGGAATACTCATCCT
m $\alpha$ -Synuclein	SNCA	F	GCAAGGGTGAGGAGGGGTA
		R	CCTCTGAAGGCATTTTCATAAGCC
mRab3a	RAB3A	F	TCTTCCGCTACGCAGATGACT
		R	TGTCGTTGCGGTAGATGGTTT
mSyn1	SYN1	F	CCAATCTGCCGAATGGGTACA
		R	GCGTTAGACAGCGACGAGAA

mITSN1	ITSN1	F	CACCAGCATTTGGTATAGGAGG
		R	GGACAGAAGATACTAAGGGTGGA
mDynamin1	DNM1	F	AATATGCCGAGTTCCTGCACT
		R	GTCTCAGCCTCGATCTCCAG
mBassoon	BSN	F	GGGCAGCCAGAGAACAACCTT
		R	GGGACAGAGTAGGGTGACG
mDBH	DBH	F	GAGGCGGCTTCCATGTACG
		R	TCCAGGGGGATGTGGTAGG
mVAMP2	VAMP2	F	GCTGGATGACCGTGCAGAT
		R	GATGGCGCAGATCACTCCC
mSyt1	SYT1	F	CTGTCACCACTGTTGCGAC
		R	GGCAATGGGATTTTATGCAGTTC
mSTX6	STX6	F	ACAGGCCGTCATGCTAGATG
		R	GGATGGCTATGGCACACCAC
mHomer1	HOMER1	F	CCCTCTCTCATGCTAGTTCAGC
		R	GCACAGCGTTTGCTTGACTION
mRab7	RAB7A	F	CCTGGGGGACTCTGGTGTG
		R	TGTCGTCCACCATCACCTCC
mRab5	RAB5A	F	AGTCTGCTGTTGGCAAATCAAG
		R	CCGTTCTTGACCAGCTGTATCC
mNPY	NPY1R	F	TGGACTGACCCTCGCTCTAT
		R	TGTCTCAGGGCTGGATCTCT
mEndoA1	SH3GL2	F	TCATTGGACATGGAAGTGAAGC
		R	ACTCGGCCGATTTCTTTAGACTCA

## 2.7 Equipment

All equipment used for this thesis is listed in Table 12.

Table 8 - List of equipment used in this study

Equipment	Manufacturer
Balance EW2200-2NM	Kern&Sohn
37°C Incubator	Memmert
Cell cracker	In-house workshop
Dounce homogenizer	Wheaton
EPC10 Amplifier	HEKA
Examiner Z1 LSM710 microscope	Zeiss
Fine balance ALJ 120-4	Kern&Sohn
Heating plate Mr3001	Heidolph
Hood Herasafe	Thermo Scientific
Imaging chamber	home-made (workshop)
Incubator Heracell 150i	Thermo Scientific
Isolation cage	home-made (workshop)

LSM 880 Airyscan microscope	Zeiss
LSM 800 microscope	Zeiss
Micromanipulator	home-made (workshop)
NanoDrop Spectrophotometer	Peqlab
Odyssey Infrared Imager	Li-Cor
Patch pipette puller	Sutter instruments
Perfusion head controller	ALA Scientific Instruments
Pipettes	Eppendorf Research
Platinum electrode stimulator	In-house built
Power source (SDS-PAGE)	Bio-Rad
Revolver wheel	Labnet
S120AT2 ultracentrifuge rotor	Sorvall
SevenEasy pH Meter	Mettler Toledo
Table centrifuge (5424)	Eppendorf
Thermomixer comfort	Eppendorf
Western blot system	Bio-Rad

## 2.8 Bacteria and virus

The bacteria and viruses used in this study are listed in Table 13.

Table 9 - List of bacteria and viruses used in the study

<b>Bacteria/Virus</b>	<b>Supplier</b>	<b>Catalog Nr.</b>
Rosetta (DE3)	Merck	70954-4
Escherichia coli BL21-CodonPlus (DE3)-RIL	Agilent Stratagene	
XL 10 Gold Ultracompetent Cells	Agilent Stratagene	200314
Dh5 $\alpha$ competent Cells	Thermo Fisher	18265017

## 2.9 Software

The software used in this study for data acquisition and analysis are listed in Table 13.

Table 10 - List of software programs used in this study

<b>Software</b>	<b>Company</b>
Adobe Illustrator CS5.1	Adobe Systems Inc.
Fiji/ImageJ	NIH
Igor Pro	Wavemetrics
Image Studio	Li-cor Bioscience
Imaris 8.0.2	Bitplane
Microsoft Office	Microsoft Corporation
Patchmaster	HEKA
Prism 6	GraphPad

Pulse/PULSEFIT	HEKA electronics
Volocity 6	PerkinElmer
ZEN black	Carl Zeiss AG
ZEN blue	Carl Zeiss AG
IMOD	bio3d.colorado.edu/imod
Sigma Plot 13	Systat Software GmbH
iTEM	EMSIS GmbH

## 2.10 Supplementary method

Here I present supplementary experiment method that is not described in the two publications in chapter 3.

### 2.10.1 Protein expression and purification procedure

Because of the abundance of non-preferred arginine codons, there was a very low expression level of amisyn under standard conditions. Thus, *Escherichia coli* Rosetta (DE3) (Merck 70954-4) competent cells transformed with pGEX-6p1-amisyn constructs were grown in Luria-Bertani medium (tryptone, yeast extract, NaCl, 50 µg/ml ampicillin, 50 µg/ml chloramphenicol) to OD<sub>600</sub> 0.7-1.0 at 37°C and 250 rpm. Amisyn WT protein was induced in bacteria by an additional 10 µM isopropyl-1-thio-β-d-galacto-pyranoside (IPTG) in the culture medium and further cultured for 12 hr at 24°C and 250 rpm. The bacteria were pelleted by centrifugation (54,000×g), washed with ice-cold PBS, and resuspended in lysis buffer (150 mM NaCl, 50 mM HEPES, 2 mM EDTA, 2 mM DTT, pH 7.5) containing one tablet of PhosStop tablet. The cells were subjected to cell fractionation (Fluidizer; Microfluidics, MA, USA); after centrifugation (25,000g, 30 min), the supernatant was loaded to the glutathione column (Protino Glutathione Agarose 4B column; Machery-Nagel, Düren, Germany) with lysis buffer at a speed of 0.5 mL/min. GST-amisyn was then eluted with reduced glutathione (10 mM, in 50 mM Tris-HCl, 100 mM NaCl, pH 8.0) at a speed of 0.5 mL/min for around 30 min. Next, the eluate was dialyzed before proteolytic cleavage (PreScission, GE Healthcare Life) to remove the GST-tag by incubation overnight at 4°C. The eluate was again affinity-purified over the glutathione column to obtain pure recombinant amisyn protein, as confirmed by SDS-PAGE analysis and western blotting.

### **2.10.2 Biochemical procedures**

Whole brains extracted from P14 WT animals were isolated and homogenized in buffer (Hepes 20 mM, NaCl 150 mM, MgCl<sub>2</sub> 1 mM, EGTA 1 mM DTT with protease inhibitor) in tissue grinders (Potter-Elvehjem). After centrifuge (1000×g, 10 min), 1% Tx-100 were added into supernatant and incubated on ice for 10 min. After further ultra-centrifuge (100000×g) for 30 min, the supernatant was mixed with GST-resin and purified GST-amisyn. The mixture was rotationally incubated at 4°C for 2 h. Supernatant mixed with GST-resin only was also incubated as a control. After incubation, the mixture was centrifuged at 2000 rpm for 10 min. Resin in the pellet was further washed three times with PBS and two times with PBS-T. After washing, the resin was mixed with 6X Laemmle loading buffer (62.5 mM Tris, 50% glycerol, 12% SDS, 0.06% bromophenol blue, 5% 2-mercaptoethanol added before use) and boiled for 3 min. The mixed samples were then loaded onto SDS-page gel. Electrophoresis was performed using a BioRad electrophoresis system (PowerPack™ Basic). The gel was then stained with Coomassie Brilliant Blue. Visualized bands on the gel were collected and sent for mass spectrometry (Mass Spec).

### **3. Results**

#### **3.1 PI(4,5)P<sub>2</sub>-dependent regulation of exocytosis by amisyn, the vertebrate-specific competitor of synaptobrevin 2**

Ilona Kondratiuk<sup>1</sup>, Shrutee Jakhanwal<sup>2,\*</sup>, Jialin Jin<sup>1,\*</sup>, Udhayabhaskar Sathyanarayanan<sup>1,\*</sup>, Benjamin Kroppen<sup>3</sup>, Ajaybabu V. Pobbati<sup>2</sup>, Anita Krisko<sup>4</sup>, Uri Ashery<sup>5</sup>, Michael Meinecke<sup>3</sup>, Reinhard Jahn<sup>2</sup>, Dirk Fasshauer<sup>2,6</sup>, Ira Milosevic<sup>1,#</sup>

<sup>1</sup>European Neuroscience Institute Göttingen – A Joint Initiative of the University Medical Center Göttingen and the Max-Planck-Society, Göttingen, Germany

<sup>2</sup>Max Planck Institute for Biophysical Chemistry, Department of Neurobiology, Göttingen, Germany

<sup>3</sup>Institute for Cellular Biochemistry, University Medical Center Göttingen (UMG), Göttingen, Germany

<sup>4</sup>University Medical Center Göttingen (UMG), Department of Experimental Neurodegeneration, Göttingen, Germany

<sup>5</sup>Tel Aviv University, George S. Wise Faculty of Life Sciences, and the Sagol School of Neuroscience, Tel Aviv, Israel

<sup>6</sup>Université de Lausanne, Département des Neurosciences Fondamentales, Lausanne, Switzerland

\*these coauthors contributed equally, in alphabetical order

**Paper 1 (submitted in PNAS)**

## **ABSTRACT**

The functions of nervous and neuroendocrine systems are mediated by fast and precisely coordinated transmitter release through SNARE-mediated exocytosis. Few proteins, including tomosyn and amisyn (STXBP6), were proposed to negatively regulate exocytosis. Little is known about amisyn, a 24 kDa brain-enriched protein with a SNARE motif. We report here that full-length amisyn transiently associates with the plasma membrane, forms a stable SNARE complex with syntaxin-1 and SNAP-25 through its C-terminal SNARE motif, and competes with synaptobrevin-2/VAMP2 for the SNARE-complex assembly. Further, amisyn contains a N-terminal pleckstrin homology (PH) domain that mediates its association with the plasma membrane of neurosecretory cells by binding to phospholipid PI(4,5)P<sub>2</sub>. However, unlike synaptobrevin-2's, the SNARE motif of amisyn was not sufficient to account for the role of amisyn in exocytosis: both the PH domain and the SNARE motif are needed for its inhibitory function. Mechanistically, amisyn interfered with the priming of secretory vesicles and the sizes of releasable pools, but not vesicle fusion properties. Our biochemical and functional analyses of this vertebrate-specific protein reveal novel aspects of negative regulation of exocytosis.

## INTRODUCTION

Ca<sup>2+</sup>-triggered exocytosis is a complex, highly controlled cascade of protein-protein and lipid-protein interactions leading to the externalization of secretory molecules and neurotransmitters. The machinery mediating and regulating exocytosis was studied in detail over the past three decades. Numerous proteins were identified and characterized, including the SNARE [soluble N-ethylmaleimide-sensitive factor (NSF) attachment protein receptor] protein superfamily, central to the later steps of regulated exocytosis and bilayer fusion. All members of the SNARE family have a characteristic conserved homologous stretch of 60-70 amino acids, referred to as a SNARE motif (1, 2).

Four SNARE motifs assemble spontaneously into a thermostable, sodium dodecyl sulfate (SDS) and protease resistant coiled-coil bundle termed the SNARE core complex (3, 4). Heptad repeats in components of the core complex form 16 conserved layers of interacting amino acid side chains that are arranged perpendicular to the axis of the complex. All layers except one contain hydrophobic amino acids; the unique central layer, termed the “0-layer”, is hydrophilic and consists of three glutamine (Q) and one arginine (R) residue that is stabilized by ionic interactions. Based on this characteristic, SNARE proteins are classified into four subfamilies: Q<sub>a</sub>-, Q<sub>b</sub>-, Q<sub>c</sub>- and R-SNAREs (4). Three or four SNARE proteins bundle together to form a Q<sub>a</sub>Q<sub>b</sub>Q<sub>c</sub>R complex: this arrangement contributes to specific Q- and R-SNARE pairing.

Among the large number of SNARE proteins, the members of the neuronal SNARE complex are most intensely studied. This complex, first purified in (5), is comprised of three proteins: syntaxin-1 (6), synaptosome-associated protein of 25 kDa (SNAP-25; 7) and synaptobrevin2/vesicle associated membrane protein 2 (VAMP2) (8, 9), and comprises a minimal fusion machinery. Yet, fusion mediated only by SNARE proteins is slow and uncoordinated, which conflicts with the physiology of neuronal and neuroendocrine cells that require fast, spatially coordinated secretion. Consequently, accessory factors are needed to modulate the SNARE-driven exocytosis, like synaptotagmins that sense the rise in calcium (Ca<sup>2+</sup>) levels and

Sec1/Munc18 (SM) proteins that are essential for several exocytic steps (10, 11). Additional regulators bind to SNARE complexes and/or to neuronal SNARE proteins, e.g. complexin, tomosyn (also known as syntaxin binding protein 5, STXBP5) and amisyn (also known as syntaxin binding protein 6, STXBP6) (12, 13, 14), to promote, or interfere with, the SNARE complex formation.

Very little is known about amisyn, a 24 kDa protein reported to contain an uncharacterized N-terminal domain and a C-terminal SNARE motif (14). This brain-enriched protein co-immunoprecipitated with syntaxin-1a and syntaxin-4 (14). It was mostly cytosolic, but a fraction co-sedimented with membranes (14, 15). Like tomosyn's SNARE motif, the recombinant SNARE motif of amisyn formed a ternary complex with the neuronal SNARE proteins syntaxin-1a and SNAP-25 (14). Addition of amisyn SNARE domain is reported to inhibit secretion from cultured neuroendocrine PC12 cells (14). Amperometry-based experiments revealed that overexpression of full-length amisyn in rat chromaffin cells had no effect on the basic characteristics of the amperometric spikes, but it reduced the number of spikes elicited, and increased the lifetime of the pre-spike foot (15). Yet, the inhibition of secretion was independent of amisyn's interaction with syntaxin-1 (15) and the mechanisms of amisyn action in exocytosis are not clear. Overexpression of amisyn also inhibited secretion from human insulin-secreting  $\beta$ -cells (16). Recently, the cAMP-sensor Epac2 is reported to restrict fusion pore expansion by acutely recruiting amisyn and GTPase dynamin-1 to the exocytic site in insulin-secreting  $\beta$ -cells (17). Of note, amisyn is linked to several diseases, e.g., diabetes (16, 17), autism (18, 19) and cancer (20, 21). Consequently, this poorly studied protein necessitates detailed characterization of its biochemical, structural and functional roles.

Here, we report that amisyn is a vertebrate-specific protein that transiently associates with the plasma membrane and binds phosphatidylinositol-4,5-bisphosphate [PI(4,5)P<sub>2</sub>] through its pleckstrin homology (PH) domain. Full-length amisyn formed stable SNARE complexes with syntaxin-1a and SNAP-25, yet both PH and SNARE domains were needed to mediate its role in neurosecretory cell exocytosis. Elevated

amisyn levels interfered with docking/priming and fusion of secretory vesicles and resulted in reduced number of amperometric spikes, but did not alter the fusion pore properties. Finally, elevated amisyn potently inhibited exocytosis, most likely as a competitor of synaptobrevin-2.

## RESULTS

### **Amisyn is a conserved vertebrate-specific protein that forms a ternary SNARE complex with neuronal SNAP-25 and syntaxin-1**

We first used the full-length coding region of human amisyn to identify orthologues in the animal kingdom with moderate stringency conditions (see Methods): orthologues of amisyn were identified in all classes of vertebrates (**Table 1**), but not in other orders of animal kingdom, in agreement with (35). The comparative protein sequences revealed that amisyn is evolutionary conserved (**Table 1**).

Amisyn contains the SNARE motif at its C-terminus (14), while the structural and functional nature of the N-terminal region is unclear. We next aligned the SNARE motifs of syntaxin-1, SNAP-25 and synaptobrevin-2 with that of amisyn, and detected the characteristic heptad repeats (layers -7 to +8) essential for the putative amisyn-SNARE complex formation (**SI Appendix, Fig. S1A**; layers -7 to +8 are shaded grey; SNARE motifs are boxed). Notably, amisyn contains a R-SNARE motif like synaptobrevin-2, implying that amisyn may participate in the SNARE complex formation, possibly instead of synaptobrevin-2.

Given a suggested role for the SNARE motif of amisyn in the SNARE complex assembly (14), supported by the sequence alignment (**SI Appendix, Fig. S1A**), we examined the biochemical properties of full-length amisyn protein in the context of its interactions with other neuronal SNAREs. Full-length amisyn was reported as difficult to express heterologously and poorly soluble (14). We confirmed that the full-length protein expresses poorly under commonly used expression conditions, but it was nevertheless soluble. By subsequent optimization of the expression conditions

(see Methods), we achieved high expression levels, and succeeded to purify soluble amisyn protein (~5 mg amisyn/L medium). Moreover, the amisyn R-SNARE motif (amisyn-SNARE) was expressed and purified to even higher concentrations. Both proteins were >95% pure, as assessed by SDS-PAGE (**SI Appendix, Fig. S2**). We noted, however, that both proteins were inactivated by freeze-thawing, and were active only when kept on ice for up to 3-4 days.

Analysis by circular dichroism (CD) spectroscopy revealed the change in the secondary structure when syntaxin-1a and SNAP-25a were added to the purified SNARE motif of amisyn (**SI Appendix, Fig. S1B**). Specifically, the characteristic  $\alpha$ -helical spectrum showed minima at 208 and 222 nm. The structural change occurred after the addition of the SNARE motif of amisyn, similar as observed with the SNARE motif of synaptobrevin-2 (36), and the SNARE motif of tomosyn (37, 38). Our data further revealed that the SNARE motif of amisyn interacts with syntaxin-1a and SNAP-25a to form an SDS-resistant ternary complex, as originally reported in (14). Also the full-length amisyn protein, and not only the SNARE motif, formed a stable, SDS-resistant ternary complex with the neuronal Q-SNAREs *in vitro* (**SI Appendix, Fig. S1C-D**; note that the complexes dissociated after heating at 95°C).

Detailed characterization of amisyn-containing SNARE complex formation was performed by a comprehensive set of fluorescence anisotropy experiments using recombinant purified SNARE proteins (see Methods). Firstly, fluorescence anisotropy spectra of syntaxin-1a (syx1<sup>1-288OG</sup>; 1  $\mu$ M) revealed that its interaction with full-length amisyn (1  $\mu$ M) occurred only in the presence of SNAP-25a (1.5  $\mu$ M) (**Figure 1A**). Secondly, fluorescence anisotropy spectra of synaptobrevin-1 (syb<sup>1-96OG</sup>) showed that full-length amisyn (0.25  $\mu$ M - 2  $\mu$ M) competes for the SNARE complex formation in the presence of SNAP-25a (1.5  $\mu$ M) and syntaxin-1a (1 $\mu$ M) in a concentration-dependent manner (**Figure 1B**). Thirdly, when the cysteine residue at position 210 of amisyn's C-terminus was labelled with Oregon Green dye

(amisyn-SNARE<sup>210OG</sup>), we observed unchanged fluorescence anisotropy spectra of amisyn-SNARE<sup>210OG</sup> after addition of Q-SNARE motifs of SNAP-25a (1.5  $\mu$ M) or syntaxin-1a (1  $\mu$ M) (**Figure 1C**). In contrast, a robust increase in fluorescence anisotropy was observed when both SNAP-25a and syntaxin-1a were present (**Figure 1C**). Similarly, the fluorescence anisotropy of syntaxin-1a, labelled at position 197 with Oregon Green (syx1-H3<sup>197OG</sup>,  $\sim$ 0.5  $\mu$ M), did not change after the addition of the SNARE motif of amisyn (amisyn-SNARE, 1  $\mu$ M) (**Figure 1D**). Yet, an increase in anisotropy was evident when both amisyn-SNARE (1  $\mu$ M) and SNAP-25a (1  $\mu$ M) were added to syntaxin-1a<sup>197OG</sup> (**Figure 1D**). From the complex-forming and fluorescence anisotropy experiments, we concluded that full-length amisyn can form stable ternary complexes with syntaxin-1 and SNAP-25.

Taken together, our observations conclusively show that full-length amisyn interacts with syntaxin-1 and SNAP-25, two key neuronal Q-SNAREs, through its SNARE domain. Furthermore, amisyn interacts with the Q-SNARE proteins in a similar manner as synaptobrevin-2 (**Figure 1**), and the SNARE motif of tomosyn (38). We thus propose that amisyn, with the arginine residue in the centre layer position (**SI Appendix, Fig. S1A**), is a competitor of synaptobrevin-2 for a ternary SNARE complex formation (**SI Appendix, Fig. S1E**).

### **Amisyn inhibits liposome fusion *in vitro***

One common approach to investigate the function of a SNARE protein is by reconstituting complementary SNARE proteins into liposomes and examining liposomal fusion by Förster resonance energy transfer (FRET) between two fluorophore-labelled lipid analogs (31). We used an established liposome-based fusion assay (28) to examine if exogenously added amisyn interferes with liposome fusion. Addition of purified full-length amisyn inhibited liposome fusion (**Figure 1E**), and the effect was concentration-dependent (**Figure 1F**). The lack of a detectable trans-membrane domain in amisyn implied that the amisyn-containing SNARE complex was ‘fusion-inactive’, supporting the hypothesis that amisyn acts as a

negative regulator of exocytosis.

### **Amisyn is enriched at the plasma membrane in rodent nerve terminals**

We next aimed to study the sub-cellular distribution of native amisyn protein using an affinity-purified, custom-made polyclonal antibody (see Methods). This antibody could specifically recognize amisyn, both native, expressed and recombinant forms (**SI Appendix, Fig. S3**), and was thus used to investigate the distribution of amisyn in the mouse brain subcellular fractions. Notably, in the mouse brain, amisyn was conspicuously absent from supernatant fractions S3, LS1 and LS2, but was enriched in synaptosomal membranes (LP1) and in crude synaptosomal vesicles (LP2) (**SI Appendix, Fig. S1F; Figure 1G**). The evident implication was that the majority of amisyn associates with the membranes in nerve terminals of mouse brains. These data are in agreement with (14) and (15), who reported that a fraction of amisyn is membrane-bound.

We next cloned human amisyn (aa 1-210) fused to enhanced green fluorescent protein (EGFP) and expressed this construct in pheochromocytoma PC12 cells, neuroendocrine cells isolated from rat adrenal medulla. We noted, besides cytosolic localization, the significant association of amisyn-EGFP with the plasma membrane (**Figure 2A-B**). The binding of amisyn to the plasma membrane was further confirmed by an *in vitro* assay in which cultured cells are unroofed by a single sonication pulse (23, 39), as demonstrated in **Figure 2H-J**.

### **The N-terminal sequence of amisyn is a pleckstrin homology (PH) domain**

Despite the absence of membrane anchor sequences, amisyn associated considerably with the plasma membrane in living cells and isolated membrane fractions (**Figure 1G and Figure 2A**). Of note, the N-terminal part of amisyn remains to be explored for as yet unknown functions. This part of amisyn protein showed sequence homology (~32%) to Sec3-like protein, and we noted that Sec3 contains a pleckstrin homology (PH) domain implicated in functional tethering. Furthermore, homology was noted

with the *C. elegans* homologue Uso1p, also known as a tethering protein. We consequently scrutinized the uncharacterized N-terminal domain of amisyn for potential lipid-binding sequences and activity.

Firstly, we modelled the N-terminal domain of amisyn using as template the yeast exocyst subunit Sec3p (PDB code 3A58) (**Figure 2C-D**). The 89 residues of the amisyn N-terminal domain (68% coverage) was modelled using the protein threading method with 99.7% confidence (see Methods). As evidenced by the structural alignment with the template structure (rmsd 0.56 Å), as well as with the PH domain from the exchange factor ARNO in mouse (PDB code 1U27, rmsd 2.23 Å), the N-terminal amisyn sequence represented a typical PH domain, with a distinct fold consisting of an antiparallel beta sheet followed by an alpha helix. In addition, the molecular docking simulation revealed a potential binding site for PI(4,5)P<sub>2</sub>, with the highlighted lysine residues (K64 and K66) located at the putative PI(4,5)P<sub>2</sub> binding site. Moreover, in analogy with homologous proteins where the N-terminal domains is flexibly linked to the SNARE domain, we refer to 17 residues stretch between the putative N-terminal PH domain and C-terminal SNARE domain in amisyn as a linker region (**Figure 2E**).

To experimentally verify the predicted PH-domain in amisyn, we attempted to prepare amisyn crystals, but failed to obtain suitably refracting crystals. Thus, we experimentally approached our prediction that the PH-domain of amisyn was responsible for its membrane interactions. We prepared a mutated amisyn with the lysine residues predicted to interact with PI(4,5)P<sub>2</sub> based on molecular docking and analogy with phospholipase C-d<sub>1</sub> and with Sec3p as PI(4,5)P<sub>2</sub>-binding proteins (40). We constructed and expressed several mutants, including the quadruple amisyn mutant: K30A, K32A, K64D, K66D, denoted AADD-amisyn (**Figure 2E**). In transfected PC12 cells, we noted that the expressed AADD-amisyn failed to locate at the plasma membrane (**Figure 2F-G**). Moreover, plasma membrane sheets from transfected PC12 cells expressing either WT amisyn-EGFP, or AADD-amisyn-EGFP, confirmed that WT amisyn was bound to the plasma membrane, while the

AADD-amisyn was not (**Figure 2H-J**).

Next, we expressed and purified WT and AADD-amisyn heterologously (mutant showed similar CD spectra and gel filtration profile as WT amisyn (**SI Appendix, Fig. S2**), suggesting that the mutations did not alter the local and the overall protein fold. Upon incubation with the freshly-prepared PC12 plasma membrane sheets only recombinant WT amisyn-EGFP, and not AADD-amisyn-EGFP, bound to the isolated membranes (**Figure 3A-C**). Of note, we observed that fluorescently-labelled amisyn bound membranes in a non-uniform punctate pattern (**Figure 3B**; the plasma membrane sheets generated from PC12 cells expressing amisyn-EGFP showed non-uniform pattern as well, see **Figure 2I**). We concluded from the combined experiments that amisyn interacts with membranes through its N-terminal PH domain.

We next used liposome-based assay fusion assay (as shown in **Figure 1E-F**) to examine if AADD-amisyn or SNARE domain of amisyn alone, can alter liposome fusion. While addition of either AADD amisyn mutant, or SNARE domain of amisyn, had a negative effect on liposome fusion, neither had an effect as potent as the inhibition observed with full-length WT amisyn (**Figure 3D-E**; a mean of three independent experiments is shown in **Figure 3F**).

### **PI(4,5)P<sub>2</sub> controls amisyn binding to membranes in living PC12 cells**

We next performed the series of *ex vivo* and *in vitro* experiments to explore if amisyn interaction with membranes by its PH-domain was PI(4,5)P<sub>2</sub>-dependent. Firstly, we elevated the levels of PI(4,5)P<sub>2</sub> in the inner leaflet of the plasma membrane of PC12 cells by transfection and expression of PI4P5KI $\gamma$  (23). The result revealed that the vast majority of amisyn co-expressed in PC12 cells with mRFP-PI4P5KI $\gamma$  became associated with the plasma membrane (**Figure 4A-B**). In addition, more amisyn was bound to plasma membrane sheets isolated from amisyn-EGFP/mRFP-PI4P5KI $\gamma$  co-expressing PC12 cells (**Figure 4C-D**). Next, we reduced the PI(4,5)P<sub>2</sub> levels in PC12 cells by transfection with IPP-CAAX phosphatase (23). Thereby, the

amisyn-EGFP co-expressed with mRFP-IPP-CAAX was no longer associated with the plasma membrane (**Figure 4E-F**). Moreover, less amisyn was detected on plasma membrane sheets from amisyn-EGFP/mRFP-IPP-CAAX co-expressing PC12 cells (**Figure 4G-H**). In sum, by varying the amount of PI(4,5)P<sub>2</sub> in the inner leaflet of the plasma membrane in both directions by well-established methods, we demonstrated correlating alterations in plasma membrane-anchored amisyn.

Whether amisyn requires PI(4,5)P<sub>2</sub> for the membrane binding was further tested with purified recombinant full-length WT amisyn in a co-sedimentation assay and a liposome-binding assay (**Figure 5**). We prepared unilamellar liposomes composed of phosphatidylcholine (PC), phosphatidylserine (PS) and phosphatidylethanolamine (PE) and supplemented with PI(4,5)P<sub>2</sub>, various phosphatidylinositol phosphates (PIPs) or PC only, as control. We assayed the ability of amisyn to interact with the liposome's outer membrane. Firstly, using co-sedimentation assays (**Figure 5A**) with different levels of PI(4,5)P<sub>2</sub> incorporated into the liposomes, we observed a close positive correlation between PI(4,5)P<sub>2</sub> levels and amisyn co-sedimentation (**Figure 5B**). Remarkably, WT amisyn co-sedimented with PI(4,5)P<sub>2</sub>-containing liposomes, but not with liposomes without PI(4,5)P<sub>2</sub> (**Figure 5B**), showing that amisyn interaction with the liposomal membrane is mediated by negatively charged PI(4,5)P<sub>2</sub>. In contrast to WT amisyn, amisyn AADD mutant did not co-sedimented with PI(4,5)P<sub>2</sub>-containing liposomes (**Figure 5C**). Using the same assay, we observed that amisyn, in addition to binding PI(4,5)P<sub>2</sub>-liposomes, could also bind to liposomes containing PI(3,4)P<sub>2</sub> and PI(3,5)P<sub>2</sub> and PI(3,4,5)P<sub>3</sub>, but not phosphatidylinositol (PI), suggesting that PH domain of amisyn has high affinity but low specificity for PIPs (**SI Appendix, Fig. S4**).

We next performed imaging-based membrane-binding experiments using giant unilamellar vesicles (GUV). Here, we tested the binding of purified amisyn-EGFP fusion protein to fluorescently labelled GUV with different lipid compositions (see Methods). Amisyn was thereby found to bind only to PI(4,5)P<sub>2</sub>-containing vesicles

(**Figure 5D**), because replacing PI(4,5)P<sub>2</sub> with PS or PC did not lead to any appreciable amisyn protein binding.

### **Stimulation of PC12 cells recruited amisyn-EGFP to the plasma membrane**

Depolarization of neurosecretory chromaffin cells was shown to increase PI(4,5)P<sub>2</sub> levels rapidly and transiently (41). Therefore, we analysed whether more amisyn was bound to the plasma membranes of stimulated PC12 cells, depolarized by addition of 59 mM KCl. Fractionation of the stimulated cells (see Methods) revealed more amisyn to be present in the plasma membrane fractions compared to non-depolarized cells (**Figure 6A**, quantification shown on the right panel). PC12 cells stimulated by either nicotine or ionomycin, which both increase cytosolic Ca<sup>2+</sup> levels, provoked a similar increase in amisyn membrane binding (**Figure 6B**). Finally, plasma membrane sheets prepared from KCl-stimulated amisyn-EGFP-expressing PC12 cells contained more amisyn-EGFP than plasma membrane sheets prepared from non-depolarized amisyn-EGFP-expressing cells (**Figure 6C-D**).

The kinetics of amisyn recruitment to the plasma membrane upon depolarization was analysed in a series of live imaging experiments with PC12 cells expressing amisyn-EGFP. We noted the rapid rearrangement of amisyn distribution in PC12 cells expressing amisyn-EGFP, concomitantly with the elevation in plasma membrane-bound amisyn, almost immediately upon the addition of 59 mM KCl (**Figure 6E-F**). The association of amisyn with the plasma membrane was transient, as the majority of amisyn dissociated from the membrane and returned to cytosol within 6 minutes after stimulation. We concluded that depolarization recruited amisyn-EGFP to the plasma membrane of PC12 cells, rapidly and transiently.

Upon stimulation/depolarization, the levels of intracellular calcium ions also increase rapidly and transiently. To address whether recruitment of amisyn to the plasma membrane was mediated by an increase in calcium concentration, we incubated plasma membrane sheets (isolated from non-depolarized PC12 cells) with

recombinant amisyn-EGFP protein and various concentrations of calcium ions in the specified medium (39). Imaging revealed that similar amounts of amisyn-EGFP became bound to the membranes regardless of the calcium ion concentration, and even in the complete absence of externally added  $\text{Ca}^{2+}$  (**Figure 6G-H**). We also examined the  $\text{PI}(4,5)\text{P}_2$  levels in the plasma membrane upon stimulation of PC12 cells by 59 mM KCl or nicotine. Using recombinant EGFP-PH-PLC $\beta_1$  as a specific  $\text{PI}(4,5)\text{P}_2$ -probe and plasma membrane sheet assay (23), we detected elevated  $\text{PI}(4,5)\text{P}_2$  levels in the isolated plasma membranes of stimulated PC12 cells (**Figure 6I-J**). When the same experiment was done with PC12 cell 5 min post-stimulation, the difference in  $\text{PI}(4,5)\text{P}_2$  levels were no longer observed (**Figure 6K**). These data are in agreement with Eberhard and Holz (41), who reported increased levels of PI4P and  $\text{PI}(4,5)\text{P}_2$  in whole cell lysates prepared from chromaffin cells. Given a correlation between rapid and transient amisyn recruitment and a transient increase in the plasmalemmal  $\text{PI}(4,5)\text{P}_2$  levels, we concluded that the recruitment and binding of amisyn to the plasma membrane is mediated, at least in part, by  $\text{PI}(4,5)\text{P}_2$  concentrations in the inner leaflet of the plasma membrane, and not directly by calcium ions.

### **Addition of amisyn, but not amisyn's SNARE domain, reduced secretion of adrenal chromaffin cells**

PC12 cells were instrumental for the characterization of membrane binding of amisyn, while for physiological studies primary chromaffin cells from adrenal medulla that also secrete adrenaline and noradrenaline were preferred. The secretion in adrenal chromaffin cells has been well characterized, which make these cells an ideal system to study the effects of amisyn on releasable vesicle pools and release kinetics (42).

Firstly, we attempted to express amisyn from an internal ribosome entry site (IRES)-EGFP construct in bovine adrenal chromaffin cells using Semliki Forest Virus (SFV). We noticed that the infected chromaffin cells became stressed, were detaching from the glass coverslips and eventually died. We therefore opted for acute direct

delivery of the recombinant amisyn protein through the patch pipette. Purified amisyn (5  $\mu\text{M}$ ) was included in the pipette solution, and each cell was loaded for at least 90 s before combined electrophysiological and electrochemical experiments were performed. As a control, purified EGFP (5  $\mu\text{M}$ ) was included into the pipette solution, and each cell was loaded and recorded, similarly to experiments with amisyn. This approach allowed the acute studies of amisyn function in the fast secreting primary chromaffin cells. In addition to purified amisyn, chromaffin cells were loaded via the patch pipette with the photolabile  $\text{Ca}^{2+}$  chelator nitrophenyl-EGTA and with two  $\text{Ca}^{2+}$ -sensitive dyes that enabled accurate  $\text{Ca}^{2+}$  measurements during the whole-cell patch-clamp experiments (43, 23). Flash photo-release of caged calcium commonly increase the intracellular calcium ion concentration,  $[\text{Ca}^{2+}]_i$ , resulting in robust secretion that was assayed by the increase in membrane capacitance and by amperometric current measurements. Notably, exocytosis of the chromaffin cells loaded with full-length amisyn protein was strongly inhibited compared to control cells loaded with EGFP, as measured by the lesser capacitance increase (**Figure 7A**). Acute amisyn addition robustly reduced the exocytotic burst and the sustained component of release (**Figure 7A-C**). A second flash stimulation, applied to the same cells after 90 s recovery, also triggered a smaller response in amisyn-loaded cells compared to control (**SI Appendix, Fig. S5**).

We complemented the membrane capacitance measurements, showing the net change in exocytotic and endocytotic activity, with simultaneous recordings by carbon fiber amperometry. The amperometric data provide a direct measure of catecholamine release, not influenced by endocytosis. The observed net (cumulative) amperometric signal in amisyn-loaded cells revealed a strong decrease in the number of fused catecholamine-filled secretory vesicles (**Figure 7A** and **SI Appendix, Fig. S5A** bottom panels, quantified in panels **Figure 7F** and **SI Appendix, Fig. S5F**). These results are consistent with (15), who also reports smaller cumulative number of exocytic events by amperometry in chromaffin cells expressing amisyn, and the membrane capacitance measurements described in the previous section. Further, these

data are also in agreement with (16), where the reduction in secretion in insulin-secreting  $\beta$ -cells expressing amisyn was reported. Together, our data demonstrated that increasing the levels of amisyn caused a significant decrease in secretory vesicle secretion, and that this decrease is attributable to a smaller number of fused secretory vesicles.

Remarkably, the inclusion of purified recombinant SNARE domain of amisyn (5  $\mu$ M) into the pipette solution did not affect secretion robustly, except the sustained component of release (**Figure 7A-E**). This became even more obvious by the second stimulation, applied 90 sec later (**SI Appendix, Fig. S5A-E**). The same result was obtained from amperometry measurements during first and second stimulation (**Figure 7A** and **SI Appendix, Fig. S5A** bottom panels, quantified in panels **Figure 7F** and **SI Appendix, Fig. S5F**). These data match data obtained with a well-established liposome fusion assay (**Figure 3D-F**). Nonetheless, this was a surprising observation since the SNARE domain of amisyn was shown to inhibit exocytosis of noradrenaline in cracked PC12 cells (14) and to form SNARE complex with soluble SNAP-25 and syntaxin-1 (**Figure 1**; 14). In conclusion, when injected into live chromaffin cells, only full-length of amisyn with both PH and SNARE domains could potentially inhibit exocytosis.

### **Amisyn inhibited exocytosis by attenuating docking/priming and fusion, but release time constants were unaffected**

Chromaffin cell secretion elicited by flash photolysis stimulation consists of an exocytotic burst (comprising of two pools of release-competent vesicles: RRP and SRP, corresponding to fast (~30 ms) and slow components (~200 ms), respectively), followed by the sustained phase that represents vesicle recruitment and subsequent fusion (42, 43, 44). We analysed which of these distinct phases of the exocytotic burst was affected by acute addition of amisyn, to determine the pool size by the amplitudes of the exponential fittings, and the fusion kinetics by the time constants of the exponential fittings (23). The results revealed that the amplitudes (sizes) of RRP in

amisyn-loaded cells were reduced by about 80%, and that SRP were similarly affected, compared to control cells (**Figure 7B**). The time constant of the vesicle release from RRP was not affected (**Figure 7D**). Of note, in most amisyn-loaded cells (24 out of 38) the fast component was absent, reducing the number of observations. The time constant of the vesicle release from SRP was also not significantly affected by acute addition of amisyn (**Figure 7E**). The sustained component of release, which measures the refilling of the RRP and SRP pools, was also reduced (**Figure 7C**). Altogether, the results suggested that acute amisyn addition substantially inhibited the docking/priming and fusion of vesicles into the releasable pools, but did not alter the kinetics of vesicle fusion. The results obtained with a second stimulation were almost identical to the first (**SI Appendix, Fig. S5B-E**).

Notably, the inclusion of purified recombinant amisyn SNARE domain into the pipette solution did not significantly affect the sizes of RRP and SRP, while the sustained component was reduced (**Figure 7B-C** first stimulation, **SI Appendix, Fig. S5B-C** second stimulation). Kinetics of vesicle release from RRP and SRP were not significantly affected neither during first or second stimulation (**Figure 7D-E**, **SI Appendix, Fig. S5D-E**). These data, in addition to the liposome fusion assay data, show that only the full length amisyn protein can alter docking/priming and fusion of secretory vesicles.

To further explore the putative role of amisyn in the regulation of the fusion pore stability, as recently reported in insulin-secreting  $\beta$ -cells (17), we performed a thorough examination of single amperometric spikes in bovine adrenal chromaffin cells loaded with amisyn (5  $\mu$ M) and SNARE domain of amisyn (5  $\mu$ M) (45) (**Figure 7G-Q**). Representative amperometric traces for WT, amisyn and amisyn SNARE-loaded cells are illustrated in **Figure 7G**. Significant differences were observed in the number of detected events per cell (**Figure 7I**), in agreement with (15). Single spike charge (calculated as the time integral of the amperometric current; reflects the total amount of catecholamines oxidized at the electrode) and amplitude

were not changed (**Figure 7J-K**), as well as the kinetic features of single spikes (**Figure 7L-N**). Amperometric spikes are often preceded by a pre-spike foot that reflects catecholamine leakage through the forming fusion pore (46). The pre-spike foot duration and its amplitude were not altered in chromaffin cells loaded with amisyn, or amisyn SNARE domain, for 90s (**Figure 7O-Q**), suggesting that amisyn and its SNARE domain do not alter fusion pore stability when acutely added to adrenal chromaffin cells.

Altogether, our electrophysiological and electrochemical data show that upon acute addition of recombinant proteins, only full-length amisyn, and not amisyn's SNARE domain, can strongly inhibit exocytosis by attenuating secretory vesicle docking/priming and fusion, while the release time constants and fusion pore properties were unaffected.

## **DISCUSSION**

The intracellular mechanisms governing exocytosis are regulated by numerous proteins, yet aspects of negative regulation of this complex process are poorly understood. We unequivocally show here that full-length amisyn forms a 'fusion inactive' SNARE complex with SNAP-25 and syntaxin-1, and acts as a vertebrate-specific competitor of synaptobrevin-2. In addition to the SNARE-domain, amisyn also contains a N-terminal PH domain that mediates amisyn's association with the plasma membrane by binding to phospholipid PI(4,5)P<sub>2</sub>. Importantly, both the PH and SNARE domains of amisyn are needed to inhibit docking/priming and fusion of secretory vesicles.

Amisyn has been implied to play a role in several disorders, including diabetes, autism and cancer, by way of its regulatory functions in exocytosis (15, 16, 17, 47). Our research on this functionally largely unknown protein was motivated by its inhibitory role in membrane fusion and a presence of the SNARE domain in amisyn. We first explored its biochemical properties with respect to SNARE complex formation *in vitro*. We document that full-length amisyn is as effective in forming a

stable SDS-resistant SNARE complex with syntaxin-1 and with SNAP-25 as the SNARE motif fragment of amisyn (14). Detailed biochemical studies were required because the SNARE domain of amisyn alone does not efficiently inhibit exocytosis, unlike the SNARE domain of synaptobrevin 2.

While amisyn does not contain a distinct trans-membrane sequence nor recognizable lipidation motif(s), we and others (14, 15) found it to be enriched at the membranes. In our study, the subcellular fractionation of mouse brain indicated that amisyn was largely absent from the soluble fractions. It is possible that amisyn is indirectly attached to the plasma membrane through its interaction partner syntaxin-1. Yet, we have not observed a correlation between syntaxin-1a and amisyn levels associated with the plasma membrane. In contrast, we observed that amisyn association with the plasma membrane was dependent on the membrane concentration of PI(4,5)P<sub>2</sub> *in vitro* and *ex vivo*. This dependence of amisyn on PI(4,5)P<sub>2</sub>, considerable sequence homology to yeast Sec3p that contains a PH-domain and a review by Barg and Guček (47), inspired us to explore whether the N-terminal domain of amisyn contained a functional PH-domain. We first attempted to obtain amisyn structure through crystallography but had little success. Thus, we performed a series of mutagenesis-based experiments that led to the construction of a AADD mutant incapable of PI(4,5)P<sub>2</sub> binding *ex vivo*. Altogether, it was revealed that amisyn's PH domain mediates its interaction with the plasma membrane and is needed for its regulatory role in vesicle priming and fusion. Indeed, intricate regulation of exocytosis can be achieved by varying the levels and types of phosphatidylinositides, which, in turn, alter the nature and composition of the recruited exocytic machinery (23, 48). The PH domain may allow amisyn to act as a PI(4,5)P<sub>2</sub>-dependent effector, contributing to the spatial and temporal regulation of exocytosis. Additional research is needed to distinguish if amisyn's PH domain is just a recruiting device to create a high local concentration of the inhibitory SNARE motif, or amisyn's N-terminal domain mediates more than membrane binding.

Of note, the N-terminal part of amisyn corresponds to the N-terminal domain of the exocyst component Sec3p. This yeast protein is targeted to the budding tip through interactions with PI(4,5)P<sub>2</sub> and the small GTPase Rho/Cdc42. Consequently, Sec3 was used as structural model and template, similar also to the *C. elegans* homologue of the tethering protein Uso1 (49), with unknown structure and function. This connection of amisyn to the exocyst complex is intriguing. We envisage that amisyn may have taken over a part of the function of Sec3 (given the documented interaction of the N-terminal domain of Sec3 with sso2/syntaxin; 50), and could act in concert with other exocyst components as ExoC8, and possibly Exo84. In addition, Klöpper (35) proposed that amisyn evolved with the vertebrates, likely containing the SNARE-motif of tomosyn, the gene of which was possibly duplicated and evolved with a different N-terminal domain. Tomosyn is evolutionary very old: it belongs to the SNARE repertoire of the last common ancestor of all eukaryotes. Despite tomosyn and Lgl (a protein that likely arose from tomosyn or a predecessor that lost its SNARE domain) are active in different contexts, we speculate that amisyn is related to tomosyn, and possibly Lgl. Like amisyn, Lgl and tomosyn regulate secretion of vesicles, presumably independently of calcium.

In any case, the role of amisyn in exocytosis goes beyond its SNARE motif: at difference to (14) where amisyn's SNARE domain was sufficient to inhibit secretion in cracked PC12 cells, the whole protein was needed to block exocytosis efficiently, as seen by *in vitro* liposome fusion assays and fast electrophysiological and electrochemical recordings in live chromaffin cells. Notably, the inhibition of exocytosis by amisyn was directly proportional to its concentration: the higher the levels, the more potent was the exocytic block (high levels of amisyn were detrimental for the cells). Mechanistically, we document that amisyn interfered with the docking/priming and fusion of secretory vesicles, and with the sizes of releasable pools. Fusion kinetics of releasable vesicle pools (RRP and SRP) were not altered upon acute addition of amisyn protein in chromaffin cells, nor were the single spike features (only the number of detected spikes was lower, in agreement with (15, 16).

The only difference to (15) is that we do not detect a significant difference in foot duration and charge when amisyn was acutely loaded into cells through the patch pipette. Yet, we do not exclude that amisyn can affect fusion pore expansion under different conditions, as suggested earlier (15, 17). Of note, recombinant amisyn was delivered through a patch pipette in our studies, which may cause a diffusion of small molecules like cAMP (possibly also cAMP effector proteins, e.g. EPAC2) out of the cell and prevent detecting the effect of amisyn on fusion pores as reported in (17). Furthermore, amisyn has a strong inhibitory effect on exocytosis, making these experiments difficult: the number of detected amperometric spikes was severely reduced and many amisyn-loaded cells showed little or no secretion.

### **Putative model of amisyn role in exocytosis**

Amisyn's enrichment in the plasma membrane suggests that amisyn exerts its main functions there. The R-SNARE motif of amisyn interacts with the Q-SNAREs syntaxin-1 and SNAP-25 as effectively as synaptobrevin-2. In addition, amisyn acts primarily on the regulation of number of released vesicles from RRP, SRP and during sustained secretion. Therefore, one could envision that amisyn acts as a negative regulator of SNARE complex assembly by competing with the 'fusion-active' synaptobrevin-2 for SNAP-25/syntaxin-1 binding (**Figure 8**). Since amisyn does not contain any trans-membrane domain(s), it most likely forms a 'fusion-inactive' SNARE complex, as originally suggested by (14). Nonetheless, at difference to (14), our model does not assume that amisyn holds SNAP-25/syntaxin-1 in a conformation ready for synaptobrevin-2 to replace it before membrane fusion takes place. We rather propose that amisyn controls the number of fused vesicles and timing of exocytosis, which may be important for brain development and autism, as well as insulin-secreting  $\beta$ -cells and diabetes. Furthermore, amisyn interacts with the plasma membrane in a PI(4,5)P<sub>2</sub>-dependent manner through its N-terminal PH domain that may serve as the protein's recruiting device, and, in turn, generate the required high local concentrations of amisyn that are needed to outcompete the abundant and membrane-anchored synaptobrevin-2. PI(4,5)P<sub>2</sub>-sensitive PH domain is also able to

provide temporal and spatial characteristics needed for the regulation of exocytosis. Such a model could elegantly explain key observations in amisyn's studies, including decreased exocytosis efficiency (14, 15, 16 our work) and enhance our understanding of membrane fusion timing control.

Given the complexity of the exocytic machinery, it is not surprising that regulatory proteins like amisyn are needed to balance and control exocytosis, and by extension, that the proteins involved are potentially relevant in various diseases. Further studies are needed to comprehend this conserved, vertebrate-specific yet overlooked protein. Understanding amisyn both structurally and functionally is not only fundamentally important for our knowledge of the physiology of neurosecretory and neuronal cells, but may also help to unravel complex pathological processes, like in diabetes and autism.

## **Methods**

### **Plasmids**

Cloning of pEGFP(N1)-amisyn WT, pEGFP(N1)-amisyn SNARE domain, pEGFP(N1)-amisyn AADD, pEGFP(N1)-amisyn PH domain, pGEX-6p1-amisyn WT, pGEX-6p1-amisyn SNARE domain, pGEX-6p1-amisyn AADD and pGEX-6p1 amisyn PH domain are described in the Supporting Information (SI). All constructs were checked by both control restriction enzyme digestions and by sequencing. Besides amisyn, the following SNARE expression constructs were used: rat syntaxin1a H3 domain (aa 180-262) (4), rat syntaxin-1 with its transmembrane region (aa 183-288) (22), rat SNAP-25a (aa 1-206) (4), soluble rat synaptobrevin-2 (aa 1-96) (4), and synaptobrevin-2 with trans-membrane domain (aa 1-116) (22). EGFP-PH-PLC $\delta_1$ , mRFP-PI4P5KI and mRFP-IPP1-CAAX (23), or empty pEGFP-N1 (Clontech) as control, were used as indicated.

### **Cell culture, cell transfections and cell stimulations**

The neuroendocrine cell line PC12 (ATCC CRL-1651<sup>TM</sup>) was maintained and propagated as detailed in the SI. PC12 cells (until passage 14) were transfected with plasmids expressing amisyn-EGFP, mRFP-PI4P5KI and mRFP-IPP1-CAAX (23). In some experiments, EGFP expressed from pEGFP-N1 was used as a control. Cell transfection was performed using Lipofectamine (ThermoFisher Scientific, San Jose, CA, USA), after which the cells were maintained in fresh growth medium for 18-30 hrs before analysis. PC12 cells were either imaged live, used for plasma membrane sheet preparations, or fixed in 3.7% paraformaldehyde (PFA) in Phosphate-Buffered Saline (PBS) for 30 min at room temperature and further processed for confocal microscopy. Stimulation of PC12 cells was achieved with 59 mM KCl (Sigma), nicotine (Merck, N0267), or ionomycin (Merck, I0634) in Tyrode's buffer (119 mM NaCl, 5 mM KCl, 25 mM HEPES pH 7.4, 2 mM CaCl<sub>2</sub>, 1 mM MgCl<sub>2</sub>, 6g/l glucose), as indicated in the figure legends.

The primary culture of bovine chromaffin cells (BCCs) was prepared as described (23). BCCs ( $\sim 5 \times 10^5$  cells) were plated on Ø18 mm glass coverslips that had been pre-treated with a 0.1 mg/ml poly-L-lysine (Sigma, St Louis, MS, USA) for 30 min and kept at 37°C in 8% CO<sub>2</sub>. Cells were used for experiments 24 h after plating.

### **Protein expression, purification and labelling**

Due to the abundance of non-preferred arginine codons, the full-length amisyn could be expressed only at very low levels under standard conditions. Thus, *Escherichia coli* BL21-CodonPlus(DE3)-RIL (Stratagene; these cells contain plasmids that encode the non-preferred tRNAs) or Rosetta (DE3) (Merck 70954-4) competent cells transformed with pGEX-6p1-amisyn constructs were grown in Luria-Bertani medium (LB; tryptone, yeast extract, NaCl, 50 µg/ml ampicillin, 50 µg/ml chloramphenicol) to OD<sub>600</sub> 0.6-0.8 at 37°C. Amisyn recombinant protein (amisyn WT, amisyn SNARE and amisyn AADD) expression was induced by the addition of 10 µM isopropyl-1-thio-β-d-galacto-pyranoside (IPTG) and further culturing for 12 hr at 18°C and 250 rpm. The cells were pelleted by centrifugation (54,000xg), washed with

ice-cold PBS and resuspended in equilibration buffer (150 mM NaCl, 50 mM HEPES, 2 mM EDTA, 2 mM DTT, pH 7.5) containing 1mM phenylmethylsulfonyl fluoride (PMSF). The cells were subjected to cell fractionation (Fluidizer; Microfluidics, MA, USA), after centrifugation (25,000g, 20 min) the supernatant was loaded to the glutathione column (Protino Glutathione Agarose 4B column; Machery-Nagel, Düren, Germany; equilibration buffer - 150 mM NaCl, 50 mM HEPES, 2 mM EDTA, 2 mM DTT, pH 7.5). GST-amisyn was eluted with reduced glutathione (10 mM, in 50 mM Tris-HCl, 100 mM NaCl, pH 8.0). Next, the eluate was dialysed before proteolytic cleavage (PreScission, GE Healthcare Life) to remove the GST-tag by incubation overnight at 4°C. The eluate was again affinity-purified over the glutathione column to obtain the pure recombinant amisyn protein, as confirmed by SDS-PAGE analysis and Western blotting.

EGFP-PH-PLC $\beta_1$  was expressed and purified as in (23). Unless otherwise stated, proteins from other expression constructs were expressed through the pET28a expression vector (Novagen) in *E. coli BL 21* (DE3) competent cells (Merck), purified and labelled as described in the SI.

### **Antibodies**

Custom-made polyclonal amisyn antibody was generated against full-length recombinant amisyn, expressed and purified as detailed above. The rabbit was immunized with 300  $\mu$ g recombinant protein emulsified in Freud's adjuvant complete (Merck, Cat No. F5881). Booster injections (150  $\mu$ g recombinant protein emulsified in Freud's adjuvant) were given every 2-3 weeks for 4 months. The blood was obtained from the ear veins of the rabbit and processed to remove the blood cells. The serum with polyclonal anti-amisyn antibody was then aliquoted, and stored at -80°C. This anti-amisyn antibody (Aminchen #172) was affinity purified using the immobilized recombinant amisyn protein. The column was washed with 0.1% Tween in Tris-buffered saline (TBS; 50 mM Tris-Cl pH 7.3, 150 mM NaCl) and TBS alone, before elution with 0.1 M glycine. The eluate was immediately neutralized with 1.5 M Tris (pH 7.3). The titer and specificity of the amisyn antibodies was verified using

both native, expressed and recombinant amisyn blotted onto nitrocellulose membranes, as detailed in Results and SI Appendix, Fig. S2. The list of commercial antibodies and their dilutions is presented in the SI.

### **DNA sequence analysis and structural modelling of amisyn**

We searched available databases for possible homologues of amisyn using BLAST (24) against the non-redundant dataset (nr) with default parameters. We restricted the search to insects, molluscs, arachnids, crustaceans (all invertebrates), as well as all vertebrates, and separately mammals and primates. Homologous protein sequences (e-value  $<10^{-5}$ , and sequence coverage  $>70\%$ ) were collected and multiple sequence alignments were performed using the T-Coffee server (25).

Using the Phyre2 web portal for protein modelling, prediction and analysis with default parameters (26), the tertiary structure of the N-terminal domain of amisyn and its SNARE motif were modelled. The N-terminal domain of 89 amino acids (68% of the query sequence) was modelled with 99.7% confidence, using the tertiary structure of the yeast Sec3p exocyst subunit (PDB code 3A58). The C-terminal domain, previously described as the SNARE domain, was modelled on the tomosyn (PDB code 1urq) as template. The model was obtained with 99.8% confidence on a stretch of 58 amino acids (94% of the query sequence).

The resulting PDB files of models of the N-terminal domain and the SNARE domain of amisyn were used to perform structural alignments using the TM-align server (27). The N-terminal domain was aligned with its template (PDB code 3a58), as well as with several typical PH domains, e.g. PH domain from the exchange factor ARNO (*Mus musculus*, PDB code 1u27). The SNARE domain was aligned with its template (PDB code 1urq). PyMol software was used for protein visualization.

### **Anisotropy measurements**

Anisotropy measurements were performed as described (28) on a Fluorolog 3 spectrometer with magnetic stirrer and built-in T-configuration equipped for polarization (Model FL322, Jobin Yvon). The interaction of amisyn and syntaxin-1

was examined using 200 nM syntaxin-1 (aa 1-288) labelled with Oregon Green<sup>TM</sup> 488 (ThermoFischer, O-10241). For competition assays, different concentrations of synaptobrevin2 (aa 1-96) labelled with Oregon Green at the position C28 were used. The concentrations of amisyn are indicated in the Figures, while the concentration of the syntaxin-1:SNAP-25 complex was 400 nM. Anisotropy ( $r$ ) was calculated using the formula  $r = (IVV_G \times IVH)/(IVV + 2 \times G \times IVH)$ , where “I” denotes the fluorescence intensity, and the first and second subscript letters indicate the polarization of the exciting light and the emitting light, respectively. For Oregon Green-labelled synaptobrevin-2 or syntaxin-1, the excitation wavelength was set to 490 nm and the emission wavelength was set to 520 nm. All experiments were performed at 37°C and in a reaction volume of 600  $\mu$ l.

### **Giant Unilamellar Vesicles (GUVs) preparation and GUV assays**

GUVs were prepared as described in (29) and lipid composition as indicated in the SI. GUV visualisation experiments were carried out using the spinning-disc confocal setup (UltraVIEW VoX, Perkin Elmer, Waltham, MA, USA) with an inverted microscope (Nikon Ti-E Eclipse) and a 14-bit electron-multiplying charge-coupled device camera (C9100; Hamamatsu) using Volocity 6.3 software for image acquisition. The experiments were carried out using a 250  $\mu$ l borosilicate chamber (Lab-Tek). To avoid disruption of the GUV on contact, the chamber was coated with Bovine Serum Albumin (BSA) and 50  $\mu$ l GUVs (300 mM sucrose, 10 mM HEPES, pH 7.4) were added to 150  $\mu$ l 192 mM NaCl, 10 mM HEPES, pH 7.4. Osmolality of GUV suspension and buffer was matched to that of the protein solutions. Proteins were added to a final concentration of 2.2 mg/ml, and solution was mixed by gently rotating the pipette tip.

For a liposome sedimentation assay, freshly-prepared liposomes (as detailed in the SI) were incubated with 10  $\mu$ M recombinant amisyn for 20 min at 37°C. The liposomes were then centrifuged for 1 hr at 70,000 rpm (Sorvall RC-M120, rotor S120-AT3). Supernatant and pellet were separated, analysed by SDS-PAGE, and the gel was scanned (EPSON Perfection V700 Photo).

### **Liposome fusion assays**

Liposome fusion was studied using a lipid de-quenching assay (31). The  $\Delta N$  ternary complex, which contains the SNARE motif and transmembrane domain of syntaxin-1 (residues 183-288), SNAP-25 and Synaptobrevin-2 (Syb) (49-96) was incorporated into a population of liposomes, termed the acceptor liposomes. The full-length Syb protein (1-116) was incorporated into another population of liposomes, termed donor liposomes. The donor liposomes contained quenched populations of two fluorophores 7-nitro-2-1,3-benzoxadiazol-4-yl (NBD) and Rhodamine (ThermoFischer) coupled to lipids. Fusion with acceptor liposomes increases the total surface area and therefore the average distance between the fluorophores, resulting in an increase in donor (NBD) fluorescence. Liposome fusion reactions were performed at 30°C with 15  $\mu$ l labelled and unlabelled liposomes mixed in a total volume of 1.2 ml, resulting in final protein concentrations of 200 nM for both liposome populations. Fluorescence de-quenching was measured at 460 nm excitation and 538 nm emission wavelengths. Fluorescence intensities were normalized to the initial fluorescence intensity.

### **Isolation of plasma membranes from PC12 cells**

Crude PC12 cell membranes were prepared as described in (32) with minor modifications. Cells were resuspended by pipetting in PBS containing 2 mM EDTA at RT, and pelleted by centrifugation (300 g, 5 min, 4°C). The pellet was resuspended in low ionic strength TEP buffer (20 mM Tris-HCl pH 7.4, 1 mM EDTA) containing protease inhibitors (Roche) and homogenized with 20 strokes of a tight-fitting glass-glass homogenizer. Intact cells and nuclei were removed by centrifugation (300 g, 7 min). The supernatant was centrifuged (50,000 g, 30 min) and the pelleted membranes resuspended in TEP buffer. Protein content was determined with the bicinchoninic acid method (BCA; Pierce Chem. Co., Rockford, IL) using BSA as the standard. Protein electrophoresis and immunoblotting was performed as described in the SI.

### **Live PC12 cells and plasma membrane sheet experiments**

Experiments with live PC12 cells and plasma membrane sheets were performed and imaged as described in the SI. Digital image analysis of data shown in Figures 3H, 4D, 5D, 5H, 7D and 7H were performed using ImageJ (33) as detailed in the SI.

### **Electrophysiology and electrochemistry**

Capacitance and amperometric measurements on bovine adrenal chromaffin cells were performed concurrently at room temperature (22-24°C), and as described in the SI. Recombinant amisyn (5 µM), or SNARE-amisyn mutant (5 µM), were added to the intracellular pipette solution (in mM: 100 Cs-glutamate, 8 NaCl, 4 CaCl<sub>2</sub>, 32 Cs-HEPES pH 7.25, 2 Mg-ATP, 0.3 GTP, 0.4 Fura4F and 0.4 Furaptra, 5 NPE, osmolarity ~295 mOsm/kg), and kept cold until injection into cells through the custom-made glass patch pipette (NPI Electronic, GB150TF-8P, prepared with P-97 Flaming/Brown Micropipette Puller, Sutter Instruments). Analysis of amperometric recordings were performed by IGOR Pro (Wave Metrics) as in (34).

### **Statistical analysis**

Unless otherwise stated, all statistical analysis was done using Prism (GraphPad) software. Where indicated, nonparametric one-way ANOVA tests were used for comparing population means with significance set at  $p < 0.05$ . Unpaired two-sided t-test with Tukey's correction were used for comparisons between specific groups. Cumulative frequency distributions were compared using the Kolmogorov–Smirnov test. Electrophysiological data were analysed statistically by the Kruskal-Wallis test with Dunn's multiple comparison test. Unless otherwise stated, data are presented as mean±SEM.

### **ACKNOWLEDGEMENTS**

We thank D. Schwitters and B. Ide for excellent technical assistance, J. Peña del Castillo for help with amperometry analysis, J. Ferreira for protein expression

assistance, and Dr. I. Gottfried for initial discussion about amisyn's PH domain. This work was supported by the Schram-Stiftung T287/25457 and the Deutsche Forschungsgemeinschaft (Emmy Noether Young Investigator Award MI-1702/1 and SFB1190/P02) to IM, SFB803/B09 and SFB1190/P12 to BK and MM, and the Engelhorn-Stiftung fellowship to IK.

**Author contribution:** Conceptualization IM; Investigation and/or Analysis: IK, JJ, SJ, US, BK, AVP, DF, JPC, AK, IM; Reagents: UA, RJ, DF, IM; Writing: IM (with inputs from all co-authors); Revision: JJ and IM with inputs from all co-authors. Authors declare no competing financial interests.

#### **Data contribution**

IK (Figure 1-6,8 S1, S2), IM (Figure 6-8, S4, S5), JJ (Figure 2, 3, 5, 8, Figure S2-5), SJ (Figure 1,3), AK(Figure 2), US (Figure S2, S4)

#### **REFERENCES**

1. D. M. Terrian, and M. K. White, Phylogenetic analysis of membrane trafficking proteins: a family reunion and secondary structure predictions. *Eur. J. Cell Biol.* 73, 198–204 (1997).
2. T. Weimbs, K. Mostov, S. H. Low, K. Hofmann, A model for structural similarity between different SNARE complexes based on sequence relationships. *Trends Cell Biol.* 8(7):260-2 (1998).
3. R. B. Sutton, D. Fasshauer, R. Jahn and A. T. Brunger, Crystal structure of a SNARE complex involved in synaptic exocytosis at 2.4 Å resolution. *Nature* 395, 347–353 (1998).
4. D. Fasshauer, W. K. Eliason, A. T. Brunger, and R. Jahn, Identification of a minimal core of the synaptic SNARE complex sufficient for reversible assembly and disassembly. *Biochemistry* 37, 10354–10362 (1998).

5. T. Sollner, M. K. Bennett, S. W. Whiteheart, R. H. Scheller, and J. E. Rothman, A protein assembly-disassembly pathway in vitro that may correspond to sequential steps of synaptic vesicle docking, activation, and fusion. *Cell* 75, 409–418 (1993).
6. M. K. Bennett, N. Calakos, and R. H. Scheller, Syntaxin: a synaptic protein implicated in docking of synaptic vesicles at presynaptic active zones. *Science* 257, 255–259 (1992).
7. G. A. Oyler, G. A. Higgins, R. A. Hart, E. Battenberg, M. Billingsley, F. E. Bloom, M. C. Wilson, The identification of a novel synaptosomal-associated protein, SNAP-25, differentially expressed by neuronal subpopulations. *J. Cell. Biol.* 109:3039-52 (1989).
8. W. S. Trimble, D. M. Cowan, R. H. Scheller, VAMP-1: a synaptic vesicle-associated integral membrane protein. *Proc. Natl. Acad. Sci. U. S. A.* 85(12):4538-42 (1988).
9. M. Baumert, P. R. Maycox, F. Navone, P. De Camilli, R. Jahn, Synaptobrevin: an integral membrane protein of 18,000 daltons present in small synaptic vesicles of rat brain. *EMBO J.* 8(2):379-84 (1989).
10. Q. Zhou, Y. Lai, T. Bacaj, M. Zhao, A. Y. Lyubimov, M. Uervirojnangkoorn, O. B. Zeldin, A. S. Brewster, N. K. Sauter, A. E. Cohen, S. M. Soltis, R. Alonso-Mori, M. Chollet, H. T. Lemke, R. A. Pfuetzner, U. B. Choi, W. I. Weis, J. Diao, T. C. Südhof, A. T. Brunger, Architecture of the synaptotagmin-SNARE machinery for neuronal exocytosis. *Nature.* 525(7567):62-7 (2015).
11. E. A. Prinslow, K. P. Stepien, Y. Z. Pan, J. Xu, J. Rizo, Multiple factors maintain assembled trans-SNARE complexes in the presence of NSF and  $\alpha$ SNAP. *Elife.* 8. pii: e38880 (2019).
12. H. T. McMahon, M. Missler, C. Li, T. C. Südhof, Complexins: cytosolic proteins

that regulate SNAP receptor function. *Cell* 83(1):111-9 (1995).

13. Y. Fujita, H. Shirataki, T. Sakisaka, T. Asakura, T. Ohya, H. Kotani, S. Yokoyama, H. Nishioka, Y. Matsuura, A. Mizoguchi, R. H. Scheller, Y. Takai, Tomosyn: a syntaxin-1-binding protein that forms a novel complex in the neurotransmitter release process. *Neuron* 20(5):905-15 (1998).

14. S. J. Scales, B. A. Hesser, E. S. Masuda, R. H. Scheller, Amisyn, a novel syntaxin-binding protein that may regulate SNARE complex assembly. *J. Biol. Chem.* 277(31):28271-9 (2002).

15. J. R. Constable, M. E. Graham, E. Morgan, R. D. Burgoyne, Amisyn regulates exocytosis and fusion pore stability by both syntaxin-dependent and syntaxin-independent mechanisms. *J. Biol. Chem.* 280(36):31615-23 (2005).

16. S. C. Collins, H. W. Do, B. Hastoy, A. Hugill, J. Adam, M. V. Chibalina, J. Galvanovskis, M. Godazgar, S. Lee, M. Goldsworthy, A. Salehi, A. I. Tarasov, A. H. Rosengren, R. Cox, P. Rorsman, Increased expression of the diabetes gene SOX4 reduces insulin secretion by impaired fusion pore expansion. *Diabetes* 65(7):1952-61 (2016).

17. A. Guček, N. R. Gandasi, M. Omar-Hmeadi, M. Bakke, S. O. Døskeland, A. Tengholm, S. Barg, Fusion pore regulation by cAMP/Epac2 controls cargo release during insulin exocytosis. *Elife* 8. pii: e41711 (2019).

18. D. Castermans, B. Thienpont, K. Volders, A. Crepel, J. R. Vermeesch, C. T. Schrandt-Stumpel, W. J. Van de Ven, J. G. Steyaert, J. W. Creemers, K. Devriendt, Position effect leading to haploinsufficiency in a mosaic ring chromosome 14 in a boy with autism. *Eur. J. Hum. Genet.* 16(10):1187-92 (2008).

19. D. Castermans, K. Volders, A. Crepel, L. Backx, R. De Vos, K. Freson, S. Meulemans, J. R. Vermeesch, C. T. Schrandt-Stumpel, P. De Rijk, J. Del-Favero, C. Van Geet, W. J. Van De Ven, J. G. Steyaert, K. Devriendt, J. W. Creemers, SCAMP5,

NBEA and AMISYN: three candidate genes for autism involved in secretion of large dense-core vesicles. *Hum. Mol. Genet.* 1;19(7):1368-78 (2010).

20. S. V. Fernandez, K. E. Snider, Y. Z. Wu, I. H. Russo, C. Plass, J. Russo, DANN methylation changes in a human cell model of breast cancer progression. *Mutat. Res.* 688(1-2):28-35 (2010).

21. G. Lenka, M. H. Tsai, H. C. Lin, J. H. Hsiao, Y. C. Lee, T. P. Lu, J. M. Lee, C. P. Hsu, L. C. Lai, E. Y. Chuang, Identification of methylation-driven, differentially expressed STXBP6 as a novel biomarker in lung adenocarcinoma. *Sci. Rep.* 15;7: 42573 (2017).

22. M. Margittai, H. Otto, R. Jahn, A stable interaction between syntaxin 1a and synaptobrevin 2 mediated by their transmembrane domains. *FEBS Lett.* 5;446(1):40-4 (1999).

23. I. Milosevic, J. B. Sørensen, T. Lang, M. Krauss, G. Nagy, V. Haucke, R. Jahn, E. Neher, Plasmalemmal phosphatidylinositol-4,5-bisphosphate level regulates the releasable vesicle pool size in chromaffin cells. *J. Neurosci* 25 (10), 2557-65 (2005).

24. S. F. Altschul, W. Gish, W. Miller, E. W. Myers & D. J. Lipman, Basic local alignment search tool. *J. Mol. Biol.* 215:403-410 (1990).

25. C. Notredame, D. G. Higgins, J. Heringa, T-Coffee: A novel method for multiple sequence alignments. *J.M.B.*, 302, 205-217 (2000).

26. L. A. Kelley, S. Mezulis, C. M. Yates, M. N. Wass, M. J. E. Sternberg, The Phyre2 web portal for protein modeling, prediction and analysis. *Nature Protocols* 10, 845-858 (2015).

27. Y. Zhang, J. Skolnick, TM-align: A protein structure alignment algorithm based on TM-score, *Nucleic Acids Research*, 33: 2302-2309 (2005).
28. A. V. Pobbati, A. Stein, D. Fasshauer, N- to C-terminal SNARE complex assembly promotes rapid membrane fusion. *Science*. 4;313(5787):673-6 (2006).
29. D. Tarasenko, M. Barbot, D. C. Jans, B. Kroppen, B. Sadowski, G. Heim, W. Möbius, S. Jakobs, M. Meinecke, The MICOS component Mic60 displays a conserved membrane-bending activity that is necessary for normal cristae morphology. *J. Cell. Biol.* 3;216(4):889-899 (2017).
30. D. Fasshauer, W. Antonin, M. Margittai, S. Pabst, R. Jahn, Mixed and non-cognate SNARE complexes. Characterization of assembly and biophysical properties. *J. Biol. Chem.* 274(22):15440-6 (1999).
31. T. Weber, B. V. Zemelman, J. A. McNew, B. Westermann, M. Gmalch, T. H. Parlati, T. H. Sollner, J. E. Rothman, SNAREpins: minimal machinery for membrane fusion. *Cell* 92(6): p. 759-72 (1998).
32. N. Sharma, G. D'Arcangelo, A. Kleinlaus, S. Halegoua, J. S. Trimmer, Nerve growth factor regulates the abundance and distribution of K<sup>+</sup> channels in PC12 cells. *J. Cell. Biol.* 123:1835-43 (1993).
33. W. S. Rasband, ImageJ, U. S. National Institutes of Health, Bethesda, Maryland, USA, <https://imagej.nih.gov/ij/> (1997-2018).
34. E. V. Mosharov, D. Sulzer, Analysis of exocytotic events recorded by amperometry. *Nat. Methods*. 2(9):651-8 (2005).
35. T. H. Kloepper, C. N. Kienle, D. Fasshauer, SNAREing the basis of

multicellularity: consequences of protein family expansion during evolution. *Mol. Biol. Evol.* 25(9):2055-68 (2008).

36. D. Fasshauer, H. Otto, W. K. Eliason, R. Jahn, A.T. Brünger, Structural changes are associated with soluble N-ethylmaleimide-sensitive fusion protein attachment protein receptor complex formation. *J. Biol. Chem.* 272(44):28036-41 (1997).

37. K. Hatsuzawa, T. Lang, D. Fasshauer, D. Bruns, R. Jahn, The R-SNARE motif of tomosyn forms SNARE core complexes with syntaxin 1 and SNAP-25 and down-regulates exocytosis. *J. Biol. Chem.* 278(33):31159-66 (2003).

38. A. V. Pobbati, A. Razeto, M. Böddener, S. Becker, D. Fasshauer, Structural basis for the inhibitory role of tomosyn in exocytosis. *J. Biol. Chem.* 279(45):47192-200 (2004).

39. I. Milosevic, Spatial and temporal aspects of phosphoinositides in endocytosis studied in the isolated plasma membranes. *Methods Molecular Biology: Clathrin-Mediated Endocytosis*, Volume 1847, Springer ISBN 978-1-4939-8717-7 (2018).

40. R. Pleskot, L. Cwiklik, P. Jungwirth, V. Žárský, M. Potocký, Membrane targeting of the yeast exocyst complex. *Biochim. Biophys. Acta.* 1848(7):1481-9 (2015).

41. D. A. Eberhard and R. W. Holz, Calcium promotes the accumulation of polyphosphoinositides in intact and permeabilized bovine adrenal chromaffin cells. *Cell Mol. Neurobiol.* 11(3):357-70 (1991).

42. E. Neher, A comparison between exocytic control mechanisms in adrenal chromaffin cells and a glutamatergic synapse. *Pflugers Arch* 453(3), 261-8 (2006).

43. T. Voets, Dissection of three  $\text{Ca}^{2+}$ -dependent steps leading to secretion in chromaffin cells from mouse adrenal slices. *Neuron*. 28(2):537-45 (2000).
44. T. Xu, T. Binz, H. Niemann, E. Neher, Multiple kinetic components of exocytosis distinguished by neurotoxin sensitivity. *Nat. Neurosci.* 1(3):192-200 (1998).
45. E. V. Mosharov, Analysis of single-vesicle exocytotic events recorded by amperometry. *Methods Mol. Biol.* 440:315-27 (2008).
46. R. H. Chow, L. von Ruden, E. Neher, Delay in vesicle fusion revealed by electrochemical monitoring of single secretory events in adrenal chromaffin cells. *Nature* 5;356(6364):60-3 (1992).
47. S. Barg , A. Guček, How Kiss-and-Run Can Make Us Sick: SOX4 Puts a Break on the Pore. *Diabetes* 65(7):1791-3 (2016).
48. K. O Schink, T. W Tan, H. Stenmark, Phosphoinositides in Control of Membrane Dynamics. *Annu Rev. Cell. Dev. Biol.* 32:143-171 (2016).
49. H. Nakajima, A. Hirata, Y. Ogawa, T. Yonehara, K. Yoda, M. Yamasaki, A cytoskeleton-related gene, *uso1*, is required for intracellular protein transport in *Saccharomyces cerevisiae*. *J. Cell Biol.* 113(2), 245-60 (1991).
50. P. Yue, Y. Zhang, K. Mei, S. Wang, J. Lesigang, Y. Zhu, G. Dong, W. Guo, Sec3 promotes the initial binary t-SNARE complex assembly and membrane fusion. *Nat. Commun.* 8:14236 (2017).

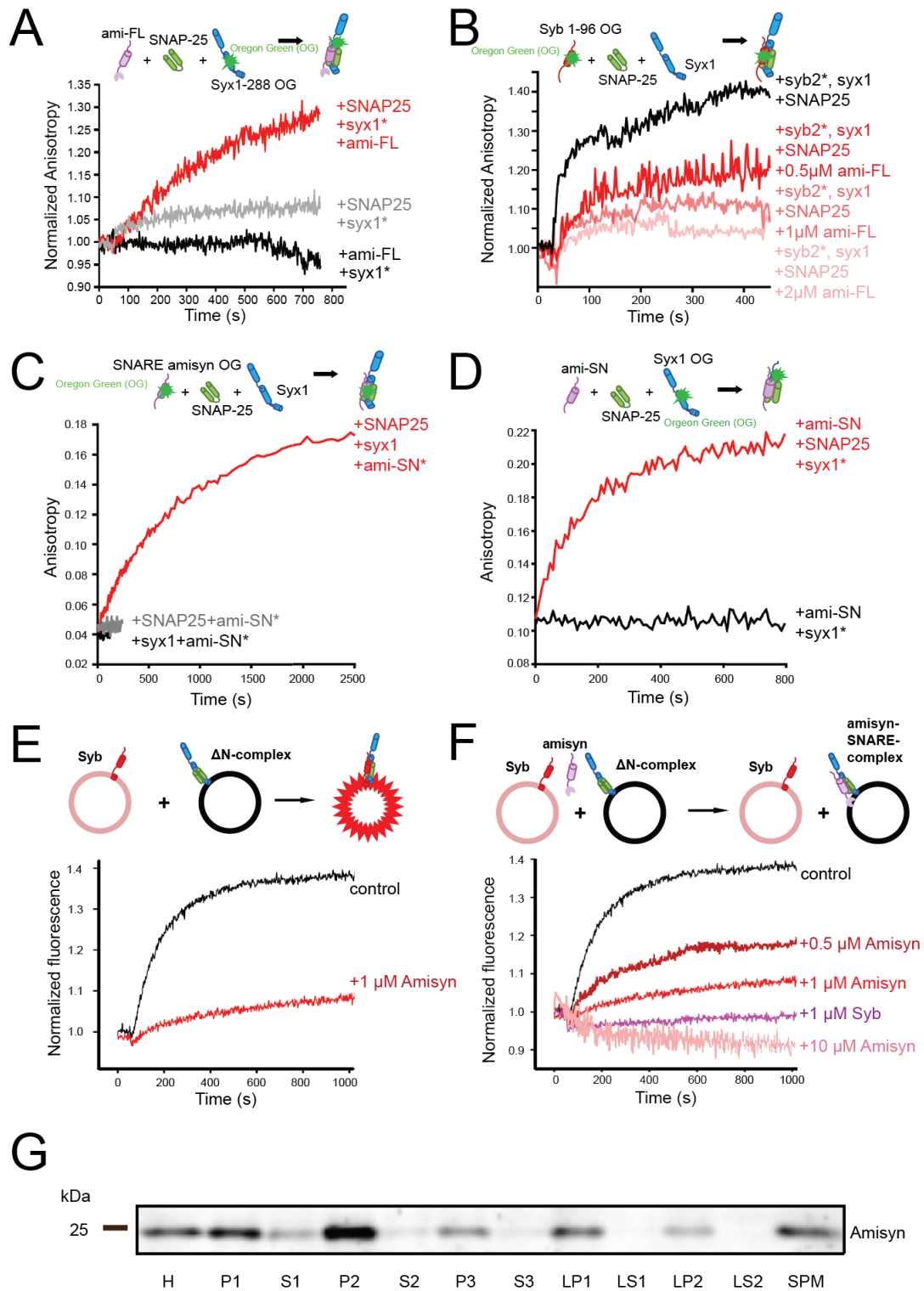


**Figure 1 Amisyn forms SNARE complex with syntaxin-1 and SNAP-25 and inhibits liposome fusion *in vitro*.**

(A) Fluorescence anisotropy of syntaxin-1 ( $\text{syx1}^{1-288\text{OG}}$ ; 1  $\mu\text{M}$ ) revealed interaction with full-length amisyn (ami-FL; 1  $\mu\text{M}$ ) in the presence of

full-length SNAP-25 (1.5  $\mu$ M) (red trace), versus SNAP-25 (grey trace) and amisyn alone (black trace).

- (B) Fluorescence anisotropy of synaptobrevin-2 (syn2<sup>1-96OG</sup>) revealed interaction with syntaxin-1 in the presence of SNAP-25 (1.5  $\mu$ M) and full-length amisyn (0.5, 1 or 2  $\mu$ M). Competition between amisyn and synaptobrevin-2 is demonstrated by decrease in anisotropy upon adding full-length amisyn in a concentration-dependent manner.
- (C) Anisotropy of the SNARE motif of amisyn (100 nM), labelled at cysteine-210 with Oregon Green, did not change by addition of the H3-syntaxin-1a (syx1, 1  $\mu$ M) or SNAP-25 (SNAP25) (1.5  $\mu$ M). In contrast, increased anisotropy was observed when both syx1 and SNAP-25 were added.
- (D) Anisotropy of H3-syntaxin-1a (syx1), labelled at position 197 with Oregon Green (syx1<sup>197OG</sup>), did not change by addition of the SNARE motif of amisyn (Ami-SN). Increased anisotropy was evident when both ami-SN and SNAP-25 (SNAP25) were added to syx1<sup>197OG</sup>.
- (E) In amisyn's presence, liposome fusion is severely impaired. Schematic representation of the liposome fusion assay is shown above the graph. Donor liposomes contain Syb-2 (1-116) and two fluorophores NBD and Rhodamine coupled to lipids, thereby quenching their fluorescence. Acceptor liposomes contain  $\Delta$ N ternary complexes of SNAP-25, syntaxin1a and C-terminal fragment of Syb-2. When donor (200 nM) and acceptor (200 nM) liposomes are mixed, they fuse due to trans-SNARE complex formation, which causes NBD fluorescence changes, allowing de-quenching of the NBD fluorescence and kinetic and quantitative measurements of the fusion process. Amisyn caused less de-quenching, indicative of inhibition of the fusion process.
- (F) Inhibition of liposome fusion by amisyn is concentration-dependent. Monitoring of NBD dequenching fluorescence after mixing liposomes revealed that higher concentrations of amisyn blocked liposome fusion more efficiently. Note that soluble synaptobrevin-2, that competes with

synaptobrevin-2 on the liposomes for the SNARE complex formation, was added as a control.

- (G) Fractionation of mouse brain homogenates to define the sub-cellular distribution of amisyn. Abbreviations: H mouse brain homogenate; P1 1,400xg pellet; S1: supernatant, further centrifuged (13,800xg, 10 min) to yield pellet P2: crude synaptosomes. P2 was lysed and centrifuged (32,800xg, 20 min) to yield pellet LP1: crude synaptic plasma membranes and supernatant LS2: synaptic vesicles and synaptosomal cytosol. S2: crude cytosol further centrifuged (165,000xg, 1 hr) to obtain P3: membranes and S3: cytosol. Fraction LP1 was further differentiated by sucrose gradient centrifugation to isolate synaptic membranes (SPM). Fraction LS1 was centrifuged (165,000xg, 1 hr) to yield pellet containing crude synaptic vesicles (SV) (LP2) and supernatant containing synaptosomal cytosol (LS2). Amisyn is predominantly present in membrane fractions.

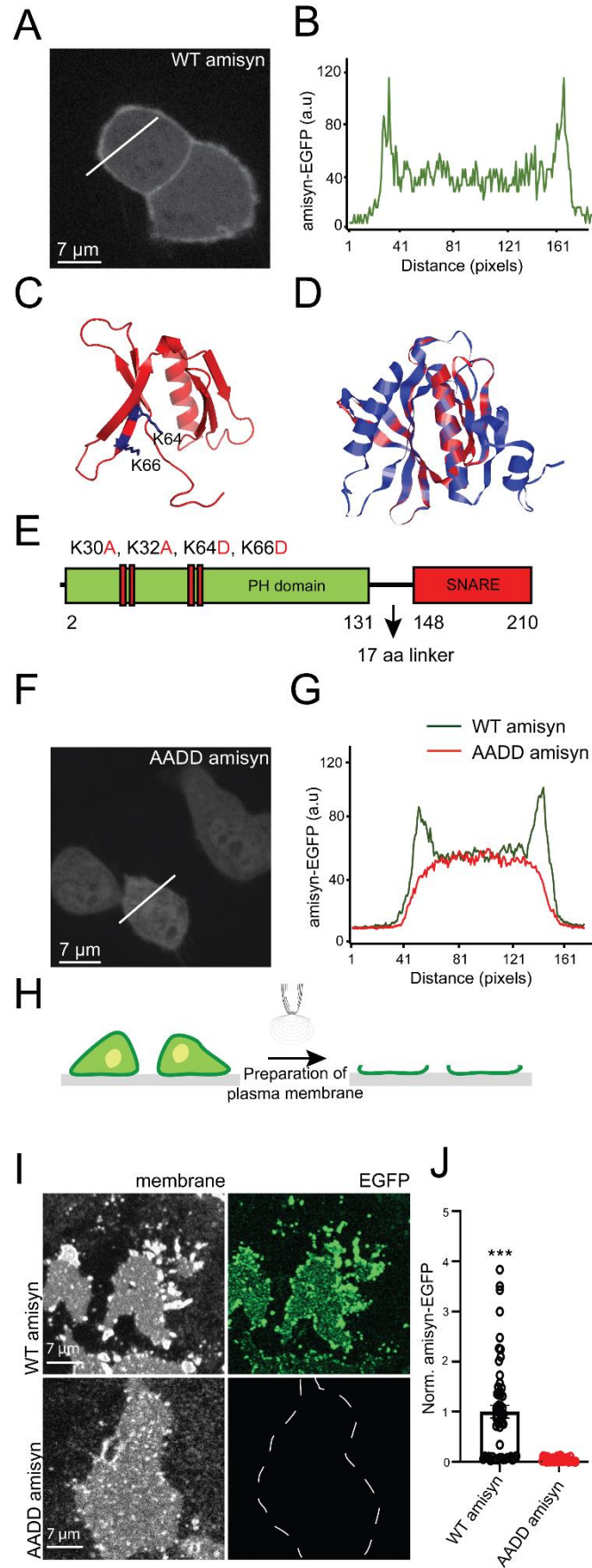


**Figure 2. Amisyn binds to membranes by its N-terminal PH-domain.**

- (A) Distribution of amisyn-EGFP in PC12 cells reveals binding to the plasma membrane. Cells were fixed and imaged 20 hr after transfection.
- (B) The fluorescence intensity line profile according the white line in (A).
- (C) Model of the N-terminal domain of amisyn that assembles into a PH-like domain. The essential Lysine residues (K64 and K66) are marked in blue.
- (D) Alignment of the identified PH-domain of amisyn (red) with that of PLC $\delta_1$  (blue) as template.
- (E) Schematic representation of amisyn with the PH and SNARE domains separated by the 17 aa linker sequence. The mutant AADD-amisyn protein contained 4 point-mutations in the PH domain: K30A, K32A, K64D, K66D.
- (F) The mutant AADD-amisyn failed to bind to the plasma membrane. Confocal images of AADD amisyn-EGFP expressed in PC12 cells. Cells were fixed and imaged 20 hr after transfection.
- (G) The fluorescence intensity profiles of PC12 cells expressing WT amisyn-EGFP (green trace) and AADD amisyn-EGFP (red trace; from the white line in F).
- (H) Schematic of isolated PC12 plasma membrane sheet preparation by sonication.
- (I) Isolated membrane sheets from PC12 cells expressing either WT or AADD amisyn-EGFP (indicated by the captions on the left). Representative images are shown of the membranes (left panels) and the associated fluorescence (right panels).
- (J) Quantification of the fluorescence signals (as shown in panel I) of WT and AADD amisyn-EGFP. 3 independent experiments, WT (31 cells) and AADD (33 cells). Unpaired two-sided t-test, mean $\pm$ SEM, \*\*\*p<0.001.

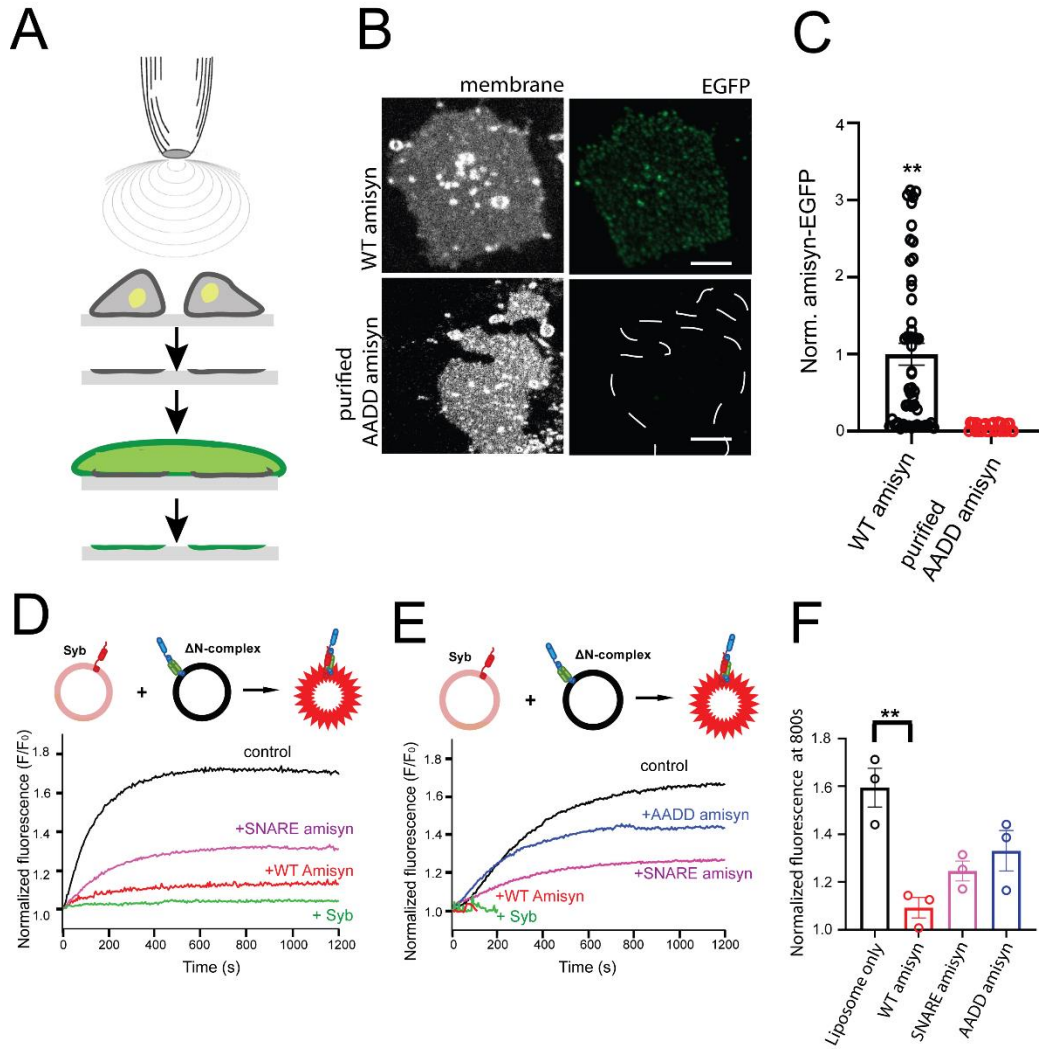


**Figure 3. Recombinant amisyn binds to plasma membranes *in vitro*.**

- (A) Schematic of PC12 plasma membrane sheet preparation by sonication and subsequent immediate incubation with purified recombinant amisyn protein.
- (B) Binding of recombinant WT and AADD-amisyn to membranes from PC12 cells. The purified WT amisyn-EGFP (1 $\mu$ M) or AADD amisyn-EGFP (1 $\mu$ M) were incubated with freshly prepared membranes at RT. WT but not AADD-amisyn-EGFP bound to the membranes (stained with TMA-DPH).
- (C) Quantitative analysis of data as shown in panel (B). Unpaired two-sided t.test, At least 49 sheets/condition from 3 experiments; mean $\pm$ SEM, \*\*\*p<0.001.
- (D) Representative experiment showing full-length WT amisyn inhibiting liposome fusion more efficiently than its SNARE domain. Fluorescence de-quenching of NBD fluorophore labelled liposomes containing

synaptobrevin-2 (Syb) after mixing with liposomes containing  $\Delta$ N complex. Soluble synaptobrevin-2 that competes with synaptobrevin-2 on the liposomes for the SNARE complex formation was added as a control.

- (E) Representative experiment showing that WT amisyn inhibits liposome fusion more efficiently than AADD amisyn mutant. Fluorescence de-quenching of NBD fluorophore labelled liposomes containing synaptobrevin-2 (Syb) after mixing with liposomes containing  $\Delta$ N complex.
- (F) Fluorescence de-quenching of NBD fluorophore labelled liposomes at 800s reveals that WT amisyn inhibits liposome fusion more efficiently than its SNARE domain alone, or AADD-amisyn. Three independent experiments. Mean $\pm$ SEM.

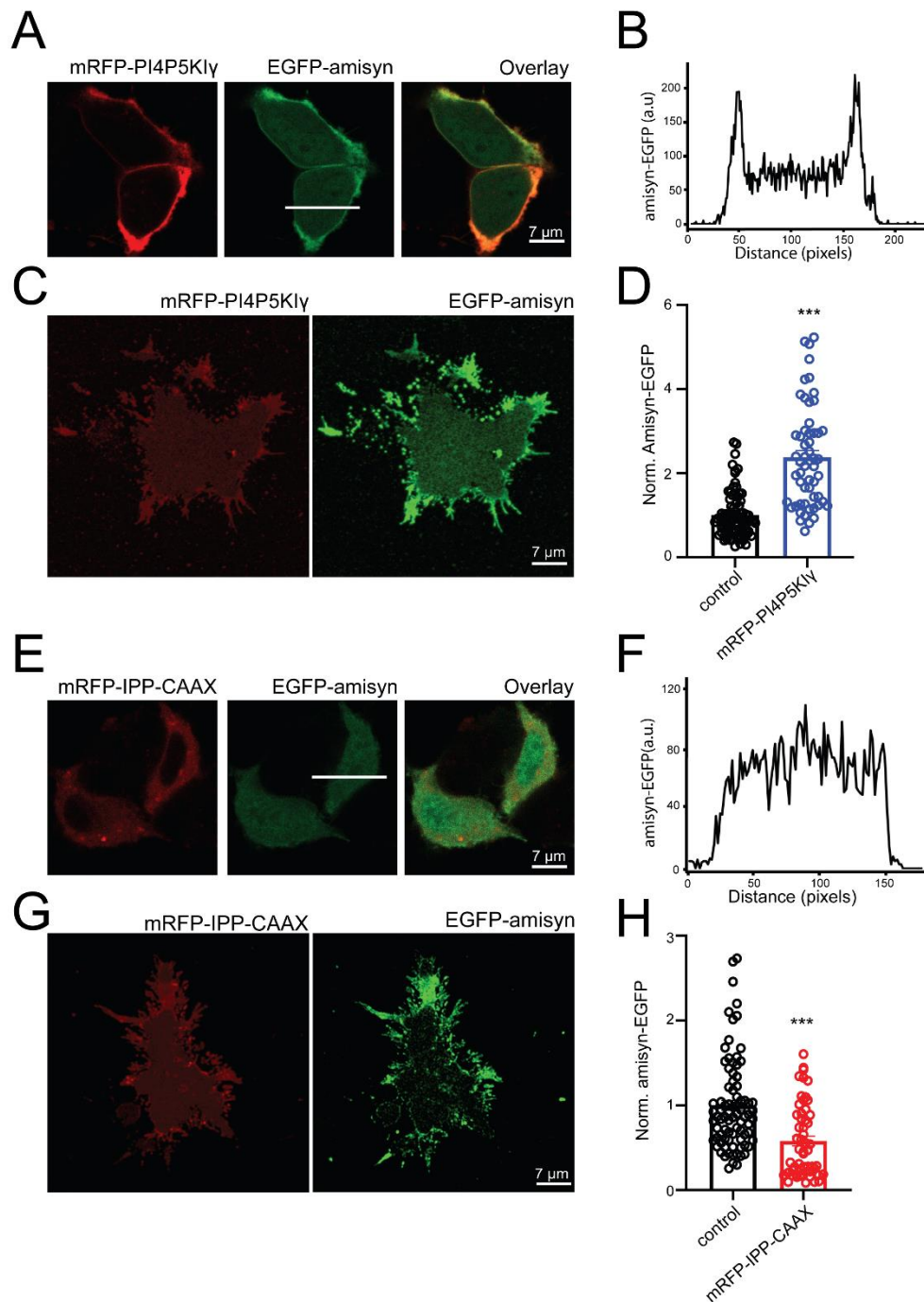


**Figure 4. PI(4,5)P<sub>2</sub> levels control membrane binding of amisyn in PC12 cells.**

- (A) Confocal images of PC12 cells expressing either amisyn-EGFP or mRFP-PI4P5KI $\gamma$ , or both to increase PI(4,5)P<sub>2</sub> in inner leaflet of membrane, resulting in more amisyn associated with the plasma membrane.
- (B) Fluorescence profile of amisyn-EGFP expressing cell through a white line in (A).

- (C) Plasma membrane sheets isolated from co-transfected PC12 cells as in panel (A) contain more amisyn-EGFP.
- (D) Quantitation of amisyn-EGFP fluorescence on the plasma membrane sheets isolated from transfected PC12 cells. 50 sheets/condition, two independent experiments; mean $\pm$ SEM, unpaired two-sided t-test, \*\*\*p<0.001.
- (E) Confocal images of PC12 cells expressing either amisyn-EGFP or mRFP-IPP-CAAX or both, to decrease levels of PI(4,5)P<sub>2</sub> in the inner leaflet of the plasma membranes, resulting in less amisyn-EGFP bound to the plasma membrane.
- (F) Fluorescence profile through amisyn-EGFP expressing cell through a white line in (E).
- (G) Membrane sheets isolated from co-transfected PC12 cells as in panel (E) contain less amisyn-EGFP.
- (H) Quantitative determination of amisyn-EGFP fluorescence intensity on membrane sheets from transfected PC12 cells. 50 sheets/condition, 3 experiments. Mean $\pm$ SEM, unpaired two-sided t-test, \*\*\*p<0.001.

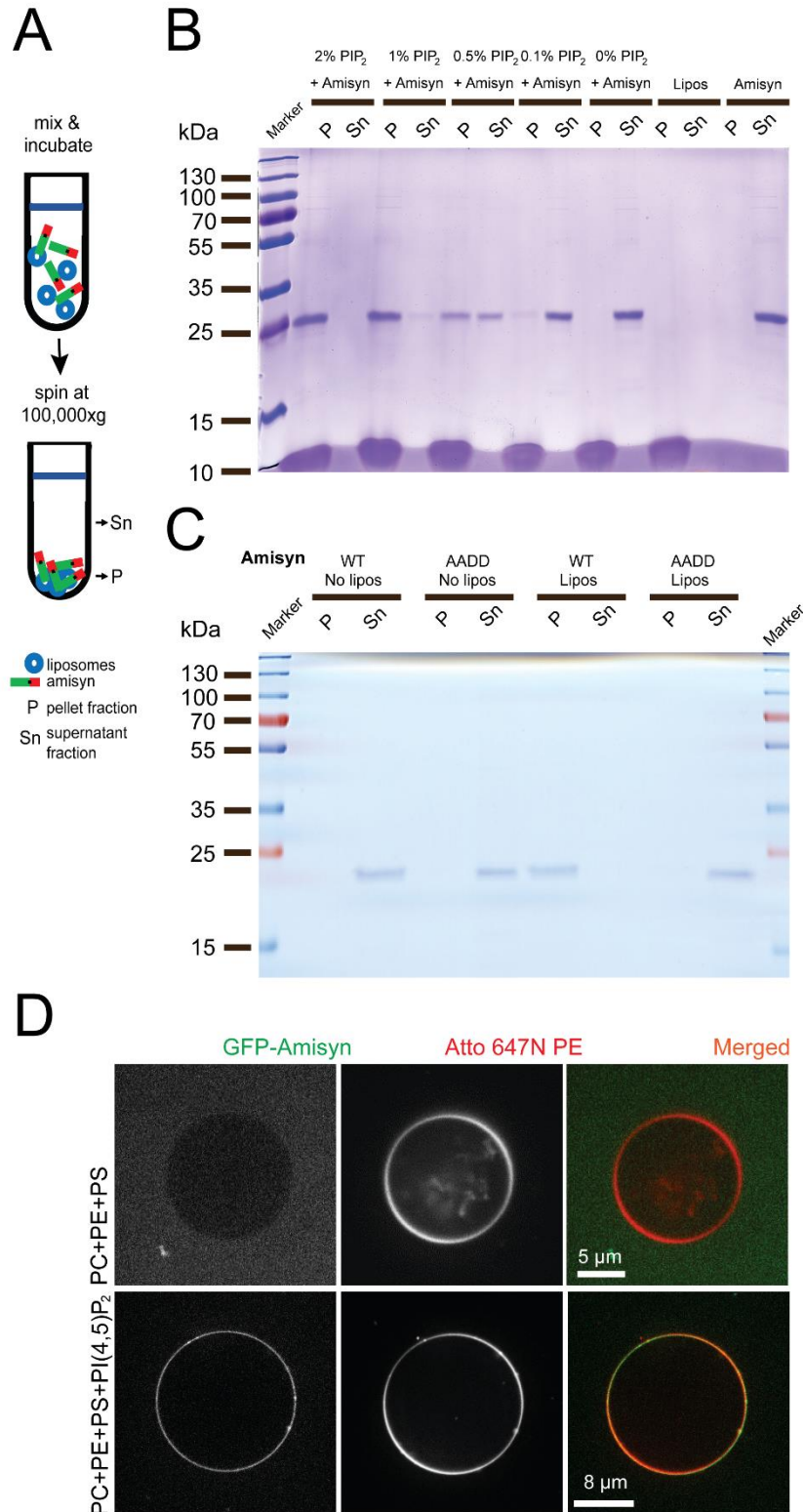


**Figure 5. Liposome binding of amisyn is dependent on PI(4,5)P<sub>2</sub>.**

(A) Schematic representation of a co-sedimentation assay.

(B) Representative co-sedimentation of amisyn with liposomes depends on their PI(4,5)P<sub>2</sub> content (shown in captions over each lane). Representative

SDS-PAGE gel (12%) shows that PI(4,5)P<sub>2</sub> levels in liposomes correlate with more amisyn bound to liposomes co-sedimenting in the pellets (P) relative to the supernatant (Sn). Three independent experiments were performed.

(C) Representative co-sedimentation assay shows that AADD amisyn mutant does not bind well PI(4,5)P<sub>2</sub>-containing liposomes (2%). Representative SDS-PAGE gel (12%) of sedimentation assay. P – pellet, Sn – supernatant; three independent experiments were performed.

(D) Recombinant amisyn-EGFP bound only to liposomes containing PI(4,5)P<sub>2</sub>. Representative confocal images of liposomes without or containing PI(4,5)P<sub>2</sub> (captions on the left). Two experiments with independently purified amisyn-EGFP were performed, each time numerous technical replicates were performed.

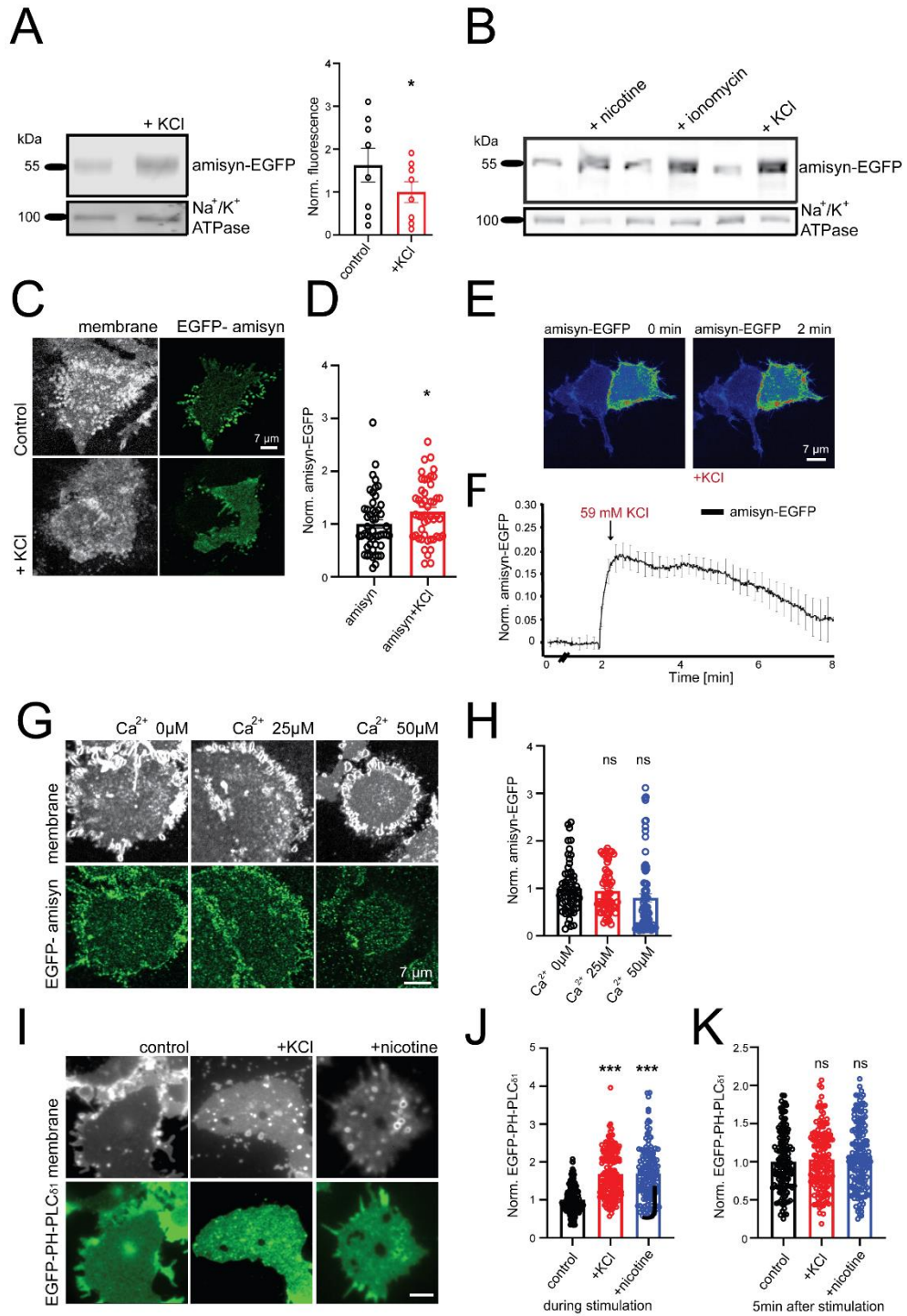


**Figure 6. Stimulation recruits amisyn-EGFP to the plasma membrane of PC12 cells.**

(A) Membranes isolated from PC12 cells after stimulation (59 mM KCl, 5 s) contain more amisyn-EGFP, relative to membranes isolated from naive cells. Na<sup>+</sup>/K<sup>+</sup> ATPase is used as internal loading control and membrane marker. (Left

- panel) Representative Western blots from 8 experiments. (Right panel) quantification. Mean $\pm$ SEM, unpaired two-sided t-test, \* $p < 0.1$ .
- (B) Representative Western blot of membranes isolated from naive PC12 cells and after stimulation as shown in the captions (100  $\mu$ M nicotine, 1  $\mu$ M ionomycin, 59 mM KCl, 5 s). Na<sup>+</sup>/K<sup>+</sup> ATPase was used as internal loading control and membrane marker.
- (C) Membrane sheets generated from stimulated PC12 cells (59 mM KCl, 5 s) contain more amisyn-EGFP than membrane sheets from naive cells.
- (D) Fluorescence quantified from samples as in panel (C) (n=41 sheets/condition, 3 experiments). Mean  $\pm$  SEM; unpaired two-sided t-test, \* $p < 0.1$ .
- (E) Representative confocal images of PC12 cells before and after stimulation (59 mM KCl) demonstrating that stimulation recruited amisyn to plasma membranes.
- (F) Time-course of amisyn-EGFP fluorescence on the plasma membrane in living PC12 cells stimulated with 59 mM KCl. Mean of 15 cells from 3 experiments  $\pm$  SEM.
- (G) Plasma membrane sheets from naive PC12 cells were incubated with recombinant amisyn-EGFP (3  $\mu$ M) and different calcium ion concentrations (captions). (Top) TMA-DPH-stained isolated plasma membranes; (bottom) isolated plasma membranes with bound recombinant amisyn-EGFP.
- (H) Quantification of amisyn fluorescence (as on samples in G) revealed that recruitment of amisyn-EGFP to the plasma membrane was not mediated by calcium ions. At least 46 sheets/condition from 3 experiments. Mean $\pm$ SEM; one-way ANOVA with Tukey's post-hoc test, ns - not significant.
- (I) Plasma membrane sheets isolated from stimulated PC12 cells (59 mM KCl and 100  $\mu$ M nicotine, respectively) were incubated with recombinant EGFP-PH-PLC $\delta_1$  (3  $\mu$ M) for 60 s, washed and fixed. (Top) TMA-DPH dye stains isolated plasma membranes; (bottom) isolated plasma membranes with bound recombinant EGFP-PH-PLC $\delta_1$ . Scale bar 5  $\mu$ m.

(J) Quantification of EGFP-PH-PLC $\delta_1$  fluorescence (as on samples in I) revealed elevated PI(4,5)P $_2$  levels in the plasma membranes of stimulated cells. At least 144 sheets/condition from 3 experiments. Mean $\pm$ SEM; one-way ANOVA with Tukey's post-hoc test, \*\*\*p<0.001.

(K) Plasma membrane sheets were isolated from PC12 cells 5 min post-stimulation (59 mM KCl), immediately incubated with recombinant EGFP-PH-PLC $\delta_1$  (3  $\mu$ M) for 60 s, washed and fixed. Quantification of EGFP-PH-PLC $\delta_1$  fluorescence revealed no change in the levels of PI(4,5)P $_2$  in the plasma membranes between non-stimulated and stimulated cells. At least 144 sheets/condition from 3 experiments. Mean $\pm$ SEM; one-way ANOVA with Tukey's post-hoc test, ns - not significant.

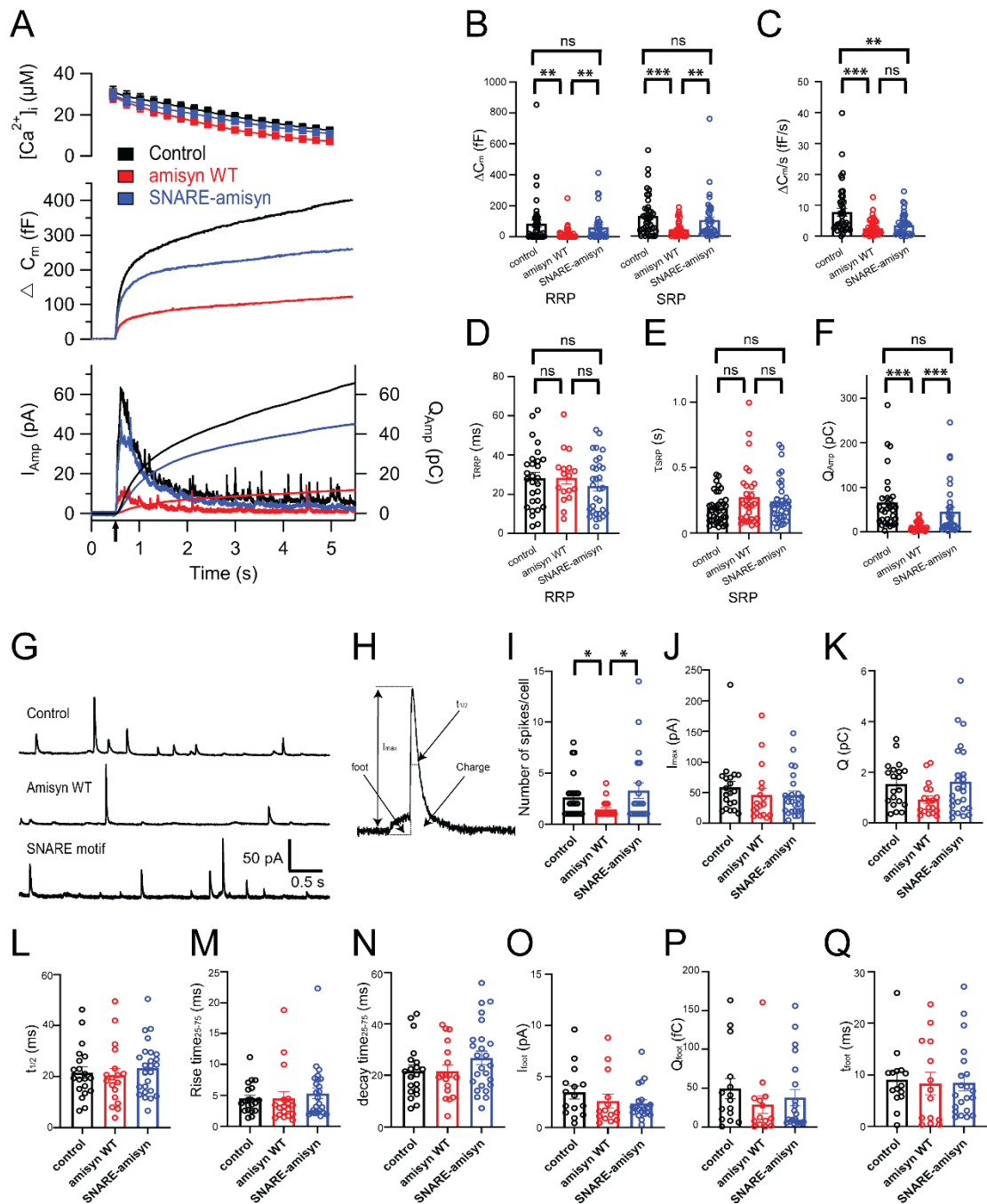


**Figure 7. Amisyn, but not amisyn SNARE-domain, reduced number of released vesicles but did not alter rates of vesicle fusion in bovine chromaffin cells.**

(A-F) Exocytosis induced by UV-flash photolysis of caged calcium ions (stimulus #1, arrow) was reduced in amisyn-loaded chromaffin cells (red trace) compared to control cells (black trace). Cells loaded with amisyn-SNARE protein (blue trace) did not differ significantly from control cells (with an exception of sustained release). 42 control cells, (black); 38 amisyn-loaded cells (red); 38 amisyn-SNARE-loaded cells (blue); from 5 independent

experiments. Kruskal-Wallis test with Dunn's multiple comparison test; ns – non significant, \*\* $p < 0.01$ , \*\*\* $p < 0.001$ .

- (A) Top: intracellular calcium level increase induced by flash photolysis (at  $t = 0.5$  s). Middle: averaged traces of membrane capacitance changes upon  $\text{Ca}^{2+}$ -induced exocytosis. Bottom: mean amperometric current ( $I_{\text{amp}}$ ) (left axis) and cumulative charge (right axis).
- (B-C) Exponential fitting of the capacitance traces revealed changes in RRP and SRP size and sustained phase of release (C). Note the marked reduction in exocytosed vesicles in amisyn-loaded cells.
- (D-E) Fusion kinetics of vesicles from RRP and SRP pools were not altered.
- (F) Reduced detection of catecholamines in chromaffin cells loaded with amisyn by amperometry: cumulative charge during 5s after stimulation.
- (G-Q) Single-spike amperometry analysis revealed problems in vesicle fusion, but no alterations in the stability of the fusion pore. Four experiments and four independent cell preparations, control (20 cells), amisyn WT (18 cells) and amisyn SNARE-domain (25 cells). Mean  $\pm$  SEM. One-way ANOVA with Tukey's post-hoc test, \* $p < 0.05$ .
- (G) Exemplary traces from single spike amperometric recordings of control, amisyn WT and amisyn SNARE-domain injected adrenal chromaffin cells.
- (H) Schematic of analysed amperometric spike parameters.
- (I) Number of fusion events per cell was significantly reduced in chromaffin cells injected with full-length amisyn.
- (J-N) Single spike amplitude (J), charge (K) and the kinetics of single fusion events, such as duration at half-maximal amplitude (L), rise time (M) and decay time (N), were unchanged.
- (O-Q) The stability of the fusion pore was not altered, as revealed by unchanged foot amplitude (O), foot charge (P) and foot duration (Q).

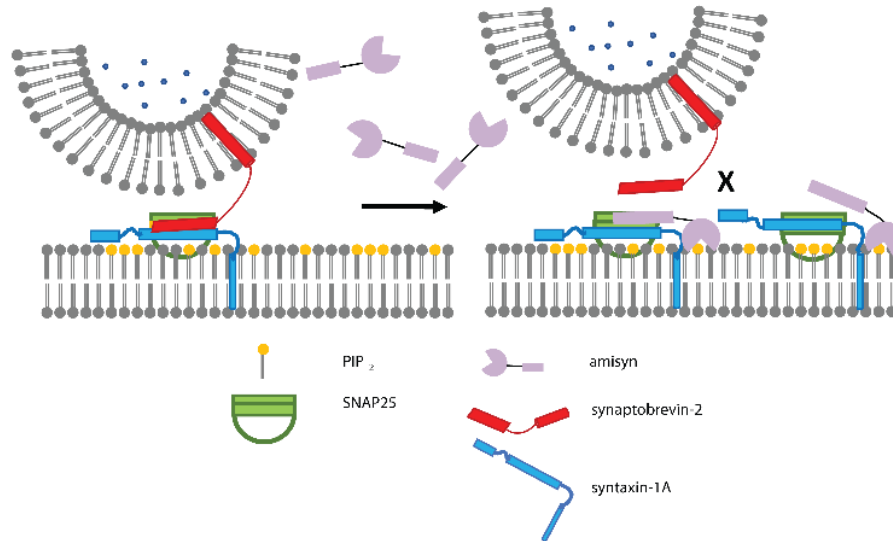
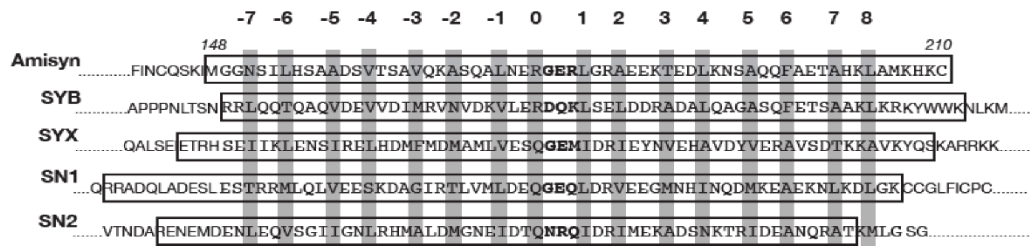


**Figure 8. Model of role of amisyn in secretory vesicle exocytosis**

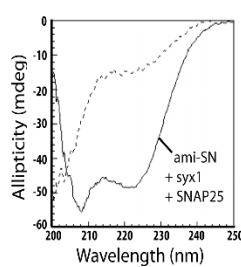
Amisyn acts as a negative regulator of SNARE complex assembly by competing with the 'fusion-active' synaptobrevin-2. Formation of the SNARE complex drives membrane fusion, whereby PI(4,5)P<sub>2</sub> recruits amisyn to the plasma membrane to compete with synaptobrevin-2 in formation of the SNARE complex and vesicle exocytosis. Since amisyn does not contain a trans-membrane domain, it forms a 'fusion-inactive' SNARE complex.

## Supplementary Figures

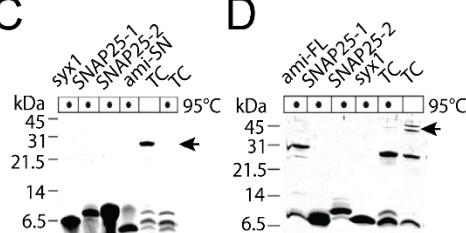
A



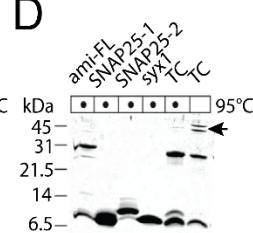
B



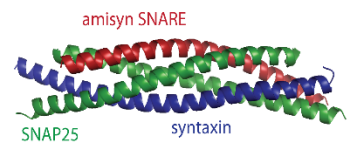
C



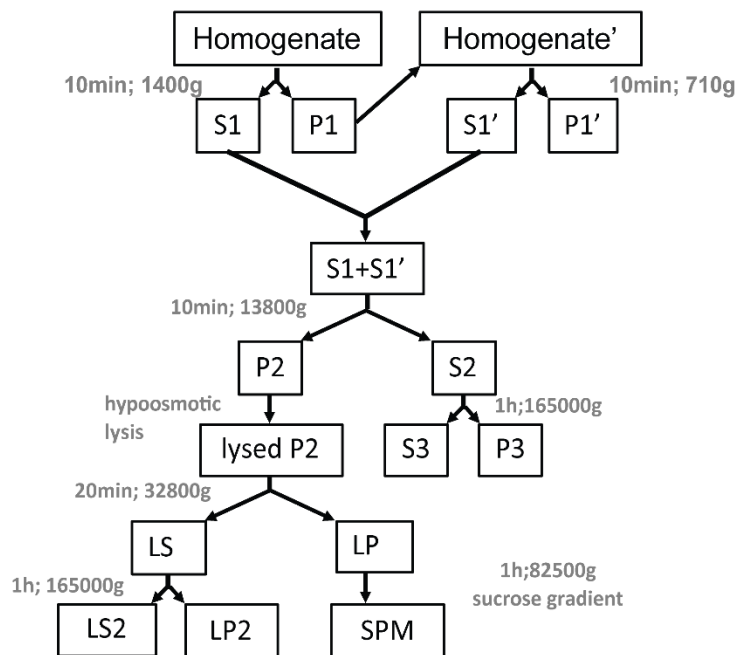
D



E



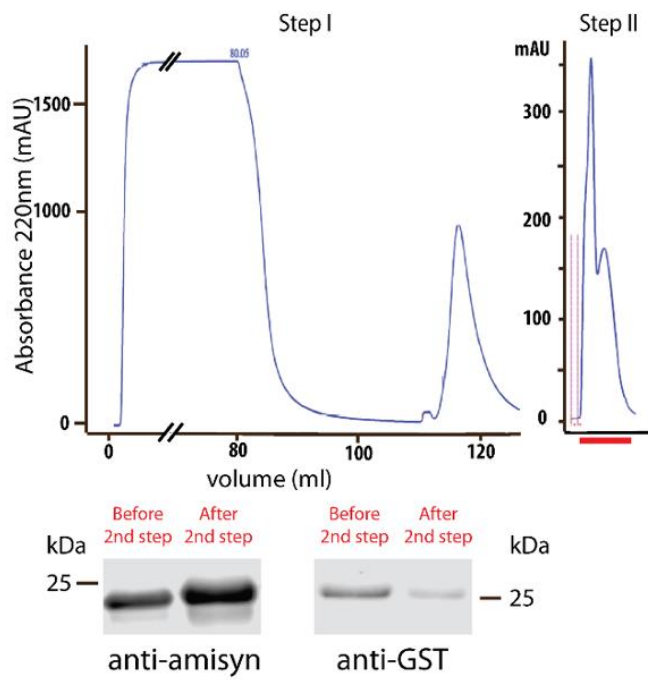
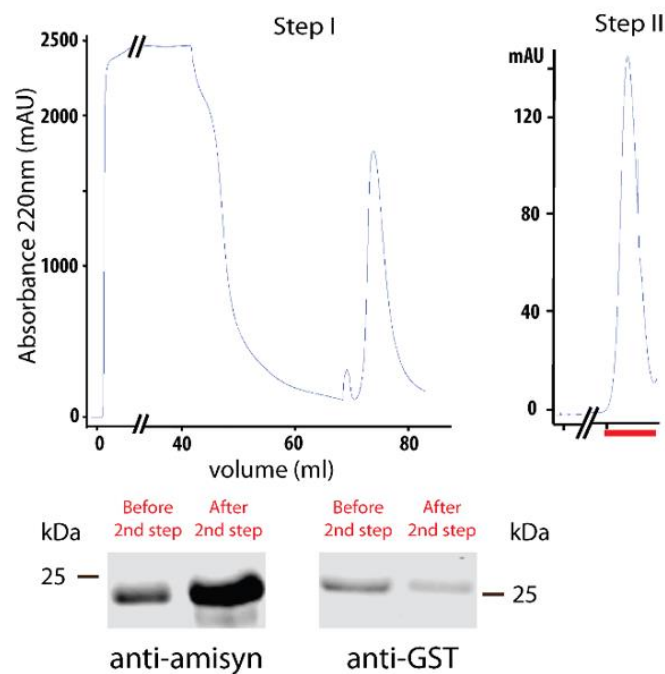
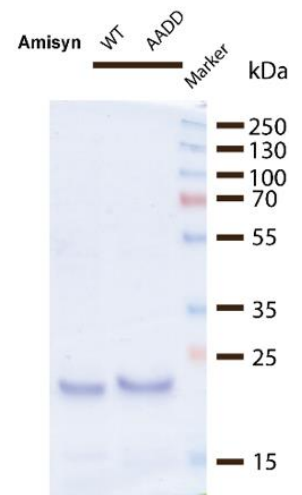
F



## Supplementary Figure S1. Amisyn is a conserved, vertebrate-specific protein that forms SNARE complex with syntaxin-1 and SNAP-25

(A) Sequence alignment of amisyn SNARE motif with those in synaptobrevin-2 (SYB), syntaxin-1a (SYX) and SNAP-25 (SN1 & SN2). The conserved positions of the heptad repeat layers (-7 to +8) are shaded in grey, with the neuronal core SNARE motifs boxed.

- (B) CD spectra reveal structural changes by formation of the amisyn-SNARE complex. The SNARE motif of amisyn (ami-SN) interacts with SNAP-25a and the H3-syntaxin-1a (syx1), and forms the  $\alpha$ -helical SNARE complex (solid tracing). The dotted line represents the theoretical non-interacting spectrum of the monomers.
- (C) The SNARE motif of amisyn (ami-SN) interacts with the Q-SNARE syntaxin-1a (syx1), the first helix of SNAP-25 (SNAP25-1) and the second helix of SNAP-25 (SNAP25-2) to form SDS-resistant ternary complex (TC) (arrowheads) that dissociates by heating at 95°C.
- (D) Full-length amisyn (ami-FL) also formed a ternary complex with Q-SNAREs. We note a presence of two bands: we are not fully aware of the biochemical composition of the second band, but both bands are SDS-resistant and dissociate by heating at 95°C.
- (E) The amisyn SNARE complex is depicted as a parallel four helical coiled-coil bundle, based on the synaptobrevin-2 SNARE complex
- (F) The schematic representation of the brain fractionation protocol used to isolate synaptic plasma membranes.

**A****B****C**

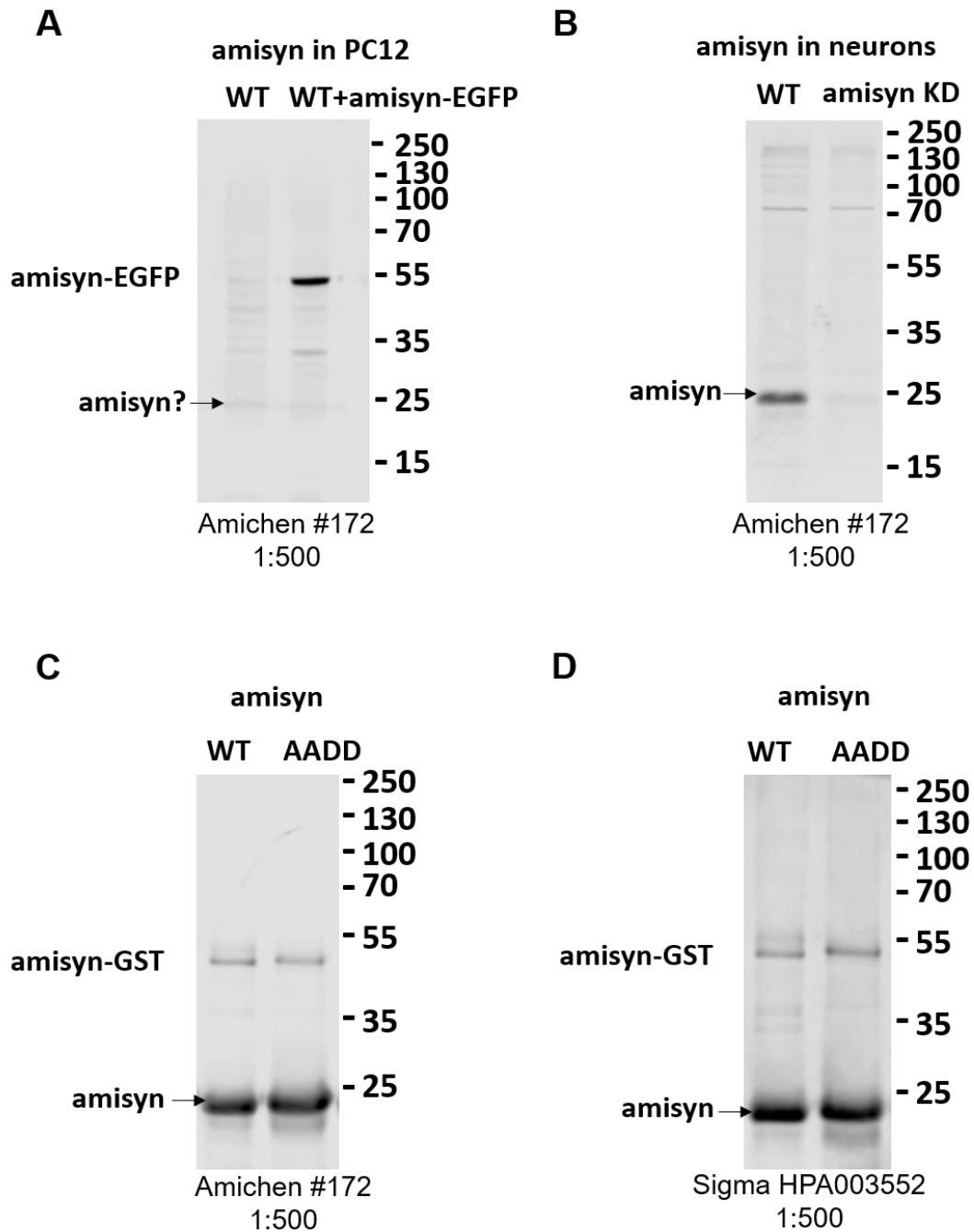
**Suppl. Figure S2. Purification of recombinant amisyn (WT and AADD mutant) proteins.**

(A) Purification of WT amisyn-GST by 2-step affinity purification of amisyn-GST on a GSTrap column before (left panel) and after (right panel) proteolytic cleavage (PreCission Protease).

Lower panels: immunoblotting with antibodies against amisyn (left panel) and GST (right panel).

(B) Purification of AADD amisyn-GST by 2-step affinity purification of amisyn-GST on a GSTrap column. Details as in panel (A).

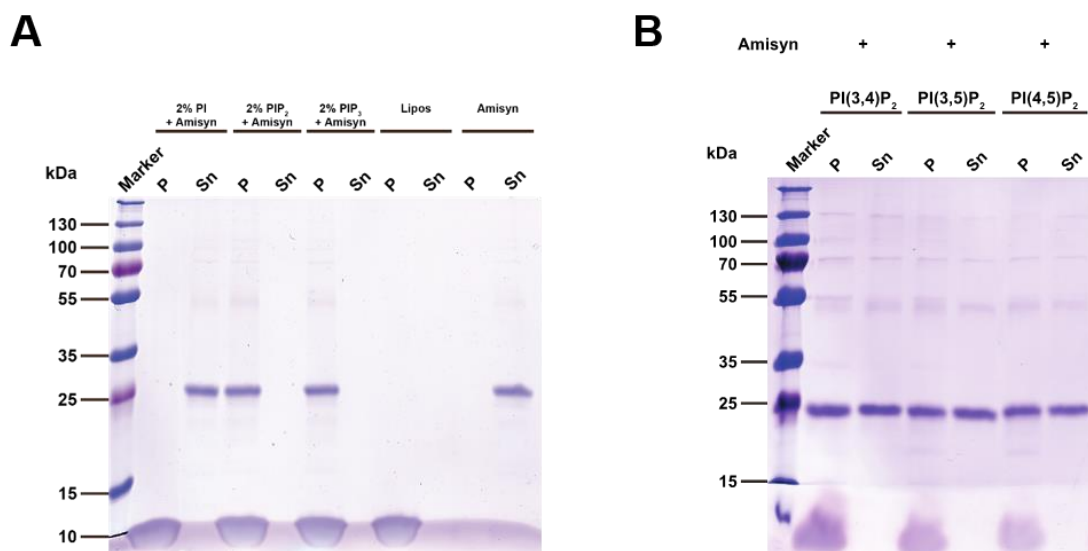
(C) Coomassie staining of SDS-PAGE gel with equal concentrations of WT amisyn and AADD amisyn. The Western blots of the same samples are shown in Suppl. Fig S3.



**Suppl. Figure S3. Specificity of custom-made anti-amisyn polyclonal rabbit antibody.**

(A) Control and amisyn-EGFP transfected PC12 cells (expression for 24h) were collected and equal protein concentrations of the samples were subjected to 12% SDS-PAGE gel. Custom-made anti-amisyn polyclonal rabbit antibody

- (Aminchen #172, 1:500) was used for Western blot. Of note, no specific antibody against amisyn was commercially available when this project started.
- (B) WT neurons and neurons with amisyn knock-down were collected and equal protein concentrations of the samples were subjected to 12% SDS-PAGE gel. Custom-made anti-amisyn polyclonal rabbit antibody (Aminchen #172, 1:500) was used for Western blot.
- (C) Equal concentration of purified recombinant WT and AADD amisyn were subjected to 12% SDS-PAGE gel and blotted with custom-made anti-amisyn polyclonal rabbit antibody (Aminchen #172, 1:500)
- (D) Equal concentration of purified recombinant WT and AADD amisyn were subjected to 12% SDS-PAGE gel and blotted with commercially available antibody from Sigma (Sigma #HPA003552, 1:500).

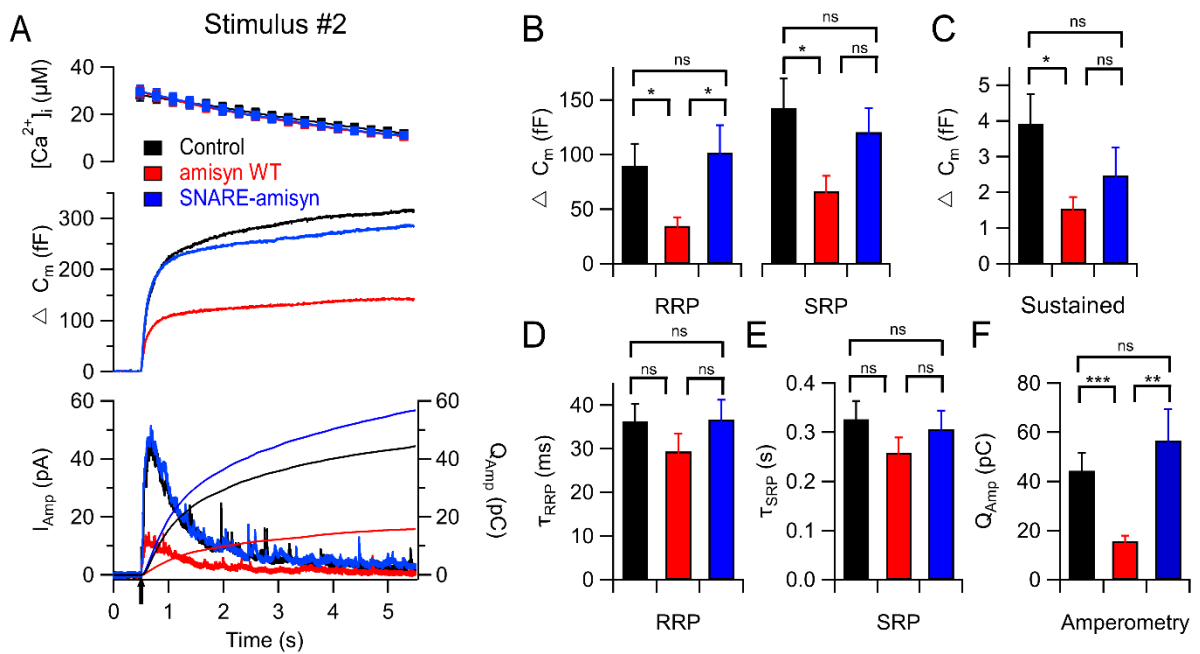


**Suppl. Figure S4. Amisyn interaction with liposomes requires the presence of phosphatidylinositol bisphosphates or phosphatidylinositol trisphosphate.**

- (A) Representative SDS-PAGE (12%) gel with co-sedimentation assay samples showing that amisyn interaction with liposomes depends on the presence of

PI(4,5)P<sub>2</sub> (2%) and PI(3,4,5)P<sub>3</sub> (2%), but not PI (2%). P – pellet, Sn – supernatant. Three independent experiments were performed.

(B) Representative SDS-PAGE (12%) gel with co-sedimentation assay samples showing that amisyn can bind to liposomes containing PI(4,5)P<sub>2</sub> (0.5%), PI(3,4)P<sub>2</sub> (0.5%) or PI(3,5)P<sub>2</sub> (0.5%). P – pellet, Sn – supernatant. Three independent experiments were performed.



**Suppl. Figure S5. Amisyn, but not amisyn SNARE-domain, reduced number of released vesicles but did not alter rates of vesicle fusion in bovine chromaffin cells.**

(A-F) Exocytosis induced by a second stimulus, elicited 100 s after the first stimulus. Similar phenotype for amisyn-loaded and amisyn-SNARE loaded cells was observed like during the first stimulus. Exocytosis induced by UV-flash photolysis of caged calcium ions (stimulus #2, arrow) was reduced in amisyn-loaded chromaffin cells (red trace) compared to control cells (black trace). Cells loaded with amisyn-SNARE protein (blue trace) did not differ significantly from control cells (with an exception of sustained release). Panels are arranged as detailed in Figure 7A-F. 32 control cells, (black); 31

amisyn-loaded cells (red); 33 amisyn-SNARE-loaded cells (blue); from 5 independent experiments. Kruskal-Wallis test with Dunn's multiple comparison test; ns – non significant, \* $p < 0.05$ , \*\* $p < 0.01$ , \*\*\* $p < 0.001$ .

(A) Top: intracellular calcium level increase induced by flash photolysis (at  $t = 0.5$  s). Middle: averaged traces of membrane capacitance changes upon  $Ca^{2+}$ -induced exocytosis. Bottom: mean amperometric current ( $I_{amp}$ )(left axis) and cumulative charge (right axis).

(B-C) Exponential fitting of the capacitance traces revealed significant changes in RRP and SRP size, and sustained phase of release (C).

(D-E) Fusion kinetics of vesicles from RRP and SRP pools were not altered.

(F) Reduced detection of catecholamines in cells loaded with amisyn by amperometry: cumulative charge during 5s after stimulation.

### **3.2 Amisyn regulates release probability at the neuronal synapse**

Jialin JIN<sup>1</sup>, Ronni Cohen<sup>2</sup>, Joana Filipa Mariano Pires<sup>1,\*</sup>, Joana Sofia Lopes Ferreira<sup>1,\*</sup>, Taylan Yazgan<sup>1</sup>, Brett Carter<sup>1</sup>, Uri Ashery<sup>2</sup>, Ira Milosevic<sup>1,3,#</sup>

<sup>1</sup>European Neuroscience Institute Göttingen – A Joint Initiative of the University Medical Center Göttingen and the Max-Planck-Society, Göttingen, Germany´

<sup>2</sup>Tel Aviv University, George S. Wise Faculty of Life Sciences, and the Sagol School of Neuroscience, Tel Aviv, Israel

<sup>3</sup>Wellcome Centre for Human Genetics, Nuffield Department of Medicine, University of Oxford, England

\*these coauthors contributed equally, in alphabetical order

#Corresponding author

**Paper 2 (Prepared for submission)**

## **ABSTRACT**

Neurotransmission is controlled both by positive and negative regulators. Amisyn is a poorly studied vertebrate-specific SNARE protein. Previous studies revealed its basic role in exocytosis of neurosecretory cells, yet the functions of this brain-enriched protein at the synapse and in neurotransmission remain unknown. We generated an amisyn mutant mouse line, which revealed amisyn's role in the regulation of synaptic vesicle pools and release probability at the presynaptic site. These changes were accompanied by an increase in the levels of peripheral synaptic vesicle proteins Rab3a and  $\alpha$ -synuclein, while the levels of VAMP2, presumed to be amisyn's competitor, decreased. Mutant mice showed autism-related behavior and impairment in learning and memory formation. Curiously, long-term potentiation was almost diminished. Our data highlight amisyn as an important factor for neurotransmission and plasticity in mammals.

## INTRODUCTION

Exocytosis, a process that mediates secretory vesicle fusion and release of its content, controls many biological events such as synaptic transmission and other secretion processes. The transmission of neural signals is crucial for brain activity and even survival. Exocytosis of synaptic vesicles is a vital process in neurotransmission, and includes a series of complex protein-protein and protein-lipid interactions. The mechanisms underlying exocytosis and its regulation have been studied since the 1980s, and many exocytosis-involved proteins have been identified and characterized. Among exocytosis regulators, SNARE (soluble N-ethylmaleimide-sensitive factor (NSF) attachment protein receptor) proteins are essential for the docking, priming, and fusion of synaptic vesicles (Terrian & White, 1997). As a common feature of this protein family, all SNARE protein contains a common, homologous domain of 60-70 amino acids, which is also called a SNARE motif (Weimbs et al., 1998). SNARE proteins are further classified into four subfamilies according to the structure of their SNARE motifs (Fasshauer et al., 1998). SNARE motifs can spontaneously form a thermostable core complex of alpha-helices, which is called SNARE complex (Sollner et al., 1993; Sutton et al., 1998). In neurotransmission, the formation of a SNARE complex helps the docking and priming of vesicles and the formation of the fusion pore (Lopez-Font, Torregrosa-Hetland, Villanueva, & Gutierrez, 2010; Misura et al., 2000). The neuronal SNARE complex contains three different SNARE proteins: syntaxin-1 (Bennett et al., 1992; Sollner et al., 1993), synaptosome-associated protein 25 (SNAP-25) (Blasi, Chapman, Link, et al., 1993; Oyler et al., 1989; Veit et al., 1996), and vesicle associated membrane protein 2 (VAMP2, also known as synaptobrevin2) (Baumert et al., 1989; Blasi, Chapman, Link, et al., 1993; Blasi, Chapman, Yamasaki, et al., 1993; Trimble et al., 1988). Syntaxin-1 and SNAP-25 reside on the plasma membrane, and are able to dock the vesicle onto the plasma membrane when they bind to VAMP2 on the vesicle membrane (Misura et al., 2000). The complex stabilizes the vesicle's interactions with the plasma membrane during the fusion and release of neurotransmitters (Jahn & Fasshauer, 2012).

Other than these three main proteins that form the SNARE complex, many other proteins coordinate the process of neurosecretion. Some proteins, such as synaptotagmins and Munc18, can promote and accelerate the exocytosis process, acting as positive regulators of exocytosis, and have been extensively studied (Prinslow et al., 2019; Zhou et al., 2015). Negative regulators of the exocytosis process have been described (An & Zenisek, 2004), but much less is known about their functions in the cell and how they regulate secretion. In general, the SNARE motifs of negative regulators are thought to interfere with the formation of the functional neuronal SNARE complex and prevent the exocytosis process. The proteins tomosyn and complexin are two examples of SNARE motif containing negative regulators of exocytosis (Fujita et al., 1998; McMahon et al., 1995).

Similar to tomosyn and complexin, amisyn (also known by its gene name as syntaxin-binding protein 6 or STXBP6) also contains a C-terminal SNARE-motif. First reported in 2002, amisyn is a 24 kDa brain-enriched protein (Scales et al., 2002). Mutations in amisyn have been associated with several diseases, including cancer, diabetes, and autism spectrum disorder (ASD) (Barg & Gucek, 2016; Castermans et al., 2008; Collins et al., 2016; Lenka et al., 2017; Y. Liu et al., 2021). Immunoprecipitation results have shown a direct interaction between amisyn and syntaxin-1a and syntaxin-4 (Scales et al., 2002). Furthermore, amisyn's SNARE-motif allows amisyn to form a complex with syntaxin-1a and SNAP-25. In addition to the SNARE-motif, amisyn also contains an N-terminal pleckstrin homology (PH) domain that allows it to bind to phosphatidylinositol-4,5-bisphosphate [PI(4,5)P<sub>2</sub>], which is a signaling lipid on the plasma membrane (Kondratiuk et al., 2020). This PH domain facilitates the recruitment of amisyn to the plasma membrane after neurosecretory cell stimulation.

It has been reported that excess full-length amisyn in cultured neurosecretory PC12 cells can inhibit neurosecretion (Constable et al., 2005). Amperometry-based experiments on chromaffin cells have also revealed that full-length amisyn reduces secretion and alters the dynamic properties of vesicle fusion (Constable et al., 2005). Furthermore, excess of externally-added amisyn also leads to a decrease of the readily

releasable vesicle pool (RRP) as well as the slowly releasable vesicle pool (SRP) size in chromaffin cells (Kondratiuk et al., 2020). Experiments have also revealed that both the SNARE-domain and the PH-domain are involved in the inhibition of secretion. In addition to neurons, overexpression of amisyn interferes with pancreatic  $\beta$ -cell insulin-secretion (Collins et al., 2016). Further studies have suggested that amisyn may be recruited to the exocytic site in  $\beta$ -cells by the cAMP-sensor EPAC2 (Gucek et al., 2019). Recent research on a mouse model that lacks amisyn revealed a decrease in body weight in comparison to the wild-type (WT) mice (C. Liu et al., 2021). Although these experimental results indicate an inhibitory function of amisyn in exocytosis, a physiological characterization of this protein is still lacking and the detailed function of amisyn in neurotransmission requires further determination.

Here, we report a newly established amisyn mutant mouse line STXBP6<sup>tm1a</sup> in which the expression of amisyn was reduced by ~90%. Physiological characterization of mutant revealed amisyn's role in the regulation of exocytosis at neuronal synapses. The mutant hippocampal synapses feature enhanced synaptic vesicle release probability, enlarged RRP size, and diminished LTP. Behavioral characterization revealed impairments in learning and memory formation, and an also autism-like phenotypes.

## **METHODS**

### **Animals**

STXBP6<sup>tm1a</sup>, also referred to as amisyn mutant mice (background: C57BL/6), were generated and used in this study. All animal procedures complied with the national animal care guidelines and were approved by the University Medical Center Göttingen board for animal welfare and the animal welfare office of the state of Lower Saxony (LAVES).

### **Behavioral experiments**

Before habituation, animals were placed under a 12/12 h light/dark reverse cycles with ad libitum access to food and water. During habituation, the light/dark cycle changed by 1 hour each day until all experimental animals were active during the daytime, while avoiding anxiety. Animals were first assessed using an Elevated Plus Maze test and the open field test. Briefly, in the open field test, mice were placed in the center of a square open field arena (a white bottom, completely opaque plastic box: length 72 cm, width 72 cm, and height 40 cm) for 10 min. The time spent in the central area (36 × 36 cm) were recorded by video tracking software (TSE system, Berlin, Germany), and the time spent on self-grooming was manually recorded later. Novel object recognition experiments were also performed using the open field arena, during which mice were placed in the open field arena with two identical objects (either set a: beverage cans, or set b: similarly sized and shaped sauce bottles) for 10 min. On the following day, one of the objects was replaced by an object from the other set, and the animals were placed in the chamber again for 10 min. The time animals spent exploring each object was recorded during the experiment. Exploration was defined as having the nose-point within ~2 cm around the objects.

Three-chamber tests were applied in a specific custom-made three-chambered arena (length 60 cm, width 20 cm, height 28 cm, outer wall opaque). The arena was separated equally into three individual chambers by partially opaque plastic walls, each of which had a door that allowed mice to pass from chamber to chamber when it opened. The left and right chamber contained a wire cage (height 10 cm, diameter 8

cm, in white color). The whole experiment consisted of two phases. In phase 1, the two wire cages were empty. The test animal was placed in the middle chamber with the two doors initially closed, and could freely explore the middle chamber for 5 min. Then, the doors were opened, and the animal was free to explore all chambers for an additional 5 min. In phase 2, a familiar, same-sex stimulus mouse (from the same housing cage) was placed in the wire cage of either the right or left chamber randomly. The test animal was placed in the central chamber with both doors open, and was allowed to explore all chambers for 10 min. Behavior was recorded and analyzed for the time test animal spent with exploring empty cage and the habituated cage (exploration was defined as the nose point being within 2cm from the cage, excluding time spent on top of the cage).

T-maze tests were applied in a custom-made T-shape maze with two 28 cm arms and one 35 cm arm. The height of the maze was 10 cm and sliding doors were set between the arms. A small well (diameter: 2 cm) was placed at the end of each arm. Before the experiment, food restriction was applied to all test animals to guarantee the allure of the bait (condensed milk) during the experiments. The experiments consisted of three different phases. In the first phase, each test animal was placed in the maze with all doors open and unlimited bait provided in the wells for 10 min. In the second phase, the test animal was placed in the long arm with the bait in its well, and was allowed to explore either short arm. Once it chose an arm, the sliding door to the opposite short arm closed. When the mouse returned to the long arm, the sliding door closed for 30 sec. This procedure continued for 10 min. In the third phase, the test animal was placed in the long arm with the bait. Upon entering one of the short arms, the door to the opposite arm closed. Once the animal returned to the initial arm, the door closed for 30 sec, and after that the animal could choose to enter a short arm again. The arm most recently visited did not contain a reward, and the other did. The same procedure was repeated for 10 min, and once a reward was consumed, the other target arm was baited for the subsequent trial. Entry into the baited arm was considered a success, and entry into the arm with no bait was considered a failure.

A fear-discrimination experiment was performed using a multi-condition system (TSE

system, Berlin, Germany) that consists of two separate closed chambers and a central control module. Each animal was kept in a small cage in the chamber, and an 0.75 mA pulse electric shock were delivered to mice as fear stimulation. During the experiment, mice were assigned to one of two different contexts. In context A, there was low light illumination, no sound, a scent of 40% ethanol, and a particular visual pattern on the inner walls. In context B, there was high light illumination, continuous white noise, the scent of 1% acetic acid, and no pattern on the inner wall. The experimental animals were randomly separated into two groups. Half the animals were assigned context A as the shocking context, and the other half were assigned context B; the other context was the non-shock context. The experiment consisted of two phases. In phase one, animals were placed in the shock context for 210 sec and received a 2s shock at the 178 sec. In phase two, animals are placed randomly in either the shock or non-shock context, and were placed in the other context after 1.5 hour. The order of contexts presented each day was pseudo-randomly assigned. The freezing time in different the context was recorded during the experiment.

### **Hippocampal slice preparation**

Wild-type (WT; +/+) and amisyn mutant (-/-) mice (P11–P17 for LTP recording, P19–P30 for other recordings, either sex) were anesthetized by diethyl ether and decapitated. The brains were quickly removed and horizontally sliced (300–400  $\mu\text{m}$ ) in an ice-cold cutting buffer using a vibratome (VT1200S, Leica). The cutting buffer composition was as follows (in mM): 26  $\text{NaHCO}_3$ , 1.25  $\text{NaH}_2\text{PO}_4$ , 4  $\text{KCl}$ , 10 glucose, 230 sucrose, 0.5  $\text{CaCl}_2$ , and 10  $\text{MgSO}_4$  (pH 7.4, osmolarity  $\sim 305$  mOsm/L; equilibrated with 95%  $\text{O}_2$  and 5%  $\text{CO}_2$ ). The brain slices were then transferred to a custom-made holding chamber containing the artificial cerebrospinal fluid (ACSF) solution, incubated at 37  $^\circ\text{C}$  for at least 30 min, and further recovered at room temperature for more than 1 hour before recording. ACSF solution composition was as follows (composition in mM): 125  $\text{NaCl}$ , 26  $\text{NaHCO}_3$ , 2.5  $\text{KCl}$ , 1.25  $\text{NaH}_2\text{PO}_4$ , 1  $\text{MgCl}_2$ , 2  $\text{CaCl}_2$ , and 25 glucose (pH 7.4, osmolarity  $\sim 305$  mOsm/L; equilibrated with

95% O<sub>2</sub> and 5% CO<sub>2</sub>).

### **Electrophysiology**

Recording patch pipettes for whole-cell recordings were pulled from borosilicate glass (GB150TF-10, Science Products) with an open-tip resistance of 2–5 MΩ (for whole-cell recordings) or a PG52151-4 (World Precision Instruments) with a resistance of 0.8-2 MΩ (for field recordings). Stimulation pipettes were pulled from borosilicate glass G-150F-4 (Warner Instruments) with a tip of ~100 μm. All pulling was conducted using a Model P-1000 puller (Sutter Instrument).

During whole-cell recordings, brain slices were placed in a custom-made recording chamber maintained at 37°C, and were continually perfused with oxygenated ACSF (rate: 2.5 ml/min). Cells were examined in a whole-cell configuration under the voltage clamp mode at a holding potential of -70 mV. Recordings were made using a custom-assembled rig consisting of a Faraday cage, a microscope (Zeiss Axio), a micromanipulator (Patchstar 360, Scientifica), a temperature manipulation model (TC-20, NPI), a perfusion system (PPS2, Multichannel system), and an amplifier (EPC10, HEKA). During recording, pyramidal cells in the CA1 region (stimulated by Schaffer collaterals) or CA3 region (stimulated by mossy fibers) were visually selected and patch clamped. Extracellular stimulation was performed using a stimulus isolation unit (DS2A, Digitimer Ltd.). Stimulus electrodes were filled with ACSF and positioned at ~500 μm from the recording electrode in the stratum radiatum (Schaffer collaterals), or the hilus adjacent to the dentate granule cell layer (mossy fibers), respectively. Data were acquired using Patchmaster software (HEKA) at an acquisition rate of 20 kHz and filtered at 2 kHz. During recordings, recording pipettes were filled with an internal solution with the following composition: 130 mM CsMeSO<sub>4</sub>, 2.67 mM CsCl, 10 mM HEPES, 1 mM EGTA, 3 mM QX-314-Cl, 5 mM TEA-Cl, 15 mM creatine phosphate disodium, 4 mM Mg-ATP, 0.3 mM Na-GTP, and 5 mM creatine phosphokinase; pH was adjusted to 7.4 using CsOH, osmolarity was measured ~305 mOsm. Uncompensated series resistance (R<sub>s</sub>) was monitored by the delivery of a 5 mV voltage step at defined points during the recording. . Recordings

were stopped or excluded if the  $R_s$  was over 20 M $\Omega$  or changed by more than 20%. For mossy fiber recordings, 10  $\mu$ M DCG-IV was added to bath solution at the end of the experiment to confirm that the recording was from mossy fiber stimulation. For miniature postsynaptic current recordings, 500 nM TTX was added in the perfusion ACSF. Events were analyzed using a custom-written macro in Igor Pro 6.36 software, as previously described in Clements et al. (Clements & Bekkers, 1997). For pool size and recovery rate estimation, data are analyzed as described by Schneggenburger et al. (Schneggenburger, Meyer, & Neher, 1999). Data were further analyzed in Igor Pro (version 6.36) and Excel, and plotted using Prism 8 (GraphPad).

During field recordings, the slices were cut between CA1 and CA3 regions before the experiment to reduce recurrent excitation. Brain slices were placed in a custom-made recording chamber kept at room temperature, and were continually perfused with oxygenated ACSF (rate: 2.5 ml/min). 10  $\mu$ M bicuculine methiodide was present in the ACSF during the recordings to block GABA<sub>A</sub>R activity. The recording pipette was filled with ACSF and placed in the stratum radiatum of CA1. Extracellular stimulation was performed using a stimulus isolation unit (DS2A, Digitimer Ltd.). Stimulus electrodes were filled with ACSF and positioned  $\sim$ 500  $\mu$ m from the recording electrode. These recordings were made using a custom-assembled rig that included a Faraday cage, a microscope (BX51WI, Olympus), a micromanipulator (MP-225 Sutter Instrument), a CV-7B patch clamp headstage (Axon Instrument), a perfusion system (PPS2 Multichannel system), and an amplifier (EPC10 HEKA). Data were acquired with multi-channel software and Igor Oro 8.0 (HEKA) at an acquisition rate of 20 kHz, and were filtered at 2 kHz. The recording procedure consisted of a 30-60 min baseline recording, 4 sets of 100 stimuli high-frequency train stimulation (100 Hz, 45 sec between each set), and a 1 h post-LTP recording. After recordings, 10  $\mu$ M NBQX was added to the bath solution to confirm that the signal originated from synaptic responses. Recordings were excluded if the baseline recording of the last 15 min changed by more than 20%. Data were further analyzed using Igor Pro 6.36 and Excel, and plotted using Prism 8 (GraphPad).

### **Plasmids and antibodies**

We generated pEGFP-amisyn WT and pGEX-amisyn WT plasmids for this study. Full-length cDNA coding for amisyn (GenBank: BC009499.2, aa 1-210) was amplified by polymerase chain reaction (PCR) using primers 5'-CCGGAATTCATGAGTGCCAAATCTGCTATCAG-3' and 5'-CGCGGATCCCCACATTTGTGCTTCATGGCAAGCT-3' (original plasmid provided by T. Weimbs, UC Santa Barbara), and was sub-cloned in the pEGFP-N1 vector using EcoRI and BamHI restriction sites. Subsequently, cDNA was amplified using primers 5'-CGGGATCCATGAGTGCCAAATCTGCTATCAG-3' and 5'-CGGAATTCCGTTATTAACATTTGTGCTTCATGGCAAGCT-3' and subcloned in the pGEX-6p1 vector using BamHI and EcoRI restriction sites. Both constructs were verified by control restriction enzyme digestions and by sequencing.

A custom-made polyclonal amisyn antibody was generated against full-length recombinant amisyn. The antibody generation process has been described by Kondratiuk et al. (Kondratiuk et al., 2020). The list of commercial antibodies and their dilutions is presented in the Supplementary Information.

### **Brain Homogenate Preparation**

The hippocampus or cortex was isolated from P14-P30 amisyn WT/mutant mice and homogenized in 1080  $\mu$ l ice-cold homogenization buffer (80 mM NaCl, 1 mM EDTA, 20 mM HEPES, Protease Inhibitor Cocktail, phosSTOP phosphatase inhibitor, 1 mM dithiothreitol, pH 7.4). Homogenization was achieved by twice oscillating with metallic beads (20-30 Hz, 1 min) on a mixer mill (Retsch, MM400). Between the two oscillations, 120  $\mu$ l 20% SDS was added. The homogenate was further mixed with a 27G needle. The protein concentration was quantified using a BCA assay kit (Thermo Scientific) with a spectrophotometer (Infinite F200, Tecan).

### **Western blotting**

Hippocampus/cortex homogenate samples were prepared by mixing the lysates with 6X Laemmli buffer (62.5 mM Tris, 50% glycerol, 12% SDS, 0.06% bromophenol

blue, 5% 2-mercaptoethanol added before use) and denatured for 5 min at 95°C. Samples were then loaded onto custom-made SDS-PAGE gels (12%, pH 8.8). A Bio-Rad electrophoresis system (PowerPack™ Basic) was used to perform the separation, depending on the protein analyzed by immunoblotting. Electrophoresis was achieved at 120 V in the presence of 1X running buffer (12 mM Tris base, 96 mM glycine, 5 ml 10% SDS in 1000 ml H<sub>2</sub>O).

After electrophoresis, the proteins were transferred onto a nitrocellulose membrane using the BIO-RAD transfer system filled with 1X transfer buffer (25 mM Tris-Base, 0.2 M glycine, 20% methanol). The transfer was done at 25 V overnight or 100 V for 90 min at 4°C. The membrane was blocked in 5% milk prepared in 1X Tris-Buffered Saline with an additional 0.1% Tween 20 at room temperature for 1 hour. It was followed by overnight incubation at 4°C with diluted primary antibody. The membrane was then washed with Tris-Buffered Saline with an additional 0.1% Tween 20 to remove any non-specific bound antibody (three short washes followed by three 5-min washes). Then, the membrane was incubated with secondary antibody for 1 hour at room temperature, followed by the washing steps already described. The fluorescent bands were then detected using an infrared imaging system (150 Odyssey, Li-Cor). The band intensity was normalized to the loading control (RPL7/GAPDH) when comparing different cell/tissue types samples.

### **Quantitative PCR**

To isolate the RNA, the hippocampus/cortex tissue from P14-30 animals was grinded into a thin powder. After adding 1 ml of Trizol into the powder, the mixture was incubated for 5 min. After the incubation, 0.2 ml of chloroform was added, followed by incubation at room temperature for 3 min and centrifugation (12000 xg, 15 min, 4°C). After centrifugation, 0.5 ml of 100% isopropanol was added to the aqueous supernatant and incubated for 10 min at room temperature. After another centrifugation (12000 xg, 10 min, 4°C), 1 ml of 75% ethanol was added to the pellet. The mixtures were centrifuged again (12000 xg, 10 min, 4°C) and the pellet was left to dry for 10 min. Finally, 20-50 µl of RNase-Free water (Biolab products, 31-00847)

was added, and the samples were incubated for 15 min at 55°C to remove the remaining ethanol.

To synthesize cDNA from the isolated RNA, a master mix composed of 5 µl nuclease-free water, 4 µl 5x iScript reaction mix, and 1 µl iScript reverse transcriptase (cDNA synthesis kit – BioRad, 1708890) (volumes/reaction) was made. Isolated RNAs were diluted with nuclease-free water in a final volume of 10 µl and an RNA mass of 1000 ng. Then, 10 µl of the master mix was added to the diluted RNA. The mixture was further put into the thermocycler (UNOII Biometra®) to run a cDNA synthesis program. After around 20 min, the cDNA was diluted with miliQ water at a ratio of 1:50.

The qPCR was done in the thermocycler (QuadStudio 6 Flex, Applied Biosystems, Life Technologies), and each reaction contained 4 µl of the master mix (90% SYBR® Green - BioLabs, M3003E, 5% reverse primer, and 5% forwarding primer) and 4 µl of the sample. The generated data were exported to an excel file by Real-Time PCR Software (QuantStudio). The CT values were converted in  $\Delta\Delta CT$  by normalizing the data to the RPL7 gene; these values were then converted into expression levels. Data were further analyzed and plotted using Prism 6 (GraphPad).

### **Statistical analysis**

Unless otherwise stated, all statistical analyses were performed using Prism (GraphPad) or Igor Pro 8 (Wavemetrics) software. Where indicated, nonparametric one-way ANOVA tests were used for comparing population means, with significance set at  $p < 0.05$ . An unpaired two-sided t-test with Tukey's correction was used for between-group comparisons. Electrophysiological data were analyzed using the Kruskal-Wallis test with Dunn's multiple comparison test. Unless otherwise stated, data are presented as the mean  $\pm$  SEM.

## RESULTS

### **Amisyn is enriched in the hippocampus, especially in the dentate gyrus**

Amisyn was originally reported to be enriched in the brain (Scales et al., 2002), but a detailed analysis of amisyn expression distribution has not previously been performed. Using brain sagittal slices and with reference to a publicly available database, the Allen Brain Atlas, the results suggest that mRNA levels of amisyn are high in the hippocampus, especially in the dentate gyrus region. To test the expression level of amisyn protein, we used a specific anti-STXBP6 antibody for immunohistochemistry experiments on WT (C57BL/6/J) sagittal slices. The experiment revealed high concentrations of amisyn in the hippocampus (**Figure 1A**). Within the hippocampus, expression in the granular cell layer of the dentate gyrus, hilus, and stratum radiatum of the CA2 region was stronger than expression in the CA1 and CA3 regions (**Figure 1A**).

### **Generation of STXBP6<sup>tm1a</sup> mutant mice and verification of new line**

Although reported 19 years ago, the physiological properties of amisyn have never been studied *in vivo* due to the lack of an adequate animal model. To overcome this barrier, we generated an amisyn mutant mouse line STXBP6<sup>tm1a</sup> using stem cells from the KOMP repository (Project #38643). First, genetically modified embryonic stem cells (JM8A3.N1 line with a mutation in the agouti gene; Pettitt et al., 2009) with an altered *STXBP6* gene (insertion of an intron tm1a in exon 2) were propagated to reach the desired number of cells suitable for injections into C57BL/6N atm1Brd female mice to generate the STXBP6<sup>tm1a</sup> mutant line (**Figure 1B**). An animal with a germline integration was selected and used as the colony founder. The colony was established by 5-times backcrossing to the C57BL/6N line.

To test whether amisyn transcription and expression levels in the STXBP6<sup>tm1a</sup> mutant mice were disrupted, we measured the mRNA and protein levels of amisyn in the hippocampus (where amisyn is most strongly expressed), and compared these to levels in the WT mice. The amisyn gene transcription level, measured using quantitative reverse transcription PCR showed a decrease of over 60% (relative to WT

littermates, **Figure 1D**). In Western blot experiments, in which protein levels in the hippocampal tissue were measured, mutant mice showed ~90% reduction of expressed amisyn (10±3% remaining, normalized to WT animal, **Figure 1E**). Given that the majority of amisyn protein was removed from the hippocampus (used as the test tissue, and the results were confirmed in the cortex), we proceeded with a characterization of the STXBP6<sup>tm1a</sup> line.

### **Amisyn absence regulates expression levels of several peripheral proteins**

We first checked if the diminished amisyn expression affected the transcription and expression of key synaptic and neuronal proteins. The levels of the majority of tested proteins were unaltered, e.g., SV2A, synaptotagmin 1, and synaptophysin 1 (**Figure 2A**). The only integral SV protein that was found to be altered was VAMP2, a competitor of amisyn, (Kondratiuk et al., 2020), whose expression levels were decreased (76±12% normalized to WT) in the STXBP6<sup>tm1a</sup> mice. Curiously, the expression levels of several peripheral SV proteins were found to be increased in the hippocampus of STXBP6<sup>tm1a</sup> mice. Rab3a expression increased to 137±9%, while  $\alpha$ -synuclein expression increased to 118±9% in comparison to WT mice (**Figure 2B**). Rab3a and  $\alpha$ -synuclein are associated with docking and priming of SVs, and changes in the levels of these two peripheral proteins could be indicative of alterations in the vesicle pool size in STXBP6<sup>tm1a</sup> mice (Bellani et al., 2010; Schluter, Basu, Sudhof, & Rosenmund, 2006). Interestingly, the transcription level of Rab3a and  $\alpha$ -synuclein remained unchanged in STXBP6<sup>tm1a</sup> mice (**Figure 2B**).

As for Q-SNARE proteins, there were no changes in either expression or transcription levels of SNAP-25, SNAP47, syntaxin 1, and syntaxin 16 (**Figure 2C**). There was also no change in the expression or transcription levels of post-synaptic proteins, including PSD95, Homer 1, and GluA2 (**Figure 2D**). The expression and transcription level of other SNARE regulators and interactors, such as tomosyn, Munc18, and Munc13, did not change in the hippocampus of STXBP6<sup>tm1a</sup> mice (**Figure 2E**).

### **Amisyn ablation causes memory and learning impairments**

As a regulator of exocytosis, amisyn could affect learning and memory abilities in mammals. To test this possibility, we performed several behavioral assays to test learning and memory in STXBP6<sup>tm1a</sup> mice. First, we tested the anxiety of animals in the Elevated Plus Maze and open field tests. There was no significant difference in anxiety level between WT and STXBP6<sup>tm1a</sup> mice (**Figure S2 A-C**).

After the anxiety test, we ran a novel object recognition test to assess recognition memory in the mice. WT animals demonstrated a better novel object identification ability than STXBP6<sup>tm1a</sup> mutant mice. During the 10 min test phase, WT mice spent 73.2±6.5 s on new subjects, and only 57.2±4.8 sec on familiar objects. The discrimination index (ratio of time spent with the familiar object and the novel object) of WT animals was 0.58±0.03. STXBP6<sup>tm1a</sup> mice, on the other hand, spent 68.3±5.6 s on the novel object and 73.9±8.3 s on the familiar object. The discrimination index of mutant animals was 0.48±0.04 s, which indicates a weaker ability to distinguish a novel object from a familiar object (**Figure 3D-F**).

We next ran a T-maze test to further characterize the learning abilities of these animals. For the three-day test, we found that WT animals achieved a 70.4±2.5% success rate, which is comparable with the result reported by Fujioka et al. (2014) and McHugh et al. (2010). Meanwhile, the success rate of WT mice on the third day was higher than on the first day, indicating successful learning. However, mutant animals only achieved a success rate of 54.5±4.9%, which suggests that mutant animals selected the arm randomly (**Figure 3G-H**). Additionally, the success rate of mutant animals remained constant during the test, which indicates that mutant animals failed to learn the baiting pattern.

To further test memory and learning, we ran a fear discrimination test. During this test, both WT and STXBP6<sup>tm1a</sup> mice froze for a longer time in the shock box compared to the non-shock box. WT animals' freezing time in the shock box (95.5±3.8 sec) was significantly longer than that of STXBP6<sup>tm1a</sup> mice (75.6±5.5 sec) (**Figure 3I-J**).

### **STXBP6<sup>tm1a</sup> mice exhibited autism-like behaviors**

Catersamn et al. reported there to be an association between amisyn and autism

(Castermans et al., 2008). Thus, we performed several behavioral assays with the STXBP6<sup>tm1a</sup> line to investigate whether there were similarities to mice models of autism (Silverman, Tolu, Barkan, & Crawley, 2010). First, we measured self-grooming time during the open field test, since repetitive behavior is a classical autism phenotype. Indeed, the WT mice spent much less time ( $12.9 \pm 1.4$  s) on self-grooming than did the STXBP6<sup>tm1a</sup> mice ( $23.2 \pm 1.7$  s) (**Figure 3A-B**).

Social communication dysfunction is another typical feature of autism (Fernandez, Mollinedo-Gajate, & Penagarikano, 2018). To test this, mice completed a three-chamber test to characterize their social behavior. In the test, WT animals spent  $65.2 \pm 2.3\%$  of the time in the chamber with another animal, while STXBP6<sup>tm1a</sup> mice spent  $54.5 \pm 4.8\%$  of the test time in the chamber with another animal. This suggests that amisyn mutants exhibited impairments in social communication (**Figure 3C**). Altogether, these results indicate that a lack of amisyn is associated with autism-like phenotypes.

### **Vesicle release probability increase in the STXBP6<sup>tm1a</sup> neurons**

Previous behavioral assays have revealed learning and memory impairments in amisyn-deficient animals. To determine whether amisyn affects synaptic transmission, we examined the electrophysiological properties of STXBP6<sup>tm1a</sup> mice using brain slices.

As the first test for synaptic function, we measured miniature excitatory postsynaptic currents (mEPSCs) from neurons in the CA1 region of the brain slices (**Figure 4A**). On average, we measured a 161% increase in spontaneous firing frequency ( $3.40 \pm 0.75$  Hz against  $1.88 \pm 0.51$  Hz for WTs) (**Figure 4B**). No significant change in mEPSC amplitude was detected (STXBP6<sup>tm1a</sup>:  $19.73 \pm 1.87$  pA; WT:  $20.51 \pm 0.84$  pA; **Figure 4C**). These results indicated that amisyn may affect presynaptic vesicle release probability.

To test this hypothesis, we stimulated Schaffer collateral inputs onto CA1 neurons to record evoked EPSCs (**Figure 4C**). We found that STXBP6<sup>tm1a</sup> mice had a larger

response ( $259\pm 36$  pA) than WTs ( $522\pm 73$  pA). Thus, a lack of amisyn may facilitate SV release.

Despite efforts to perform the experiments in a blind manner, in principle, the EPSC amplitude in brain slices may have been affected by the relative position of the electrode. Thus, we measured the paired-pulse ratio (PPR) in Schaffer collaterals to CA1 neuron synapses, as well as mossy fibers to CA3 neuron synapses, to further characterize amisyn's role in neurotransmission. In the Schaffer collaterals to CA1 synapses, the PPR at short time intervals (an inter-stimulus interval between 10 and 20 ms) was reduced in STXBP6<sup>tm1a</sup> mice relative to WTs ( $1.35\pm 0.04$  vs.  $1.70\pm 0.05$  at 10 ms interval;  $1.23\pm 0.03$  vs.  $1.41\pm 0.03$  at 20 ms interval) (**Figure 4D**).

At the mossy fibers to CA3 synapses, a similar reduction in the PPR at short time intervals was observed ( $1.67\pm 0.14$  for STXBP6<sup>tm1a</sup> vs.  $2.25\pm 0.09$  for WT at 10 ms interval;  $1.41\pm 0.09$  for STXBP6<sup>tm1a</sup> vs.  $1.69\pm 0.09$  for WT at 20 ms interval). The difference in mossy fiber reactions between mutant animals and WT animals was larger than the between-group difference in Schaffer collateral reactions, which may be due to the higher amisyn expression level in the dentate gyrus (**Figure 4F**).

To further test the functional role of amisyn in synaptic transmission, we stimulated synaptic responses with trains of stimuli at various frequencies at the Schaffer collaterals to CA1 synapses (10 stimulations at 2, 5, 10, and 20 Hz; **Figure 2G**). By comparing the tenth EPSC to the first one, we found burst-induced facilitation of the EPSC response in WT mice ( $1.19\pm 0.16$ ,  $1.22\pm 0.23$ ,  $1.30\pm 0.25$ ,  $1.37\pm 0.23$ -fold), but no such facilitation was present in mutant animals (**Figure 3G**; **Figure S1A-D**). Combining such burst-induced facilitation elimination with PPR reduction results, we could conclude that amisyn mutant animals have a loss of short-term plasticity. Considering that short-term plasticity is proportional to the release probability of synapses (as described in Zucker et al., 2002), this result demonstrates a likely negative regulation effect of amisyn on vesicle release (Zucker & Regehr, 2002).

### **Amisyn abundance positively regulates the readily releasable pool size**

It has been reported that tomosyn regulates the RRP size at synapses (Cazares et al.,

2016). . Considering the notable similarities between amisyn and tomosyn functions, amisyn could also have a role in RRP size regulation. To test this hypothesis, we measured the RRP size in Schaffer collaterals and mossy fibers in WT and mutant mice, using the method described by Schneggenburger et al. (Schneggenburger et al., 1999). With a long, high-frequency stimulation (100 stimuli, 100 Hz), the whole RRP is exhausted. Thus, we can estimate the recovery rate via the response amplitude at the end of the stimulation. Furthermore, we could calculate the size of the sRRP. The recordings of Schaffer collateral revealed that the RRP size in STXBP6<sup>tm1a</sup> neurons was 2.24±0.36-fold (after normalization) larger than that in the WT mice (**Figure 6C**). Meanwhile, the RRP recovery rate of STXBP6<sup>tm1a</sup> mice was 2.34±0.32-fold larger than of WT mice (**Figure 6D**). However, there was no difference between STXBP6<sup>tm1a</sup> mice and WT mice on the relative RRP recovery rate (recovery rate/RRP size; **Figure 6E**). The results obtained from the mossy fiber recordings were similar to those of the Schaffer collateral recordings. The RRP size at the CA3 neuron synapse was 2.34±0.92-fold (after normalization) larger than that of the WT mice (**Figure 6F**). To confirm the change of recovery rate, we measured relative recovery rate after different time durations. Firstly, we ran a long high frequency train to exhaust RRP and then measured the response after different time intervals, as in Wu et al. (Wu & Borst, 1999). There was no difference in the relative recovery rate between WT and STXBP6<sup>tm1a</sup> mice at intervals of 10 ms, 20 ms, 100 ms, and 300 ms (**Figure 6J**). These results support the previous conclusions. The relative recovery rate of WT animals (92.6±3.8% for 1 s, 108.2±3.6% for 3 s) was higher than that of the STXBP6<sup>tm1a</sup> mice (78.8±7.3% for 1 sec, 86.5±7.7% for 3 s) at intervals of 1 s and 3 s.

### **STXBP6<sup>tm1a</sup> animals have impaired long-term plasticity**

Previous studies have shown that changes in exocytosis regulation can cause changes in the long-term synaptic plasticity (LTP) (Ben-Simon et al., 2015). To determine whether amisyn depletion affects plasticity, we examined Schaffer collateral LTP (SC-LTP; **Figure 7A-B**). The results suggested that the SC-LTP was almost abolished in amisyn mutant mice (112±8%), while the SC-LTP of WT mice was robust

(137±9%). Meanwhile, post-tetanic potentiation of amisyn mutant mice (maximum potentiation in the first 3 min after stimulation) was increased after amisyn deficient (200.9±11.3% against 174.4±7.4%). The increase of post-tetanic potentiation in mutant mice was consistent with the increase of release probability (**Figure 7D**).

## **DISCUSSION**

Formation of the SNARE complex is an essential step in secretory vesicle release. Cytosolic SNARE proteins such as tomosyn and complexin have been reported as inhibitors of exocytosis (Pobbati, Razeto, Boddener, Becker, & Fasshauer, 2004; Zhou et al., 2017). As a cytosolic protein with a SNARE motif, amisyn's role in exocytosis is not well understood. Furthermore, its role in synaptic transmission has never before been addressed.

We generated a mouse line that lacks ~90% amisyn expression to study the role of amisyn in synaptic transmission and in behavior, including memory and learning. We found that amisyn reduction caused an increase in mEPSC frequency, yet no change in amplitude. The EPSC amplitude was enlarged, and there was a reduction in the PPR. Taken together, these data suggest that amisyn plays a role in negative regulation of SV release probability. Furthermore, long-term high-frequency stimulation recordings revealed that amisyn mutant mice have an increased RRP size, and a delayed recovery of the RRP. These data supported findings of an increase in selective peripheral proteins at SVs that were thought to control the size of RRP. Curiously, long-term potentiation was reduced, and learning and memory were impaired in amisyn mutant mice. Also, amisyn reduction caused autism-like features. In summary, we propose that amisyn modulates synaptic activity by regulating vesicle release probability and RRP size. In its absence, learning and memory are affected.

### **Amisyn's negative regulation of vesicle release probability**

Amisyn may negatively regulate exocytosis; its C-terminal can form a SNARE complex with syntaxin-1 and SNAP-25, making it a competitor of VAMP-2. Its N-terminal PH domain binds with PI(4,5)P<sub>2</sub> on the plasma membrane, which mediates amisyn's interaction with the plasma membrane. A previous study revealed amisyn's accumulation on the plasma membrane after stimulation (Kondratiuk et al., 2020). Taken together, these results indicate that the syntaxin-SNAP-25-amisyn complex can occupy the fusion sites of SVs at the plasma membrane. Consequently, amisyn acts as a negative regulator of exocytosis. However, the experimental evidence *in vivo* for

this model is lacking.

Transgenic mice have been considered as one of the most powerful tools to characterize the role of synaptic proteins in living animals and processes such as neurotransmission. In the initial test of synaptic function, we found that mEPSC event frequency was increased in STXBP6<sup>tm1a</sup> mice. This is consistent with the negative regulation of presynaptic release. In addition, STXBP6<sup>tm1a</sup> mice showed an increase in evoked EPSC amplitude when amisyn expression was impaired. Further tests of presynaptic function, PPR measurement, and short-burst stimulation supported the interpretation that loss of amisyn increases the initial release probability in both mossy fiber-CA3 and Schaffer collateral-CA1 synapses.

Positive regulation of release probability could arise via several different mechanisms, such as higher expression level or activity of voltage-gated calcium channels, more efficient coupling of calcium to release sensors, and upregulation of SV docking processes (Branco & Staras, 2009; Korber & Kuner, 2016). Our proteomic analyses suggested that there was no difference in the calcium channel expression level (**Supplementary Figure 3**). Thus, our findings strongly support the hypothesis that amisyn has negative regulation effect on exocytosis via occupying the fusion sites and competing with the priming of new SVs.

### **Amisyn's negative regulation of synaptic vesicle pool sizes**

Besides the regulation of release probability, regulation of the RRP size also leads to differences in exocytic activity. An increase in the RRP size and absolute recovery speed was detected in amisyn's deficiency. However, the relative recovery speed did not change. This result conformed to our recordings, which revealed no difference in recovery EPSC amplitude when the time interval was below 1 sec. The EPSC recovery at a short time interval could reflect the relative recovery speed (recovery speed according to initial RRP size). In proteomic studies, we detected an increase of synaptic vesicular peripheral protein Rab3a in amisyn mutant mice, and Rab3a has also been reported to be a positive RRP regulator (Schluter et al., 2006).

The size of the RRP can be altered due to several reasons, including a change in the

number of docked/primed vesicles, recruitment of new vesicles to the fusion sites, and priming process of vesicles, etc (Kaeser & Regehr, 2017; Millar, Bradacs, Charlton, & Atwood, 2002). For instance, mutations in VAMP2, Munc13, and other proteins involved in SNARE complex formation lead to a downregulation of RRP because the mutations interfere with vesicle docking. It is likely that amisyn occupies fusion sites for vesicles on the plasma membrane, and thus reduces the number of docked/primed vesicles. In amisyn-deficient synapses, on the other hand, more vesicles could dock on the membrane and enlarge the size of the RRP.

### **Amisyn is involved in memory formation and learning**

Apart from exocytosis regulation, we also found that SC-LTP is disrupted in amisyn mutants. There are several potential reasons for this observation. Changes in postsynaptic receptor expression, for instance, can alter LTP. However, we found no evidence of a different postsynaptic receptor expression level of amisyn mutants using proteomics. Reduction in LTP can also result from high release probability, which leads to a chronic LTP state (Gustafsson, Wigstrom, Abraham, & Huang, 1987; Schulz, 1997). Since we reported an increase of release probability in amisyn mutant mice, the defects in LTP in amisyn-deficient synapses are very likely due to higher  $P_r$ .

LTP in the hippocampus is associated with learning and memory formation (Martin, Grimwood, & Morris, 2000). From behavioral assays, including the T-maze, fear conditioning, and novel object recognition, we detected an impairment in learning and memory formation in amisyn mutant mice. A possible explanation for such impairment can be that amisyn expression in synapses assures stable LTP and short-term facilitation, which together guarantee a steady information flow in the hippocampus.

In further experiments, we also observed some typical autism-like behaviors in amisyn mutants, including social communication impairment and self-replication activity. These observations support previous links made between amisyn and autism, first reported in a case study in 2008 (Castermans et al., 2008). Of note, a recent study reported no significant difference in social and learning ability in a CRISPR-based

amisyn mouse model compared to WT animals (C. Liu et al., 2021). However, the mouse model used in this article only knocked out the SNARE motif of amisyn. Both the PH domain and SNARE domain have been shown to be involved in neurosecretory cell exocytosis (Kondratiuk et al., 2020). The PH domain amisyn may still bind with PI(4,5)P<sub>2</sub> at the active zone and substitute for some functions of amisyn.

In conclusion, we used a new mouse model to characterize the role of amisyn in neurotransmission. Electrophysiological recordings of synaptic activity revealed a reduced release probability and diminished RRP size in the mutant animals, which is consistent with a functional role of amisyn protein to negatively regulate vesicle release. Behavioral deficits in mutant animals indicated that the absence of amisyn regulation of vesicle release may impair learning and memory, and could contribute to autism-like behavioral patterns. These new characterizations of amisyn contribute to our understanding of both the physiological mechanism underlying neurotransmission and the pathological features of amisyn-related diseases.

### **Data contribution**

JJ (Figure 1-7, S1-3), RC (Figure 3, S3), JP&JF (Figure 1, Figure 2)

### **Reference**

1. Terrian DM & White MK (1997) Phylogenetic analysis of membrane trafficking proteins: a family reunion and secondary structure predictions. *Eur J Cell Biol* 73(3):198-204.
2. Weimbs T, Mostov K, Low SH, & Hofmann K (1998) A model for structural similarity between different SNARE complexes based on sequence relationships. *Trends Cell Biol* 8(7):260-262.
3. Fasshauer D, Eliason WK, Brunger AT, & Jahn R (1998) Identification of a minimal core of the synaptic SNARE complex sufficient for reversible assembly and disassembly. *Biochemistry* 37(29):10354-10362.

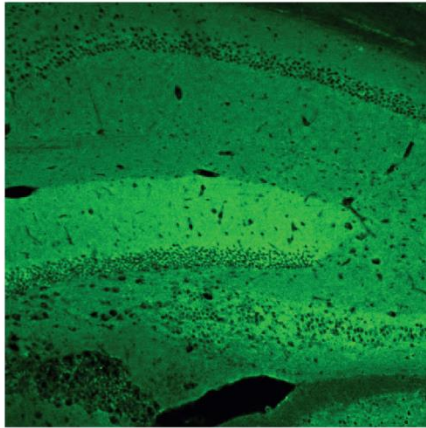
4. Sutton RB, Fasshauer D, Jahn R, & Brunger AT (1998) Crystal structure of a SNARE complex involved in synaptic exocytosis at 2.4 Å resolution. *Nature* 395(6700):347-353.
5. Sollner T, Bennett MK, Whiteheart SW, Scheller RH, & Rothman JE (1993) A protein assembly-disassembly pathway in vitro that may correspond to sequential steps of synaptic vesicle docking, activation, and fusion. *Cell* 75(3):409-418.
6. Misura KM, Scheller RH, & Weis WI (2000) Three-dimensional structure of the neuronal-Sec1-syntaxin 1a complex. *Nature* 404(6776):355-362.
7. Lopez-Font I, Torregrosa-Hetland CJ, Villanueva J, & Gutierrez LM (2010) t-SNARE cluster organization and dynamics in chromaffin cells. *J Neurochem* 114(6):1550-1556.
8. Bennett MK, Calakos N, & Scheller RH (1992) Syntaxin: a synaptic protein implicated in docking of synaptic vesicles at presynaptic active zones. *Science* 257(5067):255-259.
9. Blasi J, *et al.* (1993) Botulinum neurotoxin A selectively cleaves the synaptic protein SNAP-25. *Nature* 365(6442):160-163.
10. Ojler GA, *et al.* (1989) The identification of a novel synaptosomal-associated protein, SNAP-25, differentially expressed by neuronal subpopulations. *J Cell Biol* 109(6 Pt 1):3039-3052.
11. Veit M, Sollner TH, & Rothman JE (1996) Multiple palmitoylation of synaptotagmin and the t-SNARE SNAP-25. *FEBS Lett* 385(1-2):119-123.
12. Trimble WS, Cowan DM, & Scheller RH (1988) VAMP-1: a synaptic vesicle-associated integral membrane protein. *Proc Natl Acad Sci U S A* 85(12):4538-4542.
13. Baumert M, Maycox PR, Navone F, De Camilli P, & Jahn R (1989) Synaptobrevin: an integral membrane protein of 18,000 daltons present in small synaptic vesicles of rat brain. *EMBO J* 8(2):379-384.
14. Blasi J, *et al.* (1993) Botulinum neurotoxin C1 blocks neurotransmitter release by means of cleaving HPC-1/syntaxin. *EMBO J* 12(12):4821-4828.

15. Jahn R & Fasshauer D (2012) Molecular machines governing exocytosis of synaptic vesicles. *Nature* 490(7419):201-207.
16. Zhou Q, *et al.* (2015) Architecture of the synaptotagmin-SNARE machinery for neuronal exocytosis. *Nature* 525(7567):62-67.
17. Prinslow EA, Stepien KP, Pan YZ, Xu J, & Rizo J (2019) Multiple factors maintain assembled trans-SNARE complexes in the presence of NSF and alphaSNAP. *Elife* 8.
18. An S & Zenisek D (2004) Regulation of exocytosis in neurons and neuroendocrine cells. *Curr Opin Neurobiol* 14(5):522-530.
19. Fujita Y, *et al.* (1998) Tomosyn: a syntaxin-1-binding protein that forms a novel complex in the neurotransmitter release process. *Neuron* 20(5):905-915.
20. McMahon HT, Missler M, Li C, & Sudhof TC (1995) Complexins: cytosolic proteins that regulate SNAP receptor function. *Cell* 83(1):111-119.
21. Scales SJ, Hesser BA, Masuda ES, & Scheller RH (2002) Amisyn, a novel syntaxin-binding protein that may regulate SNARE complex assembly. *J Biol Chem* 277(31):28271-28279.
22. Castermans D, *et al.* (2008) Position effect leading to haploinsufficiency in a mosaic ring chromosome 14 in a boy with autism. *Eur J Hum Genet* 16(10):1187-1192.
23. Collins SC, *et al.* (2016) Increased Expression of the Diabetes Gene SOX4 Reduces Insulin Secretion by Impaired Fusion Pore Expansion. *Diabetes* 65(7):1952-1961.
24. Lenka G, *et al.* (2017) Identification of Methylation-Driven, Differentially Expressed STXBP6 as a Novel Biomarker in Lung Adenocarcinoma. *Sci Rep* 7:42573.
25. Liu Y, *et al.* (2021) Identification of STXBP6-IRF1 positive feedback loop in regulation of PD-L1 in cancer. *Cancer Immunol Immunother* 70(2):275-287.
26. Barg S & Gucek A (2016) How Kiss-and-Run Can Make Us Sick: SOX4 Puts a Break on the Pore. *Diabetes* 65(7):1791-1793.
27. Kondratiuk I, *et al.* (2020) PI(4,5)P2-dependent regulation of exocytosis by

- amisyn, the vertebrate-specific competitor of synaptobrevin 2. *Proc Natl Acad Sci U S A* 117(24):13468-13479.
28. Constable JR, Graham ME, Morgan A, & Burgoyne RD (2005) Amisyn regulates exocytosis and fusion pore stability by both syntaxin-dependent and syntaxin-independent mechanisms. *J Biol Chem* 280(36):31615-31623.
  29. Gucek A, *et al.* (2019) Fusion pore regulation by cAMP/Epac2 controls cargo release during insulin exocytosis. *Elife* 8.
  30. Liu C, *et al.* (2021) Behavioral and Gene Expression Analysis of Stxbp6-Knockout Mice. *Brain Sci* 11(4).
  31. Clements JD & Bekkers JM (1997) Detection of spontaneous synaptic events with an optimally scaled template. *Biophys J* 73(1):220-229.
  32. Schneggenburger R, Meyer AC, & Neher E (1999) Released fraction and total size of a pool of immediately available transmitter quanta at a calyx synapse. *Neuron* 23(2):399-409.
  33. Schluter OM, Basu J, Sudhof TC, & Rosenmund C (2006) Rab3 superprimes synaptic vesicles for release: implications for short-term synaptic plasticity. *J Neurosci* 26(4):1239-1246.
  34. Bellani S, *et al.* (2010) The regulation of synaptic function by alpha-synuclein. *Commun Integr Biol* 3(2):106-109.
  35. Silverman JL, Tolu SS, Barkan CL, & Crawley JN (2010) Repetitive self-grooming behavior in the BTBR mouse model of autism is blocked by the mGluR5 antagonist MPEP. *Neuropsychopharmacology* 35(4):976-989.
  36. Fernandez M, Mollinedo-Gajate I, & Penagarikano O (2018) Neural Circuits for Social Cognition: Implications for Autism. *Neuroscience* 370:148-162.
  37. Zucker RS & Regehr WG (2002) Short-term synaptic plasticity. *Annu Rev Physiol* 64:355-405.
  38. Cazares VA, *et al.* (2016) Dynamic Partitioning of Synaptic Vesicle Pools by the SNARE-Binding Protein Tomosyn. *J Neurosci* 36(44):11208-11222.
  39. Wu LG & Borst JG (1999) The reduced release probability of releasable vesicles during recovery from short-term synaptic depression. *Neuron*

- 23(4):821-832.
40. Ben-Simon Y, *et al.* (2015) A Combined Optogenetic-Knockdown Strategy Reveals a Major Role of Tomosyn in Mossy Fiber Synaptic Plasticity. *Cell Rep* 12(3):396-404.
  41. Pobbati AV, Razeto A, Boddener M, Becker S, & Fasshauer D (2004) Structural basis for the inhibitory role of tomosyn in exocytosis. *J Biol Chem* 279(45):47192-47200.
  42. Zhou Q, *et al.* (2017) The primed SNARE-complexin-synaptotagmin complex for neuronal exocytosis. *Nature* 548(7668):420-425.
  43. Branco T & Staras K (2009) The probability of neurotransmitter release: variability and feedback control at single synapses. *Nat Rev Neurosci* 10(5):373-383.
  44. Korber C & Kuner T (2016) Molecular Machines Regulating the Release Probability of Synaptic Vesicles at the Active Zone. *Front Synaptic Neurosci* 8:5.
  45. Millar AG, Bradacs H, Charlton MP, & Atwood HL (2002) Inverse relationship between release probability and readily releasable vesicles in depressing and facilitating synapses. *J Neurosci* 22(22):9661-9667.
  46. Kaeser PS & Regehr WG (2017) The readily releasable pool of synaptic vesicles. *Curr Opin Neurobiol* 43:63-70.
  47. Gustafsson B, Wigstrom H, Abraham WC, & Huang YY (1987) Long-term potentiation in the hippocampus using depolarizing current pulses as the conditioning stimulus to single volley synaptic potentials. *J Neurosci* 7(3):774-780.
  48. Schulz PE (1997) Long-term potentiation involves increases in the probability of neurotransmitter release. *Proc Natl Acad Sci U S A* 94(11):5888-5893.
  49. Martin SJ, Grimwood PD, & Morris RG (2000) Synaptic plasticity and memory: an evaluation of the hypothesis. *Annu Rev Neurosci* 23:649-711.

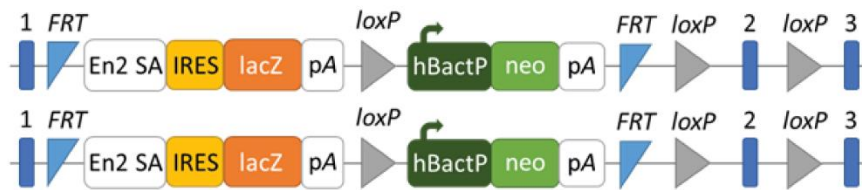
A



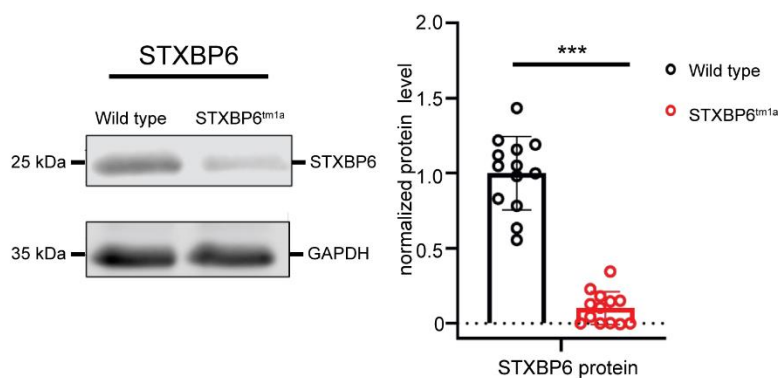
B



C



D



E

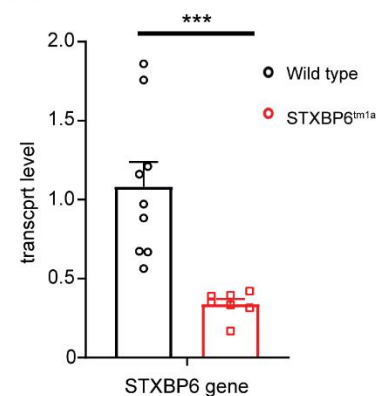


**Figure 1. Enrichment of amisyn in the hippocampus and the generation of amisyn mutant mice with conditional potential, C57BL6/N-STXBP6<sup>tm1a</sup>.** (A) Immunostaining revealed high expression levels of amisyn in the mouse hippocampus. (B) The promoter driven knockout-first strategy was used for the generation of this

mouse line. The knockout-first allele is initially a non-expressive form, but can be converted to a conditional allele via Flp recombination. (C) The STXBP6<sup>tm1a</sup> mutant mouse was viable and showed no obvious morphological changes. (D) qPCR results showed a prominent decrease of the amisyn's transcription levels in mutant brains (N = 9 WT/7 mutants). (E) Amisyn expression was largely abolished in the hippocampi of STXBP6<sup>tm1a</sup> mice (N = 13 WT/12 mutant).

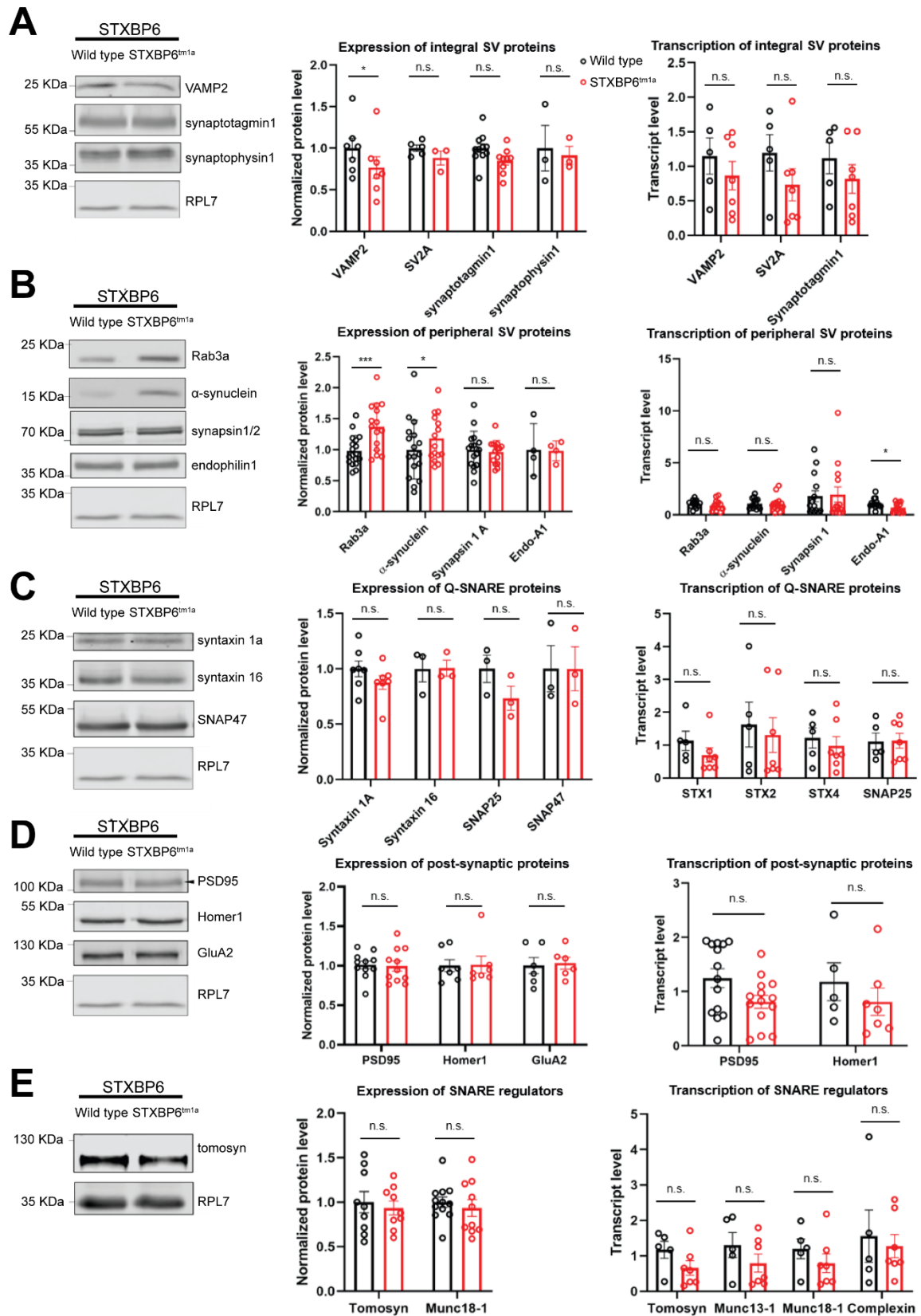
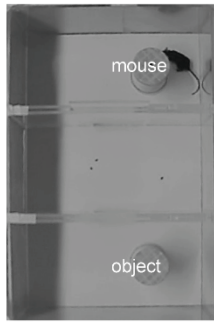


**Figure 2. Protein expression and mRNA transcription levels in amisyn mutant mice (A) Levels of selective integral vesicle proteins in WT and mutant hippocampal**

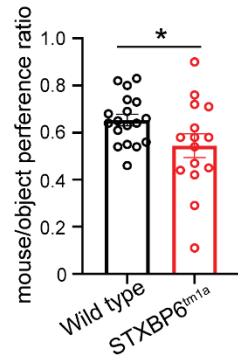
tissue. (VAMP2: 10 WT/10 mutants; SYT1 11WT/9 mutants; synaptophysin1 3WT/3 mutants) (B) Levels of peripheral vesicle proteins in the hippocampi of WT and mutant mice. (Rab3a:18 WT/15 mutants;  $\alpha$ -syn and synapsin1: 17 WT/ 15 mutants; Endo-A1: 4 WT/ 4 mutants) (C) Levels of Q-SNARE proteins present in WT and KO hippocampal tissue. (STX1A: 7 WT/ 7 mutants; STX16, SNAP-25 and SNAP-47: 3 WT/ 3 mutants) (D) Levels of postsynaptic proteins present in WT and mutant hippocampal tissue. (PSD95: 11 WT/ 11 mutants; Homer1 and GluA2: 7 WT/7 mutants) (E) Levels of exocytosis regulating proteins present in WT and mutant hippocampal tissue (Munc18-1 :9 WT/ 9 mutants; tomosyn: 5 WT/5 mutants). All of the results are normalized to the loading control. n.s.: not significant; \* $p < 0.05$ ; \*\*\* $p < 0.001$ . Results are shown as the mean $\pm$ SEM.

Sociability and Social Novelty Test

A

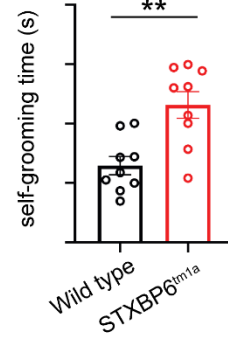


B



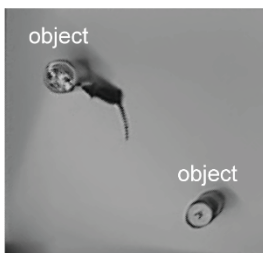
Repetitive Self-grooming Test

C

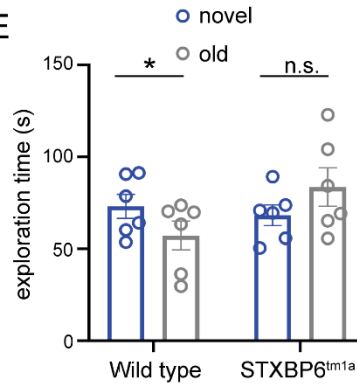


Novel Object Recognition Test

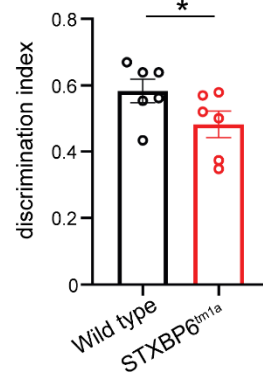
D



E



F

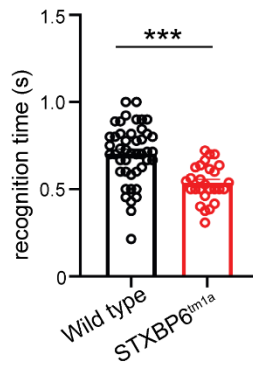


T-Maze Test

G

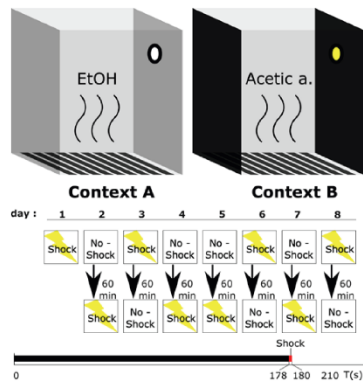


H



Fear Conditioning Test

I



J

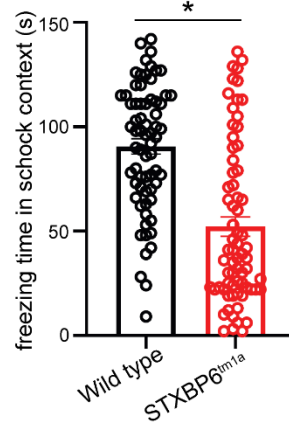


**Figure 3. Behavioral characterization of amisyn mutant mice.** (A) A three-chamber sociability test: A snap photo taken during the experiment. (B) The ratio between time spent interacting with the other mouse vs. being in the empty cage: WT mice showed a preference for interaction with the other animals, while mutant mice did not (N = 18 WT/15 mutant mice/group, \*p < 0.05). (C) The time spent grooming (out of 10 min) in an empty square arena (open field). Grooming included all sequences of face-wiping, and scratching/rubbing of head and ears (N = 9 mice/group, \*\*p < 0.01). (D) A novel object recognition test: A snap photo taken during the experiment. (E) Interaction time with a familiar vs. novel object, and (F) the discrimination index of WT and mutant mice in a 15 min test. WT mice showed a preference for the novel object, indicating recognition of the familiar object, while mutant mice failed to show such a preference (N = 16 mice/group, \*p < 0.05). (G) A T-maze test: A snap photo taken during the experiment. (H) WT mice had a significantly higher success rate than mutant mice, suggesting that mutant mice either have difficulties learning the task, or impairments in spatial memory (N = 15 WT/9 mutant mice/group, \*\*\*p < 0.001). (I) A sketch of the fear conditioning test used. (J) Amisyn mutant mice showed a shorter freezing time in the shock context, which indicates a reduced capacity for contextual-long-term memory (N = 14 WT/10 mutant mice/group, \*p < 0.05).

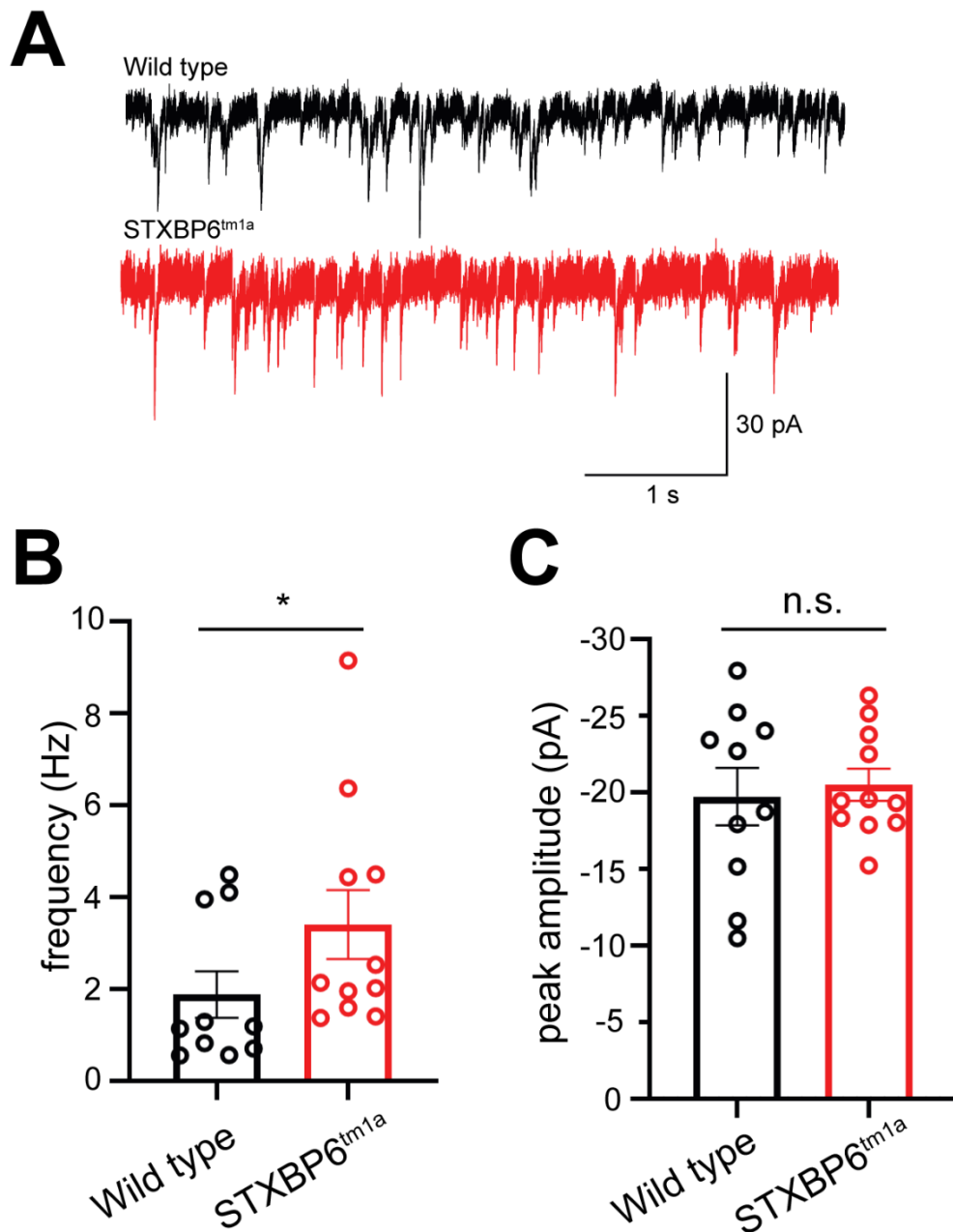


**Figure 4. mEPSC recordings in CA1 neurons from amisyn mutant mice brain slices.** (A) Representative mEPSC recordings from slices of WT and mutant mice. During the recording, a single neuron was clamped under whole-cell voltage mode under -70 mV for 10 min. (B) The mEPSC frequency increased in amisyn mutant mice (data analyzed per cell N = 10 WT/11 mutant, \* $p < 0.05$ ). (C) The mEPSC amplitude did not change in amisyn mutant mice (data analyzed per cell N = 10 WT/11 mutant).

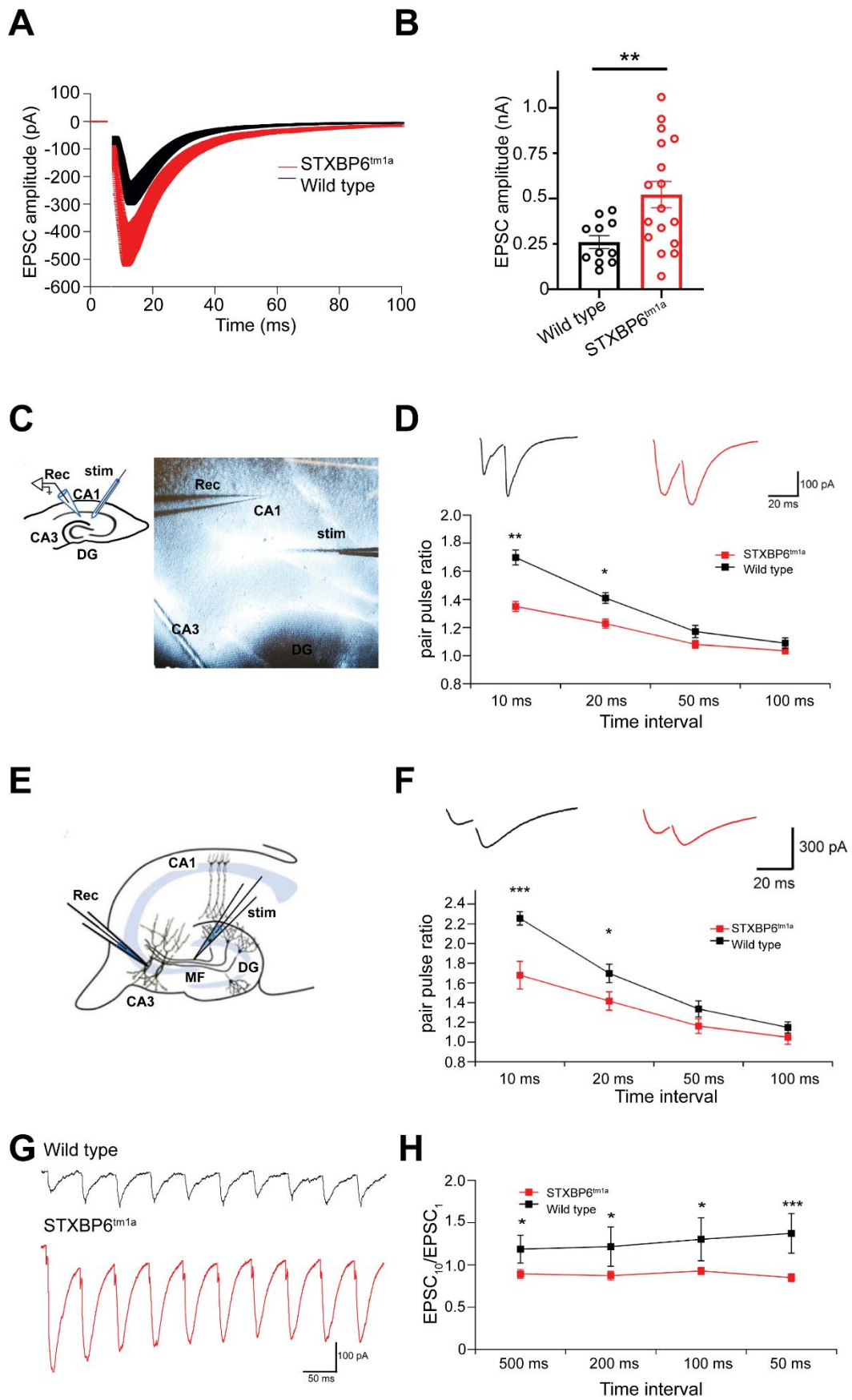


**Figure 5. Amisyn mutation altered vesicle release probability in neurons from CA1 and CA3 areas.** (A) An example of EPSC recording traces after a stimulation. (B) EPSC amplitude was higher in amisyn mutant mice (N = 11 WT/17 mutant,  $p = 0.002$ ). (C) A sketch showing EPSC recordings of CA1 neurons in a mouse hippocampus slice. A stimulation pipette was placed on the Schaffer collaterals and electrical stimuli were applied to trigger an action potential. The postsynaptic response was recorded under a voltage-clamp with a holding potential of -70 mV. (D) Paired-pulse stimulation of CA1 neurons, with time intervals of 10/20/50/100 ms, applied to Schaffer collaterals. The ratio between two EPSC responses is shown; Amisyn mutant mice had a lower paired-pulse ratio, which indicates a higher release probability (N = 15 WT/17 mutant;  $**p < 0.01$ ;  $*p < 0.05$ ). (E) Sketch showing EPSC recordings of CA3 neurons in a mouse hippocampus slice. A stimulation pipette was placed on the Mossy fibers. (F) The results of paired-pulse stimulations showed that amisyn mutant CA3 neurons also had a lower paired-pulse ratio, indicating a higher release probability (N = 6 mice/group;  $***p < 0.001$ ;  $*p < 0.05$ ). (G) An example of EPSC response traces of amisyn mutant mice and WT mice to a 20 Hz 10-stimuli train. (H)  $EPSC_{10}/EPSC_1$  significantly decreased in amisyn mutant mice at all stimulation frequencies (2 Hz, 5 Hz, 10 Hz, and 20 Hz) (N = 9 WT/20 mutant;  $*p < 0.05$ ,  $***p < 0.001$ ).

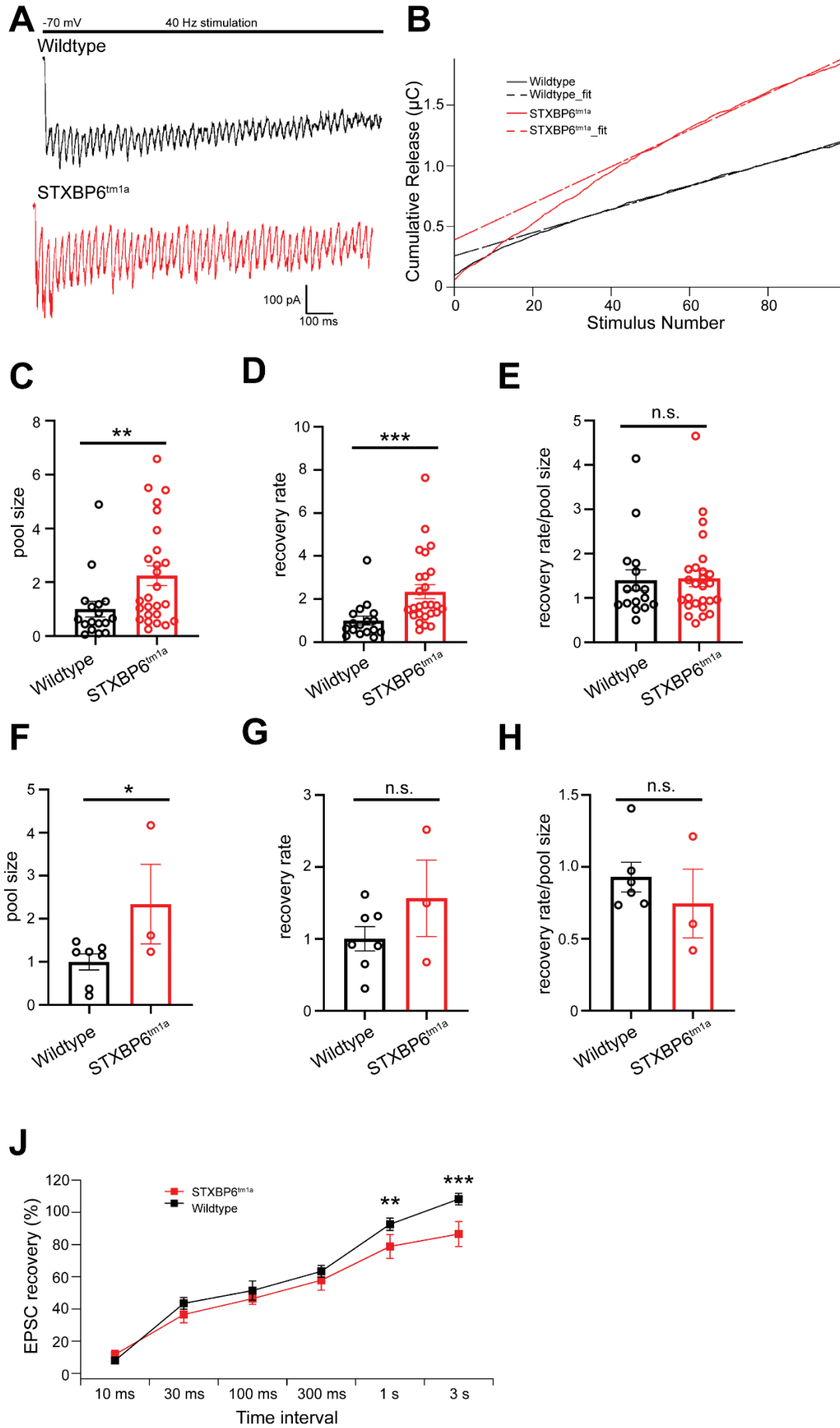


**Figure 6. High frequency stimulus train recording revealed that amisyn's absence influenced the releasable pool size.** (A) Representative train EPSC recordings from CA1 neurons of WT and mutant mice. Neurons in the CA1 region were clamped under whole-cell mode at -70 mV with stimulation at 40 Hz. (B) The cumulative release of a representative recording in (A) was calculated to further derive the pool size. (C) The CA1 neuron pool size of the mutant mice was larger than that of WT mice (N = 16 WT/26 mutant; \*\*p < 0.01). (D) CA1 neuron recovery rate of the mutant mice was faster than that of WT mice (N = 16 WT/26 mutant; \*\*\*p < 0.001). (E) CA1 neuron relative recovery rate (recovery rate/pool size) did not change in amisyn mutant animals (N = 16 WT/26 mutant). (F) The CA3 pool size of the mutant mice was larger than that of WT mice (N = 5 WT/3 mutant; \*p < 0.05). (D) CA3 neuron recovery rate did not change in amisyn mutant mice (N = 5 WT/3 mutant). (E) CA3 neuron relative recovery rate (recovery rate/pool size) did not change in amisyn mutant mice (N = 5 WT/3 mutant). (F) Recovery EPSC did not change in amisyn mutant mice at time intervals of 10 ms, 100 ms, and 300 ms. At longer time intervals (1 sec and 3 sec), amisyn mutant mice's recovery EPSC was slower than that of WT mice (N = 5 WT/7 mutant; \*\*p < 0.01, \*\*\*p < 0.001).

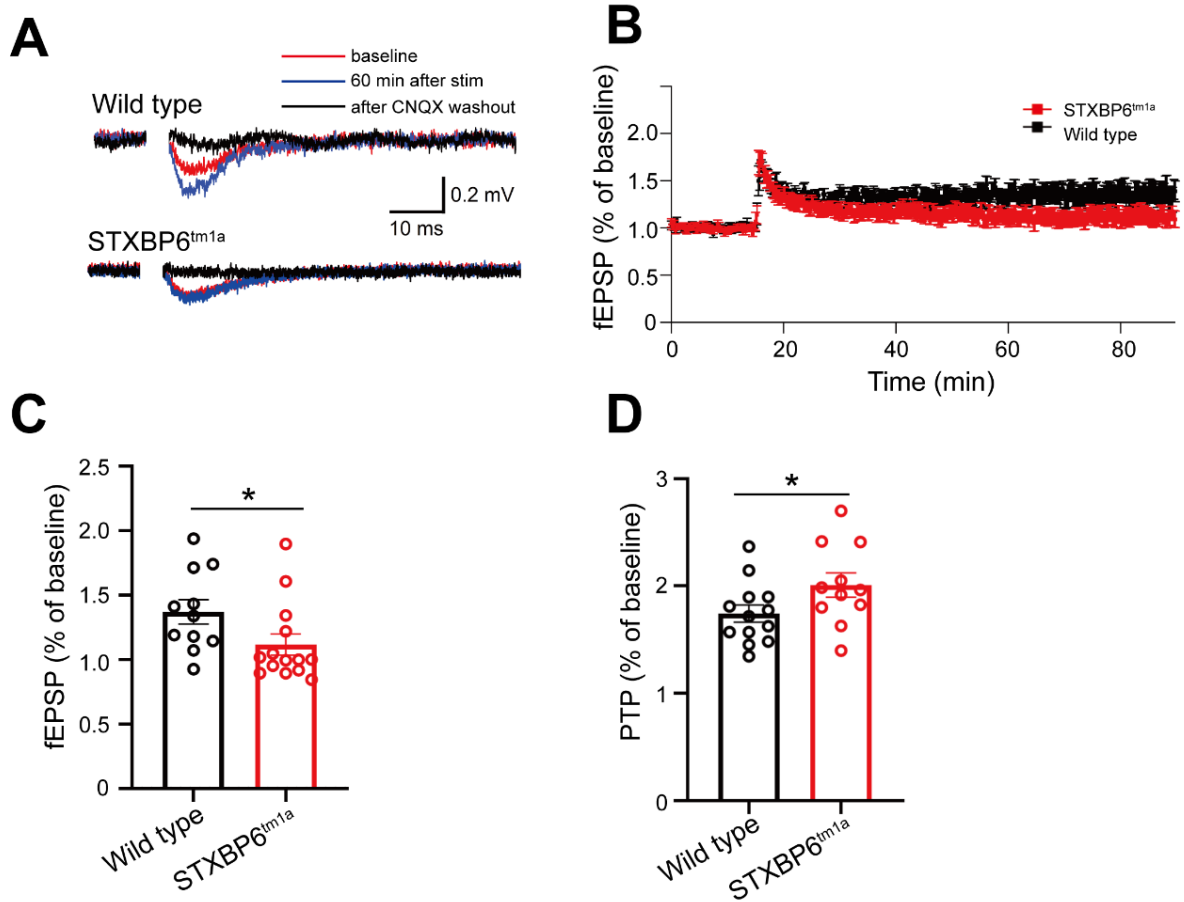
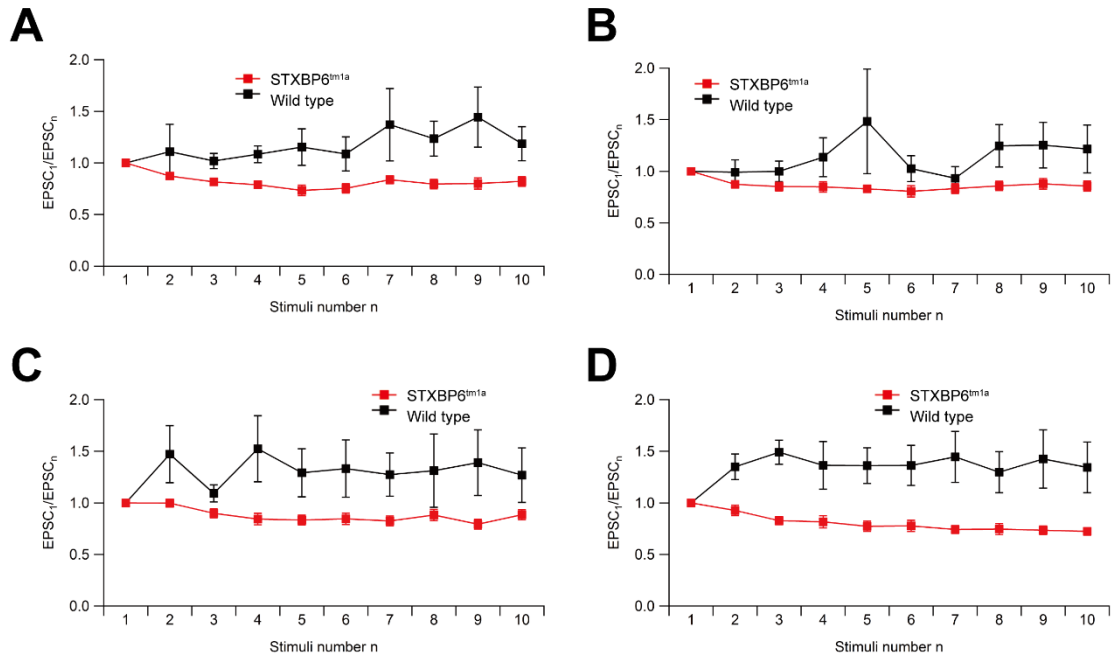
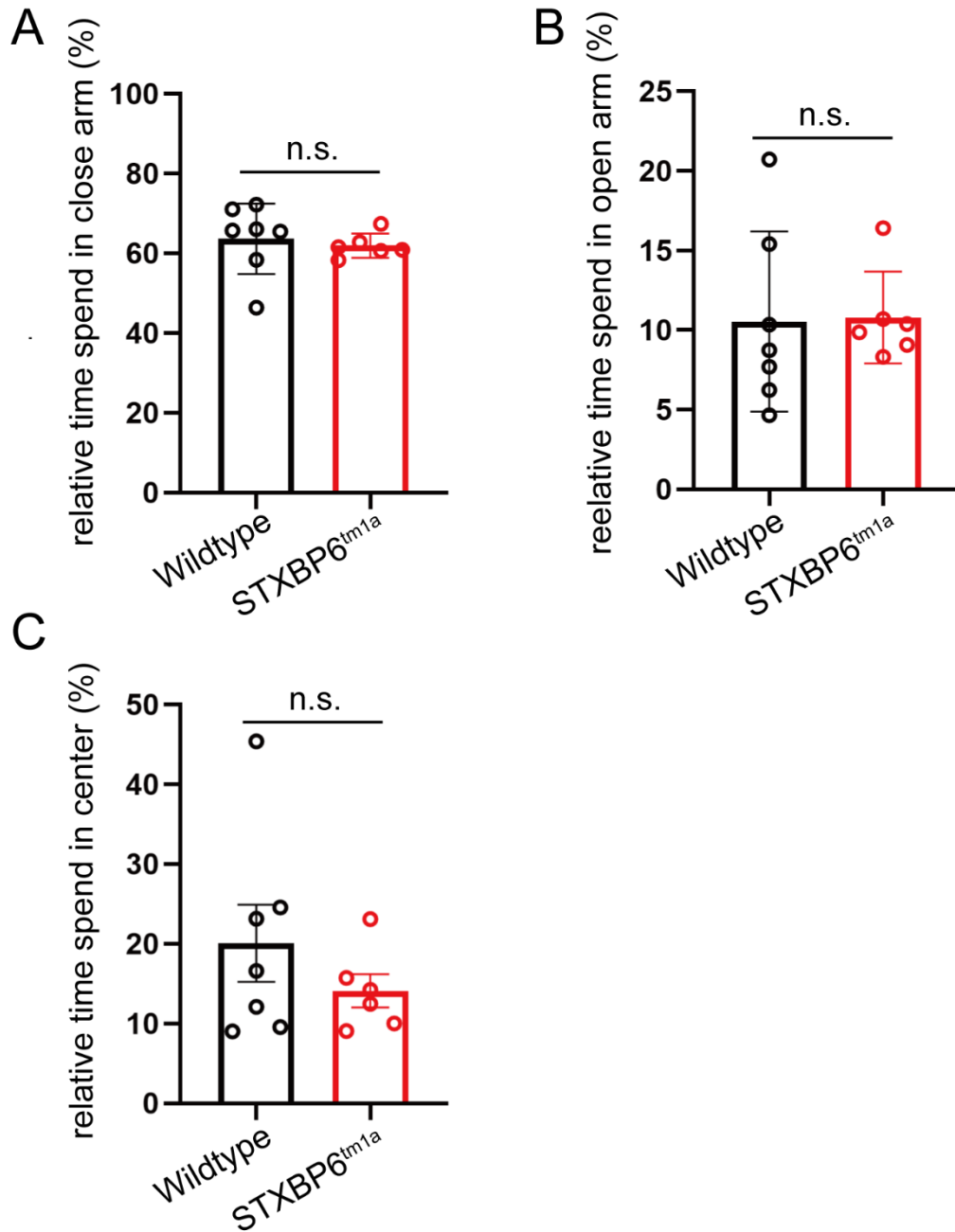


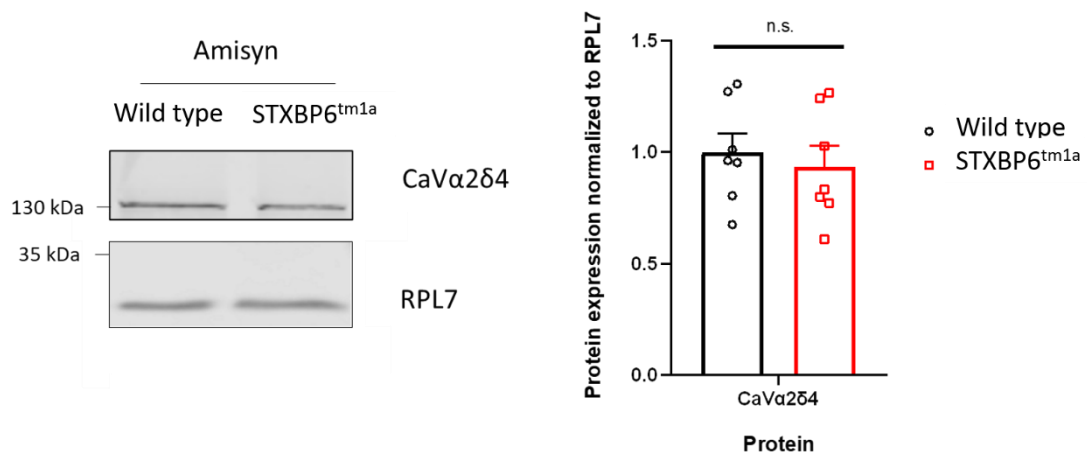
**Figure 7. Amisyn mutant mice had impaired SC-LTP.** (A) Representative fEPSP recording traces from WT (lower) and mutant (upper) mice before stimulation (red), 65-75 min after stimulation (blue), and after CNQX application (black). (B) SC-LTP in WT and amisyn mutant mice, stimulation applied at 15 min. (C) Bar plots of the mean fEPSP 65-75 min after stimulation showing that SC-LTP is abolished in amisyn mutant mice (N = 11 WT/14 mutant; \*p < 0.05). (D) Post-tetanic potentiation increase in amisyn mutant mice (N = 11 WT/13 mutant; \*p < 0.05).



**Supplementary Figure 1.** EPSCs response to a 10-stimuli train of different frequencies (A: 2 Hz, B: 5 Hz, C: 10 Hz, D: 20 Hz; N = 9 WT/20 mutant).



**Supplementary Figure 2. No anxiety differences between amisyn mutant mice and WT mice after habituation.** (A-B) Amisyn mutant mice and WT mice spent similar durations in the closed/open arm of an Elevated Plus Maze (N = 7 WT/6 mutant). (C) Time spent in the center of the open field did not change after amisyn mutation (N = 7 WT/6 mutant).



**Supplementary Figure 3.** No difference in CaVα2δ4 expression level between amisyn mutant and wild type animal's hippocampus (N = 6).

### 3.3 GST pull-down of amisyn (Supplementary results)

The first study about amisyn in 2002 reported only a few amisyn interactors, which limited the research on amisyn's characteristics. In 2002, Scale reported the interaction between amisyn and syntaxin-1, and reported that the amisyn-syntaxin dimer can form a complex with SNAP-25 (Scales et al., 2002). In the first publication included in this thesis, we described the interaction between PI(4,5)P<sub>2</sub> lipid and amisyn. We also studied other potential interactors. To this end, we used a homogenized brain from wild-type mice, purified full-length amisyn, and ran two pull-down experiments. We used the pull-down outcome to run the SDS-gel, and scans of the results are shown in Figures 7 and 8.

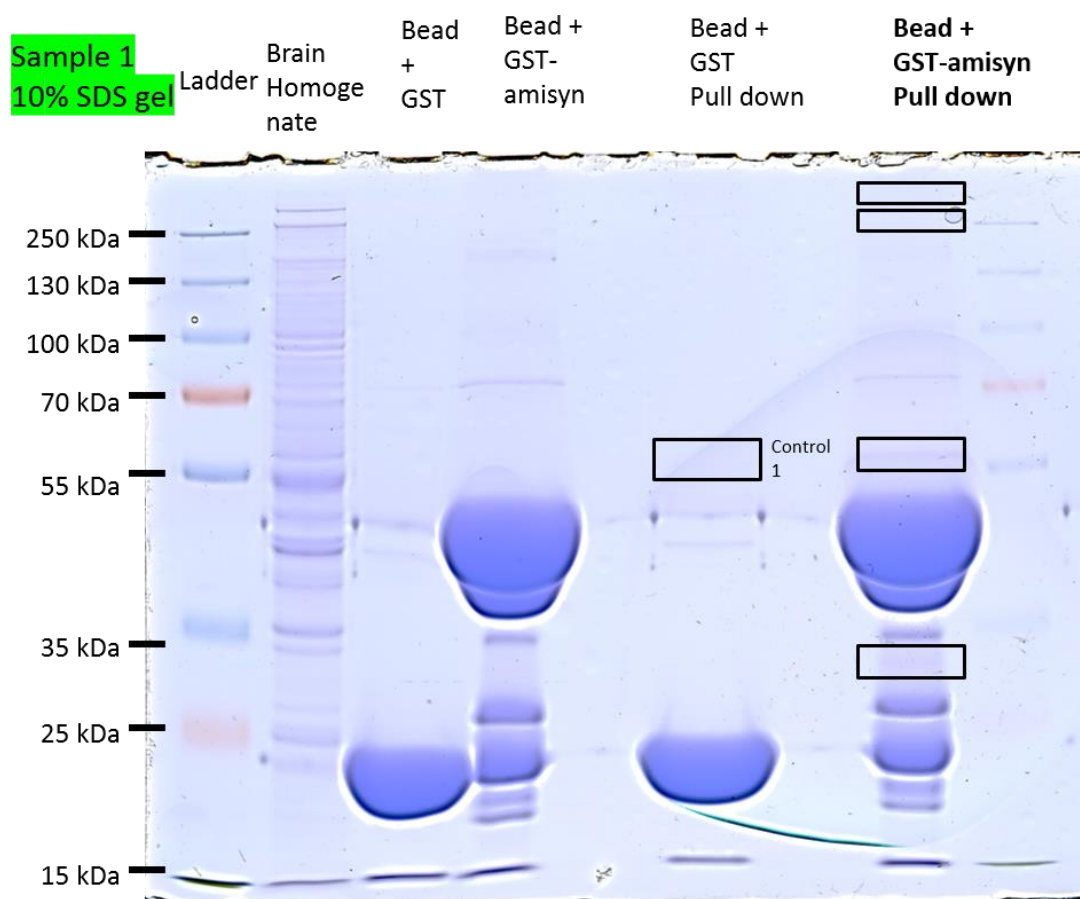


**Figure 7** Scan of the SDS gel from the first pull-down experiment. The ladder is shown in the left part of the gel. Samples from left to right are brain homogenate alone, bead + empty GST, bead + GST-amisyn, bead + empty GST + brain homogenate, and bead + GST-amisyn + brain homogenate. The cut-off parts of the gel sent for mass spectrometry are marked with a black box.

**Experiment #2**  
**10% SDS gel**

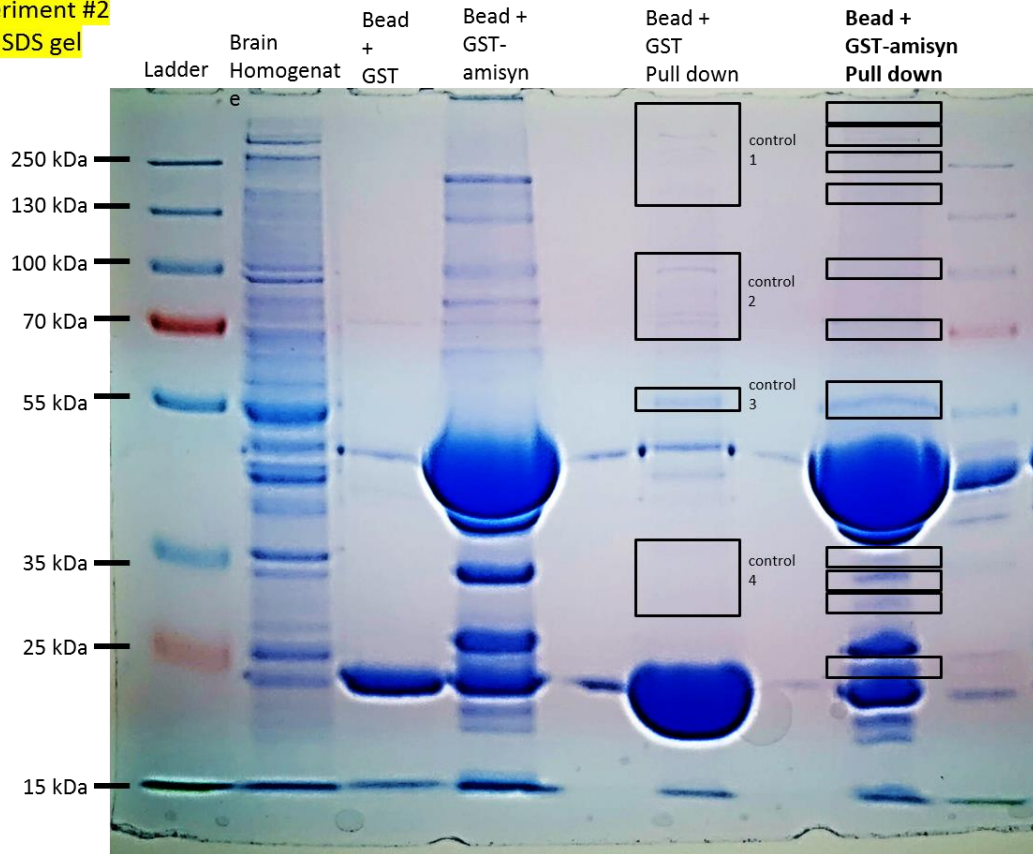


**Figure 8** Scan of the SDS gel from the second pull-down experiment. The ladder is shown on the left part of the gel. Samples from left to right are brain homogenate alone, bead + empty GST, bead + GST-amisyn, bead + empty GST + brain homogenate, and bead + GST-amisyn + brain homogenate. The cut-off parts of the gel sent for mass spectrometry are marked with a black box.

As shown in Figures 7 and 8, there were two main bands in the pull-down results, at around 50 and 25 kDa, which should be the residues of amisyn alone and GST-amisyn. As well as these two regions, we selected several bands and cut them off from the SDS gels. These samples were then sent to our collaborator, Dr. Christof Lenz from UMG, for mass spectrometry. The volcano plot of mass spectrometry result is shown in Figure 9.

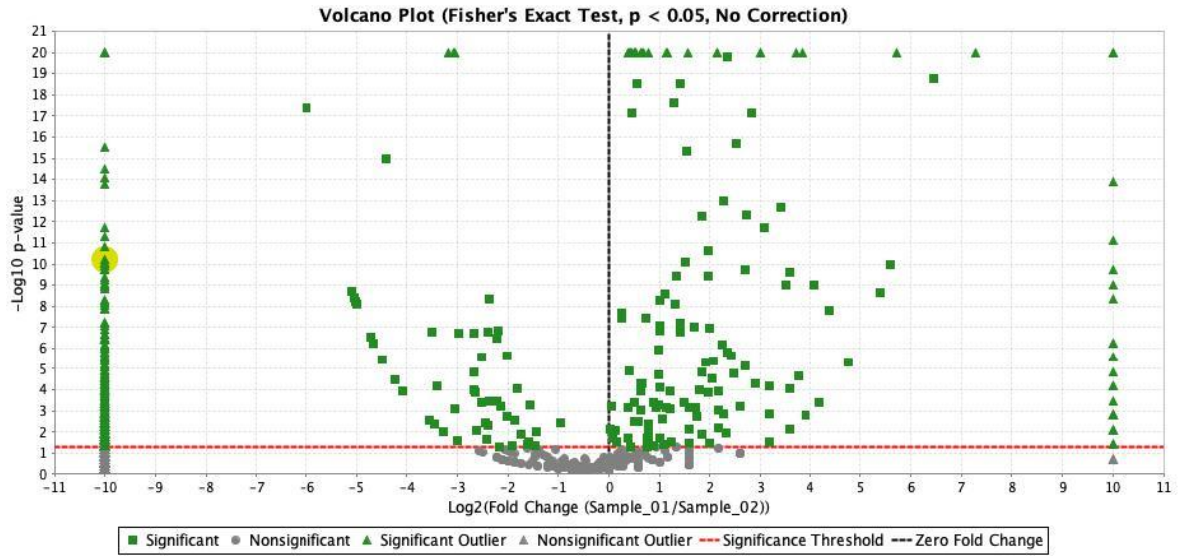


**Figure 9** Volcano plot of the mass spec result of amisyn pull-down experiment.

#### 4. Discussion

Exocytosis involves a sequence of regulated processes such as recruitment/trafficking, docking, priming, and fusion of the vesicle. It is attributed as one of the finest controlled biological processes and has been studied for several decades. Several key players, including lipids and proteins, that are involved in exocytosis have been identified and characterized (Jahn & Fasshauer, 2012). For example, the neuronal SNARE-complex is crucial to docking, priming, and fusion. It consists of three different SNARE proteins: VAMP2, syntaxin-1, and SNAP-25. (Bennett et al., 1992; Terrian & White, 1997; Trimble et al., 1988). The formation of the SNARE complex is regulated by many other proteins; for example, Munc18, Munc 13, and synaptotagmin act as promoters of SNARE-complex formation (Veit et al., 1996; Wang et al., 2020). However, usually the regulation of biological processes is of dual nature, and consist of both positive and negative regulators. A negative regulation to prevent the release of NT is necessary for neurotransmission. SNARE proteins with a VAMP2-like SNARE motif, such as tomosyn, are potential negative regulators of exocytosis owing to their structural characteristics. Their SNARE motif allows them to replace VAMP2 and conjugate with SNAP-25 and syntaxin-1 to form a SNARE complex, and interfere with the formation of neuronal SNARE complexes and inhibit exocytosis (Ashery et al., 2009; Fujita et al., 1998).

Like tomosyn, amisyn is a cytosolic protein with an R-SNARE domain. Amisyn can bind syntaxin-1 and form a thermostable complex with syntaxin-1 and SNAP-25 (Scales et al., 2002). Moreover, excess of amisyn in PC12 and chromaffin cells is found to have an inhibitory effect on secretion (Constable et al., 2005). However, the basic structural and functional properties of the N-terminal domain of amisyn are still not fully understood. Thus, the detailed mechanism for the inhibitory effect of amisyn cannot be verified. Further, the lack of an animal model makes it difficult to investigate amisyn's physiological effect *in vivo*.

As described in the first part of my thesis, the main aim was to characterize the N-terminal of amisyn. We first used sequence analysis algorithms to propose a potential structure for the N-terminal domain and modeled this structure using protein

threading. Then, we confirmed its predicted structure with several different experiments, most prominently by studying interactions between amisyn and lipids. Finally, we tested if the formation of the SNARE complex and its ability to inhibit secretion was related to amisyn's N-terminal. From all the experiment results, we proposed a new function and, consequently, a new mechanism for the inhibitory effect of amisyn on exocytosis.

The second part of my experiment mainly focused on an investigation of amisyn's physiological function. To achieve this, we used a mouse line with an amisyn mutation to characterize the physiological, protomeric, and behavioral features of mice born with downregulated amisyn. Building on this animal model, we first investigated the protein levels of amisyn interactors and other synaptic and proteins related to synaptic transmission. Via pull-down assay, we found several underlying candidates and their potential interaction matches physiological phenotype and *in silico* survey in some content. This part is not shown in the publication manuscript since the experiments were preliminary and to keep with the topic of the thesis. Hence, the result of this research will be detail discussed in the following section 4.4.

Next, electrophysiology-based methods and behavioral assays were used to characterize neurotransmission in the amisyn-mutant animals. We found an increase in vesicle release probability in the synapses of the amisyn-mutant mice. Moreover, the RRP size of neurons in the hippocampus of amisyn-mutant mice was increased. In the long-term potentiation experiment, we found that LTP was abolished in neurons lacking amisyn. Abolished LTP indicates potential impairment of learning and memorizing in amisyn-mutant mice. This deduction was confirmed by behavioral assays, including T-maze, novel object recognition, and fear conditioning tests. Additional behavioral assays also revealed the autism-like behavior of amisyn mutant animals. Finally, we used proteomics-based methods (e.g. western blotting) to investigate the levels and distribution of various neuronal proteins in amisyn mutant brains. Those results matched previous physiological recordings and support amisyn's inhibitory mechanism in the first part of this thesis.

#### **4.1 Investigation of amisyn's N-terminal domain**

Although amisyn was first reported almost 20 years ago, the N-terminal of amisyn has never been structurally or functionally characterized. From the sequencing analysis, we found the sequence of the amisyn N-terminal largely overlapped with the part of the Sec-13 protein, which contains a PH-domain. The modeling results of part of the amisyn N-terminal domain based on Sec3p yielded a confidence score of 99%. The results indicated that amisyn's N-terminal domain was very likely to have a similar character to Sec3p. Sec3p is able to associate with PI(4,5)P<sub>2</sub>. We speculated that the recruitment of amisyn to the plasma membrane after KCl stimulation was due to the association between amisyn N-terminal and PI(4,5)P<sub>2</sub> on the PM. To support this speculation, we found that amisyn could no longer bind to the PM after mutation at N-terminal. Further, experiments also proved that amisyn could bind with PI(4,5)P<sub>2</sub>, and that amisyn lost this association after N-terminal mutation. We also found a correlation between amisyn and PI(4,5)P<sub>2</sub> on the plasma membrane in vitro. Therefore, we proved that amisyn's N-terminal domain shared a similar structure and character to the PH domain of Sec3. Thus, we could consider amisyn as a protein that consists of one SNARE domain and one PH-domain.

#### **4.2 Investigation of the mechanism of amisyn-syntaxin association**

In the previous section, we showed that amisyn's N-terminal domain is actually a PH domain. We noticed that the PH domain may interact with other proteins apart from PI(4,5)P<sub>2</sub>. It is reported that the PH domain of Sec3 can interact with GTP/Cdc42, ExoC8, Exo84, and interestingly, sso/syntaxin. Thus, the PH domain may be involved in the formation of the amisyn-SNARE complex and assist with the association of the SNARE domain and syntaxin-1. In the liposome fusion experiment described in the first result part of my thesis, we found that the inhibition of liposome fusion was reduced compared with the addition of full-length amisyn when an external amisyn SNARE motif was added.

### **4.3 Investigation of exocytosis inhibition by amisyn**

Klöpffer et al. speculated that amisyn might have evolved with vertebrates, similar to the SNARE domain of tomosyn (Kloeppe et al., 2007). It is very likely that amisyn and tomosyn share a common ancestor and have developed different N-terminals during evolution. Thus, like tomosyn, amisyn is a potential calcium-free negative regulator of exocytosis and may also share the same regulatory mechanism (Ashery et al., 2009). In the previously proposed model, the SNARE motif of amisyn would compete with VAMP2 and interfere with the formation of the SNARE complex, consequently downregulating exocytosis. In this case, the inhibitory function of amisyn is only based on its SNARE motif (Scales et al., 2002). However, our experiment results pointed to a different mechanism. We found there were significant differences between the effect of full-length amisyn and the amisyn SNARE motif in the liposome fusion experiment and the electrophysiology experiment in cultured chromaffin cells. In this amperometry experiment, we found that amisyn could interfere with the docking/priming and the fusion of secretory vesicles and alter the size of both the readily available and slowly releasable pools. In this experiment, a micro-carbon fiber was placed compactly next to a chromaffin cell in a whole-cell clamp configuration. In this set-up, the secretory release of catecholamine was detected by the carbon fiber, whereas the membrane capacity of the cell was monitored by the detecting electrode in a glass pipette. As chromaffin cells are very small, the release of vast large dense-core vesicles (LDCVs) after stimulation would lead to a decrease in plasma membrane surface and be reflected by the decrease in membrane capacity (De Camilli & Jahn, 1990; Thomas-Reetz & De Camilli, 1994). Hence, we studied exocytosis by comparing the amperometry data and patch-clamp data. In our experiment, we found that there was less decrease in capacity and less secretion after stimulation when the external amisyn SNARE motif was added instead of full-length amisyn. In further spontaneous recordings, there were more spikes (each spike relates to one vesicle release event, similar to mEPSC recording) when the SNARE motif, but not full-length amisyn, was added to the chromaffin cells. The results suggested that not only the SNARE motif, but also the PH domain, was

essential for the inhibition of exocytosis. Notably, the impairment of exocytosis was not limited in the first 30 ms, which relates to the readily releasable pool, but was sustained until 200 ms after stimulation, which relates to the slow releasable pool. This result suggested that full-length amisyn regulated the full-course of exocytosis and was not only limited to the RRP.

Interestingly, we did not find a significant difference in dynamic features (foot duration of the spikes) of vesicle fusion, unlike that reported by Constable et al. (Constable et al., 2005). A possible explanation would be that amisyn regulates the kinetic features owing to the interaction between amisyn and cAMP/cAMP effector proteins. In our experiment, amisyn was directly delivered via patch clamp pipette, but not expressed by the cell itself, as in Constable's and Guček's experiment (Constable et al., 2005; Gucek et al., 2019). The delivery of amisyn inevitably led to the leak of intracellular solution and pipette internal solution, and further resulted in the dilution of cAMP concentration.

The delivery of amisyn inevitably led to a leak between the intracellular solution and the internal pipette solution, and resulted in further dilution of cAMP concentration.

In summary, we found that amisyn's PH domain was also involved in the inhibition of exocytosis, which conflicted with the original model used in Scale's research. In the prototype theory, amisyn competes with VAMP2 to form a SNARE complex with SNAP-25 and syntaxin-1. However, the amisyn-SNARE complex cannot activate the vesicle fusion process as it does not have a transmembrane domain to allow it to dock the vesicle. Thus, the original model proposes that amisyn would "hold" syntaxin-1 and SNAP-25 in a certain conformation. Once the vesicle is ready to undergo fusion, VAMP2 would replace amisyn's position in the SNARE complex and initiate exocytosis. In this model, the PH domain is not involved, and it cannot explain why amisyn can inhibit the full time-course of exocytosis, or why amisyn can be recruited transiently to the plasma membrane after stimulation.

In our new model, although amisyn's SNARE motif forms a SNARE complex with syntaxin-1 and SNAP-25, its PH domain would associate with PI(4,5)P<sub>2</sub> on the plasma membrane. After stimulation, the local composition of PI(4,5)P<sub>2</sub> at the active

zone would temporarily increase, leading to the recruitment of amisyn at the active zone. Such a high local high concentration of amisyn would outcompete VAMP2 and reduce the release probability of vesicle formation. Amisyn would continue to occupy the docking site until the concentration of PI(4,5)P<sub>2</sub> in the plasma membrane was reduced; this provides an explanation for why amisyn can regulate exocytosis until the release of SRP.

#### **4.4 Investigation of novel amisyn interactors**

In the previous section 3.3, I have shown the GST pull down result of amisyn and corresponding mass spec result, which revealed interesting results. We checked the clearest band (except the two amisyn bands), which is at 55 kDa. The result showed that the main composition of this band is alpha-tubulin and beta-tubulin. Considering tubulin is one of the most common background or contamination proteins of the pull-down assay, the formation of these bands may be due to the poor washing since the cytoskeleton protein stuck to the bead (Einarson, Pugacheva, & Orlinick, 2007b). Besides tubulins and amisyn, which was used as the bait, other proteins were also detected on mass spectrometry, but none of them showed a very strong difference between control and sample (Einarson, Pugacheva, & Orlinick, 2007a; Einarson et al., 2007b).

From these results, we were unable to identify solid candidates able to interact directly with amisyn. However, a considerable number of proteins had different relative abundances in the control and pull-down analyses and may be potential indirect interactors with amisyn. Some of those proteins were also identified in previous research and our physiological recordings. For example, we found syntaxin-1B and SNAP-25, which are known amisyn direct/indirect interactors (Scales et al., 2002). We also found synapsin 1/2 was present in the pull-down material, and this was reported as an important regulator of RRP size by Vasilev et al. in 2012 (Vasileva, Horstmann, Geumann, Gitler, & Kuner, 2012). Some other important proteins involved in memory formation and learning regulation, including RASGRF, PPP1CB, PPP1R1B, RAP1, ROCK2, PLC- $\beta$ , and PKC- $\epsilon$ , were detected in

the pull-down (Kandel, 2012; Leal, Comprido, & Duarte, 2014; Liu, Liu, Li, & Sun, 2021; Mahady, He, Malek-Ahmadi, & Mufson, 2021; Xiang et al., 2021). This may be the potential molecular explanation for the impairment of memory and learning in amisyn mutant animals. Furthermore, WDFY3, a protein linked to autophagy and brain mitophagy was also found to be significantly changed between the control and the pull-down assay (Le Duc et al., 2019).

One possible reason for such a non-ideal pull-down result could be the ultrafast centrifuge step removed most membrane proteins. Because amisyn could bind with the plasma membrane with its PH domain, some of the underlying amisyn interactors might be included in these lost membrane proteins. Over-washing of the pull-down outcome before SDS-PAGE might also lose some of the potential interactors.

#### **4.5 Electrophysiological and behavioral characteristics of amisyn mutant mice**

As discussed in the previous section, the physiological properties of amisyn have not been well studied; indeed, there is almost no research on this topic. One reason for the lack of study is the lack of specific reagents and the absence of an appropriate animal model for amisyn research. An easily accessible animal model is the CRISPR global KO model reported in 2021 (C. Liu et al., 2021). In this model, two sgRNAs were inserted into exon 3 of the amisyn gene, which prevented the translation of exon 4. In this way, the whole SNARE motif and part of the PH domain are removed from the expressed amisyn globally. However, part of the PH domain is still expressed. As the PH domain of amisyn has been proven to be involved in the regulation of neurotransmission, this incomplete knockout model may lead to phenotypes that are not sufficiently distinct to be observed. Indeed, it is reported that there was no significant difference between CRISPR KO mice and wild-type mice in several behavioral assays, and the only positive phenotype reported is weight loss.

To overcome this problem, we established an amisyn-mutant mouse line by using a promoter-driven, knock-out strategy in 2016. Protein immunoblotting results showed that the expression of amisyn was ~90% lower in the hippocampus of the amisyn-mutant mice. Using this model, we performed several different

electrophysiological and behavioral assays to investigate if amisyn deficiency would affect mammalian behavior or synaptic physiology.

In the previous model by Scale and the model presented in our first publication, amisyn is speculated to be an inhibitor of exocytosis (Scales et al., 2002). Usually, the inhibitory effect on the presynaptic side should reflect the frequency of mEPSC events. We detected an increase in mEPSC frequency on the brain slice in the CA1 region of the hippocampus from mutant animals (Turrigiano & Nelson, 2004). However, an increase in the number of synapses or an increase in postsynaptic AMPA receptors can be other possible reasons for the increased mEPSC frequency (Davenport et al., 2019; Madara & Levine, 2008). In the following proteomic measurement, we did not detect an increase in synaptic indicators or postsynaptic receptors. In the following experiment, we measured PPR in the Schaffer collaterals and mossy fibers. In both analyses, we found a decrease in PPR in the mutant animals. The pair-pulse ratio is the ratio between two EPSCs with a certain time interval between their stimulation. After the first stimulation, the internal calcium concentration would be increased owing to exocytosis. Thus, the initial calcium concentration for the second EPSC is higher than the first EPSC, which should be reflected by the higher amplitude. Such an increase in amplitude is also called synaptic facilitation. However, synaptic facilitation may be weakened or absent when the release probability is high and the time interval between two EPSCs is short, because a higher  $P_r$  would consume more vesicles in the release pool and the release pool cannot fully recover for the second stimulation (Zucker & Regehr, 2002). Besides high  $P_r$ , the increase of calcium coupling efficiency can be another possible explanation for deficient synaptic facilitation. However, we failed to find calcium sensor expression increase in mutant animals' hippocampus. Hence, amisyn mutant animals have a higher  $P_r$  compared to WT animals (Branco & Staras, 2009; Korber & Kuner, 2016; Wu & Borst, 1999). Such an increase in release probability has also been reported in tomosyn-deficient synapses (Barak et al., 2010; Yizhar et al., 2004). With this evidence, we have proven that amisyn has an inhibitory effect on mammalian synapses.

In the chromaffin cell experiment where amisyn is externally added, we found a decrease in RRP size. Using electrorheological methods, we found an increase of RRP size in CA1 and CA3 synapses with less amisyn, which consisted with chromaffin cell experiment results. The regulation of RRP is also found in tomosyn and complexin regulated animal models (Cazares et al., 2016; Zhou et al., 2017). The formation of RRP is caused by the pre-docking and priming of the vesicles. These vesicles are prepared for release directly at or near the active release site (Kaeser & Regehr, 2017; Millar et al., 2002). In the presence of amisyn, it would compete with VAMP2 and occupy the active site by binding with PI(4,5)P<sub>2</sub> on the plasma membrane. Hence, we detected an increase in RRP size when amisyn was absent. Apart from the RRP size, the vesicle recovery speed was also found to be increased in the same experiment. However, the ratio between RRP size and recovery speed remained the same, which was further supported by the result of recovery the EPSC experiments. The reason for increasing recovery speed may share the same mechanism as the increase of RRP size: the absence of amisyn provides more sites for new recycled vesicles to dock and prime (Ritzau-Jost et al., 2018). Moreover, the unchanged recovery of EPSC suggested that amisyn deficiency did not interfere with the formation and acidification of recycling vesicles. Interestingly, the RRP of the amisyn deficient synapse failed to fully recover after 1s or even 3s. The detailed mechanism behind such recovery impairment was unclear. A possible explanation could be that amisyn got involved in the disassembling of SNARE complex after the vesicle fusion.

In the immunohistochemistry experiments, we found the enrichment of amisyn in the hippocampus, which is essential for memory formation (Gustafsson et al., 1987). An essential neuronal process involved in the formation of short-term memory is LTP. LTP is a persistent enhancement of synaptic plasticity that underlies an increase in signal transmission between two neurons. LTP is abolished in tomosyn- and complexin-KD mice and we detected similar abolishment of LTP in amisyn-mutant mice (Ahmad et al., 2012; Ben-Simon et al., 2015). The expression of LTP is associated with three main parameters: the number of active release sites; the possibility of neurotransmitter release; and the postsynaptic receptors that respond to

neurotransmitters. Among these three factors, the first two are presynaptically related, whereas the third is postsynaptically related (Schulz, 1997). In previous research, it was proven that the absence of LTP in the tomosyn- and complexin-KO/KD model is postsynaptically irrelevant. We also failed to detect a difference in the expression of postsynaptic proteins in the hippocampus of the mutant mice. This evidence indicates the mechanism of LTP deficiency by amisyn. The pair-pulse ratio is strongly related to the magnitude of LTP. It is reported that LTP would be abolished when the release probability is high, and LTP would be regained when the release probability was artificially reduced. A possible explanation for such reverse correlation between LTP and the release probability is that the excess release of neurotransmitters saturates or occludes the LTP. Considering we have proven an increase in vesicle release probability in amisyn-deficient synapses, it is very likely that a high-release probability is the cause of decreased LTP in amisyn-mutant mice. Meanwhile, the binding of amisyn's PH-domain and plasma membrane may allow it to occupy the docking site for vesicles in the active zone. This could reduce the number of active release sites and support the reduction of LTP.

The diminished LTP could cause low efficiency of information transmission between neurons. If this happens in the hippocampus, the formation of memory would be impaired, and the learning ability of animals would be impaired. We performed several behavioral assays to determine if amisyn-mutant animals exhibited such phenotypes. In the T-maze test, we found that amisyn-mutant mice had difficulties with learning and reference/working memory (Patil, Sunyer, Hoger, & Lubec, 2009). The mutant animals could not memorize bait pattern after days of learning and only made choices by chance. Besides the T-maze test, which is widely used in the evaluation of working and reference learning ability, we also performed a NOR test and a fear conditioning test to investigate the visual cognition level of amisyn-mutant mice (Lueptow, 2017; Singewald & Holmes, 2019). The results indicated that the absence of amisyn also causes severe disorder of visual working memory. Mutant animals could recognize neither novel objects nor the graphic pattern of fear conditioning. In summary, we verified the disorder of learning and memorizing ability

in amisyn-mutant mice, which was highly possible owing to the deficiency of LTP in the hippocampus.

Although the function of amisyn in neurotransmission is still not fully determined, it is already associated with many physical or mental disorders. Autism, as a neurodevelopmental disorder related to social interaction and communication, is one of these disorders (Castermans et al., 2008; Castermans et al., 2010). First, the researchers found that amisyn expression was silenced in a boy with autism and eye coloboma due to mosaicism by a ring chromosome on chromosome 14. In the ultrastructural analysis of blood platelets from another patient with amisyn haploinsufficiency, the researchers found morphological abnormalities in the dense core granules. Thus, it is highly suspected that amisyn mutations may lead to autism via the disordered regulation of exocytosis. In our experiments, we also detected social communication disorders in amisyn-mutant mice. They showed no preference for spending time with other animals compared with spending time in an empty cage. We also found that amisyn-mutant animals spent more time on self-grooming. Lengthy repetitive self-grooming was considered to be an indicator of autism behavior in the mouse model, which is very similar to the hand-clapping and body-moving behavior of patients with ASD (Silverman et al., 2010).

The weight loss was reported in Liu's amisyn KO mouse model, which might associate with some diabetes or ASD phenotypes (C. Liu et al., 2021). In our amisyn mutant model, I also found a tendency of weight loss in STXBP<sup>tm1a</sup> mice. However, these data were still preliminary and need further research to study its relationship with diabetes or other diseases.

#### **4.6 Investigation of the levels and distribution of various neuronal proteins in amisyn mutant mice brains**

In addition to the electrophysiological and behavior assays, proteomic analysis is another powerful tool to characterize the features of mutant mice. By understanding the transcription and expression level of different neuronal proteins, we could infer the underlying phenotypes in the mice, and further help us to understand the

physiological mechanisms behind these phenotypes. This may also provide some clues and additional information about the interaction between amisyn and other proteins. In the western blotting and qPCR experiments, we found no change in either expression or transcription level of postsynaptic proteins, suggesting that several phenotypes, including increased mEPSC frequency and the absence of LTP, were caused by presynaptic side changes. The expression levels of Q-SNARE proteins were not changed, proving that the release probability increase in amisyn-deficient synapses was not related to the change in the expression level of other SNARE proteins. Interestingly, we found that the VAMP2 expression level was decreased in amisyn-mutant mice. This could act as negative feedback for amisyn deficiency. The amisyn mutant would lead to excess exocytosis, showing that the expression of VAMP2 was downregulated, neutralizing the effect of the absence of its competitor. The other two neuronal proteins that were found to be changed in expression were rab3a and  $\alpha$ -synuclein. Both these proteins are peripheral vesicle proteins, which play important roles in the docking and priming steps of exocytosis. It is reported that the expression level of Rab3 and  $\alpha$ -synuclein can affect vesicle release probability and RRP size at the synapses (Bellani et al., 2010; Schluter et al., 2006). Thus, the increased Rab3 and  $\alpha$ -synuclein levels in mutant mice may contribute to the increased  $P_r$  and RRP size.

## 5. Summary and outlook

### 5.1 Summary of thesis work

Neurotransmission is the basis of fundamental brain functions, such as motor control, learning, cognitive process, and memory formation. Understanding the complex recycling process of synaptic vesicles at the neuronal synapse is essential for the study of neurotransmission. The complete SV recycling process contains several different steps, including endocytosis, vesicle acidification, neurotransmitter loading, vesicle maturation, and exocytosis. Exocytosis, as it directly mediates neurotransmitter release, has been studied for decades, as well as its regulators. Among these regulators of exocytosis, amisyn or STXBP6 is still surprisingly overlooked by researchers. Although the protein was first reported almost 20 years ago, the basic structural and functional characters of this protein are still not fully understood.

Amisyn was initially reported with a C-terminal SNARE domain and an unknown N-terminal domain. It was proven *in vitro* that amisyn can bind with syntaxin-1 and further form a SNARE complex with SNAP-25. As amisyn does not contain a trans-membrane domain, the amisyn-SNARE complex is fusion-inactive. In the model developed in 2002, amisyn was proposed to compete with VAMP2 and inhibit the docking and fusion of the vesicles, until the correct time for amisyn to transfer its position to VAMP2 and initiate the fusion process. However, this model does not consider the function of the N-terminal of amisyn and failed to explain some important phenomena, including the long-lasting inhibitory effect of amisyn and the recruitment of amisyn to the plasma membrane after stimulation. The goal of my thesis was to progress the comprehension of this important exocytosis regulator, and to understand its structure and role in the neurotransmission process.

In the first study, we suspected that the N-terminal of amisyn was a PH domain, based on the sequencing analysis. This speculation was further confirmed by the association between the N-terminal of amisyn and PI(4,5)P<sub>2</sub>. We also found a correlation between amisyn and PI(4,5)P<sub>2</sub> on the plasma membrane after KCl stimulation. Furthermore, we investigated if the PH domain of amisyn was involved in the formation of the SNARE complex and the inhibition of exocytosis. In the liposome fusion experiment,

we found that full-length amisyn was required for the formation of the amisyn-SNARE complex. In the amperometry experiment, we found that the PH-domain of amisyn was necessary for a complete inhibition of exocytosis. The addition of external amisyn resulted a change in the size of RRP and SRP, but did not change the kinetic features of vesicle fusion. Based on our experiment results, we proposed a new model to explain the role of amisyn in exocytosis. In this new model, amisyn would compete with VAMP2 and form a SNARE complex with syntaxin-1 and SNAP-25, to impede the docking and priming of vesicles. After stimulation, amisyn associates with PI(4,5)P<sub>2</sub> on the active zone and blocks the active site for vesicle fusion, further inhibiting exocytosis.

In the second set of experiments, we used a newly generated amisyn-mutant mouse model to characterize the physiological properties of amisyn. We first used amisyn brain homogenate and purified amisyn to characterize the biochemical features of amisyn, as mentioned in the discussion but not the manuscript. We performed pull-down assays to investigate the interaction between amisyn and other proteins. We confirmed amisyn's interaction with syntaxin, but we did not find solid proof for a direct amisyn interactor. Despite that, we found several candidates that may be direct or indirect interactors with amisyn, and these proteins were involved in several amisyn-related biological processes, including the formation of the release vesicle pool, learning and memory formation, and autophagy. Then, we used electrophysiological and behavioral assays to characterize neurotransmission in amisyn-deficient hippocampal neurons. We reported an increase in mEPSC frequency and EPSC amplitude in the neurons in the CA1 region of mutant mice. In addition, we found that amisyn deficiency caused a decrease in the pair-pulse ratio in CA1 and CA3 synapses. These results indicated that a loss of amisyn may lead to an increased probability of vesicle release on the presynaptic side. Further experiments showed that such up-regulation of P<sub>r</sub> was accompanied by the enlargement of RRP and the elimination of LTP. In the following behavior assays, we confirmed the impairment of learning and memory formation in amisyn-mutant mice. In addition, autism-related behavior, such as social communication disorder and self-repetitive grooming, was

also observed in amisyn-mutant mice. In the proteomic analyses, we found that most synaptic proteins, especially the postsynaptic proteins and calcium channels, were not regulated after the loss of amisyn. The only proteins altered were VAMP2, rab3a, and  $\alpha$ -synuclein. The regulation of these proteins may be related to the regulation of P<sub>r</sub> and RRP.

With the help of these two studies, we have obtained the further understanding of this previously overlooked exocytosis regulator. This information may contribute to the further study of complex amisyn-involved pathological problems, such as diabetes, autism, and Parkinson's disease.

## 5.2 Future perspectives

In the two studies mentioned in this thesis, we have resolved the unknown nature of amisyn's N-terminal structure, and identified its physiological function in hippocampal neurons. However, there are still some problems about amisyn that remain unsolved.

Although we have confirmed that amisyn consists of one SNARE-domain and one PH-domain, the detailed 3D special structure of amisyn is still not confirmed. There are differences in the *in silico* predicted amisyn structures, but none of these predictions have yet been proven. The crystallization of amisyn would help to resolve these issues, contributing to further understanding of amisyn and its phosphorylation at the molecular level.

In the second study, we explored the details of the inhibitory effect of amisyn on exocytosis on the presynaptic side. However, it has been proven that many synaptic proteins are involved in more than one process. Under different spatial and temporal conditions, the same protein may have different functions in the cellular trafficking process. Tomosyn, as a protein related to amisyn, is involved in both docking, priming, fusion, and after fusion (Ashery et al., 2009). Considering that amisyn is reported to interact with syntaxin-4, it may be related to some postsynaptic processes, which require further studies (Scales et al., 2002).

In addition, the *in vivo* characterization of amisyn function on the presynaptic side is

mainly based on electrophysiological and behavioral assays. To gain an understanding of amisyn's role on the presynaptic side, other experimental assays using different technologies are required. For example, electron microscopy images would help to determine the distance between the vesicles and plasma membrane in the synapses of amisyn-mutant animals. Other fluorescence imaging experiments, including pHluorin and FM dye, would help to support our conclusion on the increased release probability and the RRP size in neurons from amisyn-mutant mice (Newton & Murthy, 2006; Seitz & Rizzoli, 2019).

In the first part of the study, we observed an interaction between the amisyn PH-domain and the lipid PI(4,5)P<sub>2</sub>. Such an interaction between a protein and a lipid is commonly regulated by phosphorylation (Milosevic, 2018). As amisyn's inhibition of exocytosis is associated with binding to the plasma membrane, the phosphorylation process of amisyn may play an essential role in the regulation of amisyn exocytosis. After phosphorylation/dephosphorylation, it may switch state and allow the binding/unbinding of amisyn with the plasma membrane. In the pull-down experiment, we found several kinases that may phosphorylate amisyn, including PKA and PKC. However, the phosphorylation sites of amisyn are still not determined. A study of the phosphorylation process of amisyn may be beneficial for further research into the mechanism of the inhibitory function of amisyn.

Moreover, PKA is essential for MF-LTP (Weisskopf, Castillo, Zalutsky, & Nicoll, 1994). Further plasticity experiments in the MF project would also contribute to the study of amisyn's phosphorylation. In the recovery EPSC experiment, we noticed an impairment of long-term RRP recovery (more than 1s) in amisyn mutant animals. In section 4.5, I suppose such impairment is relevant to the NSF combination after vesicle fusion. Further work is required to confirm this speculation.

Although we have successfully generated an animal model deficient in amisyn, it is also very important to have another model with excess amisyn for comparison. However, the overexpression of amisyn is still lethal for cultured neurons. Thus, it is important to develop effective cell and animal models with amisyn overexpression in future research.

Despite enrichment in the brain, amisyn is expressed in other organs and is involved in other biological processes. There are several pieces of research into the role of amisyn in insulin secretion in beta-cells (Barg & Gucek, 2016; Collins et al., 2016). Moreover, amisyn has been found to be related to the process of autophagy in cancer cells (Krintel et al., 2012). The study of amisyn's roles outside of the neural system would contribute to the knowledge of amisyn's function throughout the human body. The thesis was performed with the aim of understanding more about this essential, but overlooked, SNARE protein: amisyn. I sincerely hope that my work in this thesis will help researchers to understand further features of amisyn and help to understand the pathological mechanism of amisyn-related diseases.

## Reference

- Ahmad, M., Polepalli, J. S., Goswami, D., Yang, X., Kaeser-Woo, Y. J., Sudhof, T. C., & Malenka, R. C. (2012). Postsynaptic complexin controls AMPA receptor exocytosis during LTP. *Neuron*, 73(2), 260-267. doi:10.1016/j.neuron.2011.11.020
- An, S., & Zenisek, D. (2004). Regulation of exocytosis in neurons and neuroendocrine cells. *Curr Opin Neurobiol*, 14(5), 522-530. doi:10.1016/j.conb.2004.08.008
- Ashery, U., Bielopolski, N., Barak, B., & Yizhar, O. (2009). Friends and foes in synaptic transmission: the role of tomosyn in vesicle priming. *Trends Neurosci*, 32(5), 275-282. doi:10.1016/j.tins.2009.01.004
- Barak, B., Williams, A., Bielopolski, N., Gottfried, I., Okun, E., Brown, M. A., . . . Ashery, U. (2010). Tomosyn expression pattern in the mouse hippocampus suggests both presynaptic and postsynaptic functions. *Front Neuroanat*, 4, 149. doi:10.3389/fnana.2010.00149
- Barg, S., & Gucek, A. (2016). How Kiss-and-Run Can Make Us Sick: SOX4 Puts a Break on the Pore. *Diabetes*, 65(7), 1791-1793. doi:10.2337/dbi16-0019
- Baumert, M., Maycox, P. R., Navone, F., De Camilli, P., & Jahn, R. (1989).

- Synaptobrevin: an integral membrane protein of 18,000 daltons present in small synaptic vesicles of rat brain. *EMBO J*, 8(2), 379-384.
- Bellani, S., Sousa, V. L., Ronzitti, G., Valtorta, F., Meldolesi, J., & Chieregatti, E. (2010). The regulation of synaptic function by alpha-synuclein. *Commun Integr Biol*, 3(2), 106-109. doi:10.4161/cib.3.2.10964
- Ben-Simon, Y., Rodenas-Ruano, A., Alvina, K., Lam, A. D., Stuenkel, E. L., Castillo, P. E., & Ashery, U. (2015). A Combined Optogenetic-Knockdown Strategy Reveals a Major Role of Tomosyn in Mossy Fiber Synaptic Plasticity. *Cell Rep*, 12(3), 396-404. doi:10.1016/j.celrep.2015.06.037
- Bennett, M. K., Calakos, N., & Scheller, R. H. (1992). Syntaxin: a synaptic protein implicated in docking of synaptic vesicles at presynaptic active zones. *Science*, 257(5067), 255-259. doi:10.1126/science.1321498
- Blasi, J., Chapman, E. R., Link, E., Binz, T., Yamasaki, S., De Camilli, P., . . . Jahn, R. (1993). Botulinum neurotoxin A selectively cleaves the synaptic protein SNAP-25. *Nature*, 365(6442), 160-163. doi:10.1038/365160a0
- Blasi, J., Chapman, E. R., Yamasaki, S., Binz, T., Niemann, H., & Jahn, R. (1993). Botulinum neurotoxin C1 blocks neurotransmitter release by means of cleaving HPC-1/syntaxin. *EMBO J*, 12(12), 4821-4828.
- Bowers, M. R., & Reist, N. E. (2020). Synaptotagmin: Mechanisms of an electrostatic switch. *Neurosci Lett*, 722, 134834. doi:10.1016/j.neulet.2020.134834
- Branco, T., & Staras, K. (2009). The probability of neurotransmitter release: variability and feedback control at single synapses. *Nat Rev Neurosci*, 10(5), 373-383. doi:10.1038/nrn2634
- Brodal, A. (1980). [Changes in our view on the organization of the central nervous system. Have they significance for clinical neurology?]. *Tidsskr Nor Laegeforen*, 100(26), 1531-1534.
- Bykhovskaia, M. (2011). Synapsin regulation of vesicle organization and functional pools. *Semin Cell Dev Biol*, 22(4), 387-392. doi:10.1016/j.semdb.2011.07.003
- Castermans, D., Thienpont, B., Volders, K., Crepel, A., Vermeesch, J. R.,

- Schrander-Stumpel, C. T., . . . Devriendt, K. (2008). Position effect leading to haploinsufficiency in a mosaic ring chromosome 14 in a boy with autism. *Eur J Hum Genet*, *16*(10), 1187-1192. doi:10.1038/ejhg.2008.71
- Castermans, D., Volders, K., Crepel, A., Backx, L., De Vos, R., Freson, K., . . . Creemers, J. W. (2010). SCAMP5, NBEA and AMISYN: three candidate genes for autism involved in secretion of large dense-core vesicles. *Hum Mol Genet*, *19*(7), 1368-1378. doi:10.1093/hmg/ddq013
- Cazares, V. A., Njus, M. M., Manly, A., Saldate, J. J., Subramani, A., Ben-Simon, Y., . . . Stuenkel, E. L. (2016). Dynamic Partitioning of Synaptic Vesicle Pools by the SNARE-Binding Protein Tomosyn. *J Neurosci*, *36*(44), 11208-11222. doi:10.1523/JNEUROSCI.1297-16.2016
- Clary, D. O., Griff, I. C., & Rothman, J. E. (1990). SNAPs, a family of NSF attachment proteins involved in intracellular membrane fusion in animals and yeast. *Cell*, *61*(4), 709-721. doi:10.1016/0092-8674(90)90482-t
- Clements, J. D., & Bekkers, J. M. (1997). Detection of spontaneous synaptic events with an optimally scaled template. *Biophys J*, *73*(1), 220-229. doi:10.1016/S0006-3495(97)78062-7
- Collins, S. C., Do, H. W., Hastoy, B., Hugill, A., Adam, J., Chibalina, M. V., . . . Rorsman, P. (2016). Increased Expression of the Diabetes Gene SOX4 Reduces Insulin Secretion by Impaired Fusion Pore Expansion. *Diabetes*, *65*(7), 1952-1961. doi:10.2337/db15-1489
- Constable, J. R., Graham, M. E., Morgan, A., & Burgoyne, R. D. (2005). Amisyn regulates exocytosis and fusion pore stability by both syntaxin-dependent and syntaxin-independent mechanisms. *J Biol Chem*, *280*(36), 31615-31623. doi:10.1074/jbc.M505858200
- Davenport, E. C., Szulc, B. R., Drew, J., Taylor, J., Morgan, T., Higgs, N. F., . . . Kittler, J. T. (2019). Autism and Schizophrenia-Associated CYFIP1 Regulates the Balance of Synaptic Excitation and Inhibition. *Cell Rep*, *26*(8), 2037-2051 e2036. doi:10.1016/j.celrep.2019.01.092
- De Camilli, P., & Jahn, R. (1990). Pathways to regulated exocytosis in neurons. *Annu*

- Rev Physiol*, 52, 625-645. doi:10.1146/annurev.ph.52.030190.003205
- de Wit, H. (2010). Morphological docking of secretory vesicles. *Histochem Cell Biol*, 134(2), 103-113. doi:10.1007/s00418-010-0719-5
- Einarson, M. B., Pugacheva, E. N., & Orlinick, J. R. (2007a). GST Pull-down. *CSH Protoc*, 2007, pdb prot4757. doi:10.1101/pdb.prot4757
- Einarson, M. B., Pugacheva, E. N., & Orlinick, J. R. (2007b). Identification of Protein-Protein Interactions with Glutathione-S-Transferase (GST) Fusion Proteins. *CSH Protoc*, 2007, pdb top11. doi:10.1101/pdb.top11
- Fasshauer, D., Eliason, W. K., Brunger, A. T., & Jahn, R. (1998). Identification of a minimal core of the synaptic SNARE complex sufficient for reversible assembly and disassembly. *Biochemistry*, 37(29), 10354-10362. doi:10.1021/bi980542h
- Ferdaoussi, M., Fu, J., Dai, X., Manning Fox, J. E., Suzuki, K., Smith, N., . . . MacDonald, P. E. (2017). SUMOylation and calcium control syntaxin-1A and secretagogin sequestration by tomosyn to regulate insulin exocytosis in human ss cells. *Sci Rep*, 7(1), 248. doi:10.1038/s41598-017-00344-z
- Fernandez, M., Mollinedo-Gajate, I., & Penagarikano, O. (2018). Neural Circuits for Social Cognition: Implications for Autism. *Neuroscience*, 370, 148-162. doi:10.1016/j.neuroscience.2017.07.013
- Fujita, Y., Shirataki, H., Sakisaka, T., Asakura, T., Ohya, T., Kotani, H., . . . Takai, Y. (1998). Tomosyn: a syntaxin-1-binding protein that forms a novel complex in the neurotransmitter release process. *Neuron*, 20(5), 905-915. doi:10.1016/s0896-6273(00)80472-9
- Geppert, M., Archer, B. T., 3rd, & Sudhof, T. C. (1991). Synaptotagmin II. A novel differentially distributed form of synaptotagmin. *J Biol Chem*, 266(21), 13548-13552.
- Glick, B. S., & Rothman, J. E. (1987). Possible role for fatty acyl-coenzyme A in intracellular protein transport. *Nature*, 326(6110), 309-312. doi:10.1038/326309a0
- Gucek, A., Gandasi, N. R., Omar-Hmeadi, M., Bakke, M., Doskeland, S. O.,

- Tengholm, A., & Barg, S. (2019). Fusion pore regulation by cAMP/Epac2 controls cargo release during insulin exocytosis. *Elife*, 8. doi:10.7554/eLife.41711
- Gustafsson, B., Wigstrom, H., Abraham, W. C., & Huang, Y. Y. (1987). Long-term potentiation in the hippocampus using depolarizing current pulses as the conditioning stimulus to single volley synaptic potentials. *J Neurosci*, 7(3), 774-780.
- Herculano-Houzel, S. (2012). The remarkable, yet not extraordinary, human brain as a scaled-up primate brain and its associated cost. *Proc Natl Acad Sci U S A*, 109 Suppl 1, 10661-10668. doi:10.1073/pnas.1201895109
- Herculano-Houzel, S. (2014). The glia/neuron ratio: how it varies uniformly across brain structures and species and what that means for brain physiology and evolution. *Glia*, 62(9), 1377-1391. doi:10.1002/glia.22683
- Ince, C., van Bavel, E., van Duijn, B., Donkersloot, K., Coremans, A., Ypey, D. L., & Verveen, A. A. (1986). Intracellular microelectrode measurements in small cells evaluated with the patch clamp technique. *Biophys J*, 50(6), 1203-1209. doi:10.1016/S0006-3495(86)83563-9
- Jahn, R., & Fasshauer, D. (2012). Molecular machines governing exocytosis of synaptic vesicles. *Nature*, 490(7419), 201-207. doi:10.1038/nature11320
- Kaesler, P. S., & Regehr, W. G. (2017). The readily releasable pool of synaptic vesicles. *Curr Opin Neurobiol*, 43, 63-70. doi:10.1016/j.conb.2016.12.012
- Kandel, E. R. (2012). The molecular biology of memory: cAMP, PKA, CRE, CREB-1, CREB-2, and CPEB. *Mol Brain*, 5, 14. doi:10.1186/1756-6606-5-14
- Kloepper, T. H., Kienle, C. N., & Fasshauer, D. (2007). An elaborate classification of SNARE proteins sheds light on the conservation of the eukaryotic endomembrane system. *Mol Biol Cell*, 18(9), 3463-3471. doi:10.1091/mbc.e07-03-0193
- Kondratiuk, I., Jakhanwal, S., Jin, J., Sathyanarayanan, U., Kroppen, B., Pobbati, A. V., . . . Milosevic, I. (2020). PI(4,5)P2-dependent regulation of exocytosis by amisyn, the vertebrate-specific competitor of synaptobrevin 2. *Proc Natl Acad Sci U S A*, 117(12), 6453-6462. doi:10.1073/pnas.2001111117

- Sci U S A*, 117(24), 13468-13479. doi:10.1073/pnas.1908232117
- Korber, C., & Kuner, T. (2016). Molecular Machines Regulating the Release Probability of Synaptic Vesicles at the Active Zone. *Front Synaptic Neurosci*, 8, 5. doi:10.3389/fnsyn.2016.00005
- Krintel, S. B., Essioux, L., Wool, A., Johansen, J. S., Schreiber, E., Zekharya, T., . . . Hetland, M. L. (2012). CD6 and syntaxin binding protein 6 variants and response to tumor necrosis factor alpha inhibitors in Danish patients with rheumatoid arthritis. *PLoS One*, 7(6), e38539. doi:10.1371/journal.pone.0038539
- Le Duc, D., Giulivi, C., Hiatt, S. M., Napoli, E., Panoutsopoulos, A., Harlan De Crescenzo, A., . . . Jamra, R. (2019). Pathogenic WDFY3 variants cause neurodevelopmental disorders and opposing effects on brain size. *Brain*, 142(9), 2617-2630. doi:10.1093/brain/awz198
- Leal, G., Comprido, D., & Duarte, C. B. (2014). BDNF-induced local protein synthesis and synaptic plasticity. *Neuropharmacology*, 76 Pt C, 639-656. doi:10.1016/j.neuropharm.2013.04.005
- Lenka, G., Tsai, M. H., Lin, H. C., Hsiao, J. H., Lee, Y. C., Lu, T. P., . . . Chuang, E. Y. (2017). Identification of Methylation-Driven, Differentially Expressed STXBP6 as a Novel Biomarker in Lung Adenocarcinoma. *Sci Rep*, 7, 42573. doi:10.1038/srep42573
- Littleton, J. T., Barnard, R. J., Titus, S. A., Slind, J., Chapman, E. R., & Ganetzky, B. (2001). SNARE-complex disassembly by NSF follows synaptic-vesicle fusion. *Proc Natl Acad Sci U S A*, 98(21), 12233-12238. doi:10.1073/pnas.221450198
- Liu, C., Hu, Q., Chen, Y., Wu, L., Liu, X., & Liang, D. (2021). Behavioral and Gene Expression Analysis of Stxbp6-Knockout Mice. *Brain Sci*, 11(4). doi:10.3390/brainsci11040436
- Liu, L., Liu, Z., Li, Y., & Sun, C. (2021). Integration of metabolomics and proteomics to highlight altered neural development related pathways in the adult offspring after maternal folic acid supplement. *Clin Nutr*, 40(2), 476-487. doi:10.1016/j.clnu.2020.05.042

- Liu, Y., Huang, Z., Wei, Y., Zhang, M., Li, X., Yang, S., & Wang, H. (2021). Identification of STXBP6-IRF1 positive feedback loop in regulation of PD-L1 in cancer. *Cancer Immunol Immunother*, *70*(2), 275-287. doi:10.1007/s00262-020-02678-6
- Lledo, P. M., Johannes, L., Vernier, P., Zorec, R., Darchen, F., Vincent, J. D., . . . Mason, W. T. (1994). Rab3 proteins: key players in the control of exocytosis. *Trends Neurosci*, *17*(10), 426-432. doi:10.1016/0166-2236(94)90017-5
- Lopez-Font, I., Torregrosa-Hetland, C. J., Villanueva, J., & Gutierrez, L. M. (2010). t-SNARE cluster organization and dynamics in chromaffin cells. *J Neurochem*, *114*(6), 1550-1556. doi:10.1111/j.1471-4159.2010.06872.x
- Lueptow, L. M. (2017). Novel Object Recognition Test for the Investigation of Learning and Memory in Mice. *J Vis Exp*(126). doi:10.3791/55718
- Luo, G., Sui, D., Wang, K., & Chae, J. (2015). Neuron anatomy structure reconstruction based on a sliding filter. *BMC Bioinformatics*, *16*, 342. doi:10.1186/s12859-015-0780-0
- Ma, N., Niu, R. F., & Ma, Y. J. (2008). Intersectin 1: a molecular linker in the central nervous system. *Neurosci Bull*, *24*(6), 401-405. doi:10.1007/s12264-008-0715-0
- Madara, J. C., & Levine, E. S. (2008). Presynaptic and postsynaptic NMDA receptors mediate distinct effects of brain-derived neurotrophic factor on synaptic transmission. *J Neurophysiol*, *100*(6), 3175-3184. doi:10.1152/jn.90880.2008
- Magdziarek, M., Bolembach, A. A., Stepien, K. P., Quade, B., Liu, X., & Rizo, J. (2020). Re-examining how Munc13-1 facilitates opening of syntaxin-1. *Protein Sci*, *29*(6), 1440-1458. doi:10.1002/pro.3844
- Mahady, L. J., He, B., Malek-Ahmadi, M., & Mufson, E. J. (2021). Telomeric alterations in the default mode network during the progression of Alzheimer's disease: Selective vulnerability of the precuneus. *Neuropathol Appl Neurobiol*, *47*(3), 428-440. doi:10.1111/nan.12672
- Marina, N., Turovsky, E., Christie, I. N., Hosford, P. S., Hadjihambi, A., Korsak, A., . . . Gourine, A. V. (2018). Brain metabolic sensing and metabolic

- signaling at the level of an astrocyte. *Glia*, 66(6), 1185-1199.  
doi:10.1002/glia.23283
- Martin, S. J., Grimwood, P. D., & Morris, R. G. (2000). Synaptic plasticity and memory: an evaluation of the hypothesis. *Annu Rev Neurosci*, 23, 649-711.  
doi:10.1146/annurev.neuro.23.1.649
- McMahon, H. T., Missler, M., Li, C., & Sudhof, T. C. (1995). Complexins: cytosolic proteins that regulate SNAP receptor function. *Cell*, 83(1), 111-119.  
doi:10.1016/0092-8674(95)90239-2
- Millar, A. G., Bradacs, H., Charlton, M. P., & Atwood, H. L. (2002). Inverse relationship between release probability and readily releasable vesicles in depressing and facilitating synapses. *J Neurosci*, 22(22), 9661-9667.
- Miller, A. C., & Pereda, A. E. (2017). The electrical synapse: Molecular complexities at the gap and beyond. *Dev Neurobiol*, 77(5), 562-574.  
doi:10.1002/dneu.22484
- Milosevic, I. (2018). Spatial and Temporal Aspects of Phosphoinositides in Endocytosis Studied in the Isolated Plasma Membranes. *Methods Mol Biol*, 1847, 147-160. doi:10.1007/978-1-4939-8719-1\_11
- Milovanovic, D., & De Camilli, P. (2017). Synaptic Vesicle Clusters at Synapses: A Distinct Liquid Phase? *Neuron*, 93(5), 995-1002.  
doi:10.1016/j.neuron.2017.02.013
- Misura, K. M., Scheller, R. H., & Weis, W. I. (2000). Three-dimensional structure of the neuronal-Sec1-syntaxin 1a complex. *Nature*, 404(6776), 355-362.  
doi:10.1038/35006120
- Monje, M. (2018). Myelin Plasticity and Nervous System Function. *Annu Rev Neurosci*, 41, 61-76. doi:10.1146/annurev-neuro-080317-061853
- Neher, E. (2006). A comparison between exocytic control mechanisms in adrenal chromaffin cells and a glutamatergic synapse. *Pflugers Arch*, 453(3), 261-268.  
doi:10.1007/s00424-006-0143-9
- Newton, J., & Murthy, V. (2006). Measuring exocytosis in neurons using FM labeling. *J Vis Exp*(1), 117. doi:10.3791/117

- Oyler, G. A., Higgins, G. A., Hart, R. A., Battenberg, E., Billingsley, M., Bloom, F. E., & Wilson, M. C. (1989). The identification of a novel synaptosomal-associated protein, SNAP-25, differentially expressed by neuronal subpopulations. *J Cell Biol*, *109*(6 Pt 1), 3039-3052. doi:10.1083/jcb.109.6.3039
- Patil, S. S., Sunyer, B., Hoger, H., & Lubec, G. (2009). Evaluation of spatial memory of C57BL/6J and CD1 mice in the Barnes maze, the Multiple T-maze and in the Morris water maze. *Behav Brain Res*, *198*(1), 58-68. doi:10.1016/j.bbr.2008.10.029
- Perin, M. S., Fried, V. A., Mignery, G. A., Jahn, R., & Sudhof, T. C. (1990). Phospholipid binding by a synaptic vesicle protein homologous to the regulatory region of protein kinase C. *Nature*, *345*(6272), 260-263. doi:10.1038/345260a0
- Pobbati, A. V., Razeto, A., Boddener, M., Becker, S., & Fasshauer, D. (2004). Structural basis for the inhibitory role of tomosyn in exocytosis. *J Biol Chem*, *279*(45), 47192-47200. doi:10.1074/jbc.M408767200
- Prinslow, E. A., Stepien, K. P., Pan, Y. Z., Xu, J., & Rizo, J. (2019). Multiple factors maintain assembled trans-SNARE complexes in the presence of NSF and alphaSNAP. *Elife*, *8*. doi:10.7554/eLife.38880
- Raichle, M. E., & Mintun, M. A. (2006). Brain work and brain imaging. *Annu Rev Neurosci*, *29*, 449-476. doi:10.1146/annurev.neuro.29.051605.112819
- Reese, H. W. (1973). Models of memory and models of development. *Hum Dev*, *16*(6), 397-416. doi:10.1159/000271292
- Ritzau-Jost, A., Jablonski, L., Viotti, J., Lipstein, N., Eilers, J., & Hallermann, S. (2018). Apparent calcium dependence of vesicle recruitment. *J Physiol*, *596*(19), 4693-4707. doi:10.1113/JP275911
- Rosenmund, C., & Stevens, C. F. (1996). Definition of the readily releasable pool of vesicles at hippocampal synapses. *Neuron*, *16*(6), 1197-1207. doi:10.1016/s0896-6273(00)80146-4
- Saheki, Y., & De Camilli, P. (2012). Synaptic vesicle endocytosis. *Cold Spring Harb*

- Perspect Biol*, 4(9), a005645. doi:10.1101/cshperspect.a005645
- Sakmann, B., & Neher, E. (1984). Patch clamp techniques for studying ionic channels in excitable membranes. *Annu Rev Physiol*, 46, 455-472. doi:10.1146/annurev.ph.46.030184.002323
- Scales, S. J., Hesser, B. A., Masuda, E. S., & Scheller, R. H. (2002). Amisyn, a novel syntaxin-binding protein that may regulate SNARE complex assembly. *J Biol Chem*, 277(31), 28271-28279. doi:10.1074/jbc.M204929200
- Schluter, O. M., Basu, J., Sudhof, T. C., & Rosenmund, C. (2006). Rab3 superprimes synaptic vesicles for release: implications for short-term synaptic plasticity. *J Neurosci*, 26(4), 1239-1246. doi:10.1523/JNEUROSCI.3553-05.2006
- Schneggenburger, R., Meyer, A. C., & Neher, E. (1999). Released fraction and total size of a pool of immediately available transmitter quanta at a calyx synapse. *Neuron*, 23(2), 399-409. doi:10.1016/s0896-6273(00)80789-8
- Schoch, S., & Gundelfinger, E. D. (2006). Molecular organization of the presynaptic active zone. *Cell Tissue Res*, 326(2), 379-391. doi:10.1007/s00441-006-0244-y
- Schulz, P. E. (1997). Long-term potentiation involves increases in the probability of neurotransmitter release. *Proc Natl Acad Sci U S A*, 94(11), 5888-5893. doi:10.1073/pnas.94.11.5888
- Segev, A., Garcia-Oscos, F., & Kourrich, S. (2016). Whole-cell Patch-clamp Recordings in Brain Slices. *J Vis Exp*(112). doi:10.3791/54024
- Seitz, K. J., & Rizzoli, S. O. (2019). GFP nanobodies reveal recently-exocytosed pHluorin molecules. *Sci Rep*, 9(1), 7773. doi:10.1038/s41598-019-44262-8
- Shupliakov, O., & Brodin, L. (2010). Recent insights into the building and cycling of synaptic vesicles. *Exp Cell Res*, 316(8), 1344-1350. doi:10.1016/j.yexcr.2010.02.035
- Sigworth, F. J., & Neher, E. (1980). Single Na<sup>+</sup> channel currents observed in cultured rat muscle cells. *Nature*, 287(5781), 447-449. doi:10.1038/287447a0
- Silverman, J. L., Tolu, S. S., Barkan, C. L., & Crawley, J. N. (2010). Repetitive self-grooming behavior in the BTBR mouse model of autism is blocked by the mGluR5 antagonist MPEP. *Neuropsychopharmacology*, 35(4), 976-989.

doi:10.1038/npp.2009.201

- Singewald, N., & Holmes, A. (2019). Rodent models of impaired fear extinction. *Psychopharmacology (Berl)*, 236(1), 21-32. doi:10.1007/s00213-018-5054-x
- Sinha, K., & Mukhopadhyay, C. D. (2020). Quantitative detection of neurotransmitter using aptamer: From diagnosis to therapeutics. *J Biosci*, 45.
- Sollner, T., Bennett, M. K., Whiteheart, S. W., Scheller, R. H., & Rothman, J. E. (1993). A protein assembly-disassembly pathway in vitro that may correspond to sequential steps of synaptic vesicle docking, activation, and fusion. *Cell*, 75(3), 409-418. doi:10.1016/0092-8674(93)90376-2
- Stein, A., Weber, G., Wahl, M. C., & Jahn, R. (2009). Helical extension of the neuronal SNARE complex into the membrane. *Nature*, 460(7254), 525-528. doi:10.1038/nature08156
- Sudhof, T. C., & Rizo, J. (2011). Synaptic vesicle exocytosis. *Cold Spring Harb Perspect Biol*, 3(12). doi:10.1101/cshperspect.a005637
- Sutton, R. B., Fasshauer, D., Jahn, R., & Brunger, A. T. (1998). Crystal structure of a SNARE complex involved in synaptic exocytosis at 2.4 Å resolution. *Nature*, 395(6700), 347-353. doi:10.1038/26412
- Terrian, D. M., & White, M. K. (1997). Phylogenetic analysis of membrane trafficking proteins: a family reunion and secondary structure predictions. *Eur J Cell Biol*, 73(3), 198-204.
- Thomas-Reetz, A. C., & De Camilli, P. (1994). A role for synaptic vesicles in non-neuronal cells: clues from pancreatic beta cells and from chromaffin cells. *FASEB J*, 8(2), 209-216. doi:10.1096/fasebj.8.2.7907072
- Thorsten Trimbuch, C. R. (2016). Should I stop or should I go? The role of complexin in neurotransmitter release. *Nature*, 17, 118-125.
- Trimble, W. S., Cowan, D. M., & Scheller, R. H. (1988). VAMP-1: a synaptic vesicle-associated integral membrane protein. *Proc Natl Acad Sci U S A*, 85(12), 4538-4542. doi:10.1073/pnas.85.12.4538
- Turrigiano, G. G., & Nelson, S. B. (2004). Homeostatic plasticity in the developing nervous system. *Nat Rev Neurosci*, 5(2), 97-107. doi:10.1038/nrn1327

- Vasileva, M., Horstmann, H., Geumann, C., Gitler, D., & Kuner, T. (2012). Synapsin-dependent reserve pool of synaptic vesicles supports replenishment of the readily releasable pool under intense synaptic transmission. *Eur J Neurosci*, *36*(8), 3005-3020. doi:10.1111/j.1460-9568.2012.08225.x
- Veit, M., Sollner, T. H., & Rothman, J. E. (1996). Multiple palmitoylation of synaptotagmin and the t-SNARE SNAP-25. *FEBS Lett*, *385*(1-2), 119-123. doi:10.1016/0014-5793(96)00362-6
- Wang, X., Gong, J., Zhu, L., Wang, S., Yang, X., Xu, Y., . . . Ma, C. (2020). Munc13 activates the Munc18-1/syntaxin-1 complex and enables Munc18-1 to prime SNARE assembly. *EMBO J*, *39*(16), e103631. doi:10.15252/embj.2019103631
- Weber, T., Zemelman, B. V., McNew, J. A., Westermann, B., Gmachl, M., Parlati, F., . . . Rothman, J. E. (1998). SNAREpins: minimal machinery for membrane fusion. *Cell*, *92*(6), 759-772. doi:10.1016/s0092-8674(00)81404-x
- Weimbs, T., Mostov, K., Low, S. H., & Hofmann, K. (1998). A model for structural similarity between different SNARE complexes based on sequence relationships. *Trends Cell Biol*, *8*(7), 260-262. doi:10.1016/s0962-8924(98)01285-9
- Weisskopf, M. G., Castillo, P. E., Zalutsky, R. A., & Nicoll, R. A. (1994). Mediation of hippocampal mossy fiber long-term potentiation by cyclic AMP. *Science*, *265*(5180), 1878-1882. doi:10.1126/science.7916482
- Wu, L. G., & Borst, J. G. (1999). The reduced release probability of releasable vesicles during recovery from short-term synaptic depression. *Neuron*, *23*(4), 821-832. doi:10.1016/s0896-6273(01)80039-8
- Xiang, X., Wang, X., Jin, S., Hu, J., Wu, Y., Li, Y., & Wu, X. (2021). Activation of GPR55 attenuates cognitive impairment and neurotoxicity in a mouse model of Alzheimer's disease induced by Abeta1-42 through inhibiting RhoA/ROCK2 pathway. *Prog Neuropsychopharmacol Biol Psychiatry*, *112*, 110423. doi:10.1016/j.pnpbp.2021.110423
- Xu, J., Mashimo, T., & Sudhof, T. C. (2007). Synaptotagmin-1, -2, and -9: Ca<sup>2+</sup> sensors for fast release that specify distinct presynaptic properties in subsets of

- neurons. *Neuron*, 54(4), 567-581. doi:10.1016/j.neuron.2007.05.004
- Yizhar, O., Matti, U., Melamed, R., Hagalili, Y., Bruns, D., Rettig, J., & Ashery, U. (2004). Tomosyn inhibits priming of large dense-core vesicles in a calcium-dependent manner. *Proc Natl Acad Sci U S A*, 101(8), 2578-2583. doi:10.1073/pnas.0308700100
- Yoshimura, M., Furue, H., Ito, A., & Nakatsuka, T. (2002). [Functional analysis of pain pathway in posterior horn cells using spinal cord slice and in-vivo patch clamp method]. *Masui*, 51 Suppl, S79-88.
- Zarebidaki, F., Camacho, M., Brockmann, M. M., Trimbuch, T., Herman, M. A., & Rosenmund, C. (2020). Disentangling the Roles of RIM and Munc13 in Synaptic Vesicle Localization and Neurotransmission. *J Neurosci*, 40(49), 9372-9385. doi:10.1523/JNEUROSCI.1922-20.2020
- Zhou, Q., Lai, Y., Bacaj, T., Zhao, M., Lyubimov, A. Y., Uervirojnangkoorn, M., . . . Brunger, A. T. (2015). Architecture of the synaptotagmin-SNARE machinery for neuronal exocytosis. *Nature*, 525(7567), 62-67. doi:10.1038/nature14975
- Zhou, Q., Zhou, P., Wang, A. L., Wu, D., Zhao, M., Sudhof, T. C., & Brunger, A. T. (2017). The primed SNARE-complexin-synaptotagmin complex for neuronal exocytosis. *Nature*, 548(7668), 420-425. doi:10.1038/nature23484
- Zucker, R. S., & Regehr, W. G. (2002). Short-term synaptic plasticity. *Annu Rev Physiol*, 64, 355-405. doi:10.1146/annurev.physiol.64.092501.114547

## **Acknowledgements**

Here I would like to present my sincere gratitude to all the people who help me and give me support during my Ph.D. career.

I would like to thank my supervisor Prof. Dr. Ira Milosevic, who provide me this honor and opportunity to process my Ph.D. project. Her rigorous attitude towards experiments and scientific problems set a fine example to me. She provides me great deal of freedom on my own specialty. Meanwhile, she gives me considerate and detailed instruction on the techniques that I am not familiar with. Whenever I have problem either in science or in daily life, she can always offer me her wise to help me overcome those barriers.

Second, I would like to thank my thesis committee member Dr. Brett Carter and Prof. I would like to show my thankfulness especially to Dr. Brett Carter, who gives me numerous advises and helps with electrophysiology. This knowledge is an invaluable treasure for my future work. Not to mention he generously provides me his instrument to achieve some tricky experiments. Besides Brett, Prof. Schu also gives me a lot of good advice and provides me different points of view in the TAC meetings.

I would like to thank my colleagues and collaborators. Ilona helps me a lot when I start the project. Her effort makes my first half-year much easier than I thought. Udhay is always a good friend and officemate. We spend lots of good times and I also learn a lot about cloning from him. I would like to appreciate Ronni for his help on behavior assays. Although we only spend 2 months together, I have already learned tons of things about animal behavior experiments from you. And whenever I have a problem with behavior assays, I can always find your help even when you are on vacation. I would like to especially thank Taylan. We have learned a lot from each other and I particularly enjoy those unfettered scientific discussions with you. I am also grateful to the other two master students, Joana Pires and Joana Ferreira. They show great patience and endeavor in this project, although I am a rooky project leader and always failed to help them. I particularly want to thank Dirk Schwitters, our technician (and translator for some time) for his help on genotyping and

troubleshooting. And it is very joyful for me to spend time with Joanna, King, Monica, Kasia, Aman, Angela, Mariana, Joana, Renata, Kamil, and other members in Milosevic lab. I really appreciate them to provide me such a good environment for science. Also, I want to thank Dr. Nuno Raimundo for his humor and enthusiasm for science.

Besides members from Milosevic lab, I am also grateful to other supporting staff in ENI, especially Christiane Becker, Kristin Baer, Gesa Homann, and Synnöve Beckh. Also, ENI's IT team and workshop team give me a lot of help during my research.

I also want to pay my gratitude to Prof. Dr. Heinemann, who showed me not only basic knowledge about patch clamp but also the charm of electrophysiology. I won't become an electrophysiologist without his supervision.

Especially I want to thank the GGNB program and all the co-coordinators. I know sometimes I missed a lot of paperwork, but you can always help me to figure out these problems. I cannot finish my Ph.D. project without your help.

Last but definitely not least, I want to thank all my family, who continuously give me unlimited support and love whenever I have difficulty. My parents always give me good advice. My grandparents, uncle, and aunt also provide me many bits of help, and make me feel supported. Thanks a lot, Lei, you know I cannot achieve anything without you. Sometimes I just feel decant and you always give me the power to constantly strive. There are many laughs and tears during the 7 years with you, and I hope I can have the honor to continuously share those laughs and tears with you forever.

# Curriculum Vitae

## Personal Data

Name: **Jialin JIN**

Date of Birth: 26/02/1992

Place of Birth: Beijing, P.R. China

Marital Status: Single

Nationality: P.R.China

## Contact details

Jialin JIN

Ludwig-Prandtl-Straße 54

37077 Göttingen

Tel: +49 0176/ 80817554

Email: jialin.jin1992@gmail.de

## Education

07. 2019 – present **Georg-August-Universität, Göttingen, Germany**

European Neuroscience Institute

Degree: Ph. D

09. 2014 – 07.2018 **Freidrich-Schiller-Universität, Jena, Germany**

Abbe School of Photonics

Degree: Master of Photonics (M. Sc)

Mark so Far: Very Good

09. 2010 – 06. 2014 **Peking University, Beijing, P.R. China**

Physics department

Degree: Bachelor of Physics (B.Sc)

Mark: Good

09. 2004 – 06. 2010 **The Middle School Affiliated to Renmin University of China**

Final Degree: Highschool (equal to Abitur)

Mark: Very Good

## Research Experience

12. 2018 – present **European Neuroscience Institute, Göttingen, Germany**

*Research Assistant*

- Physiological characterization of novel syntaxin-binding protein amisyn

02. 2016 – 07.2018 **Freidrich-Schiller-Universität, Jena, Germany**

Institut für Biochemie und Biophysik

*Research Assistant for Master thesis*

- Manipulation of the cellular membrane potential by visible-light illumination of targeted superparamagnetic beads

06. 2015 – 02. 2016 **Freidrich-Schiller-Universität, Jena, Germany**

Institut für Biochemie und Biophysik

*Internship*

- Designing and calibration of a patch-pipette micro-thermometer
- Measurement of flash-light induced temperature change on the surface of superparamagnetic beads

01. 2014 – 07. 2014 **Tsinghua University, Beijing, P.R. China**

Center of Basic Molecular Science at Tsinghua University

*Research Assistant for Bachelor thesis*

- Synthesis, purification and test of agonist of Toll-like-receptor 4

10.2012-10.2013 **Peking University, Beijing, P.R. China**

Center of Modern Optics at Peking University

*Internship Research Assistant*

- Designing quantum dot organic solar cell with high photo-electro transition rate
- Maintaining of the Laboratory Setup

## Professional competence

- Practical skills:**
- Electrophysiology (patch-clamp technique) in both cell culture and brain slice
  - Recording and analyzing of multichannel-electrode-array (MEA)
  - Mammalian cell culture including DNA transfection
  - Fluorescence microscopy
  - Immunostaining
  - Western blotting
  - Genotyping of animal biopsies.

- Soft skills:**
- team work with my supervisor on both practical experiments and theoretical study,
  - communication skills developed in scientific conferences and weekly group meetings,
  - good at teaching other colleagues and students

## Further Knowledge

**Languages:** German (Studying), English (fluent), Chinese (native)

**IT:** Microsoft Office, Original, C Programming, Igor Programming, PatchMaster, FitMaster